ISSN 2686-7575 (Online)

ТОНКИЕ ХИМИЧЕСКИЕ ТЕХНОЛОГИИ

Fine Chemical Technologies

- Theoretical Bases of Chemical Technology
- Chemistry and Technology of Organic Substances
- Chemistry and Technology of Medicinal Compounds and Biologically Active Substances
- Biochemistry and Biotechnology
- Synthesis and Processing of Polymers and Polymeric Composites
- Chemistry and Technology of Inorganic Materials
- Analytical Methods in Chemistry and Chemical Technology
- Mathematical Methods and Information Systems in Chemical Technology

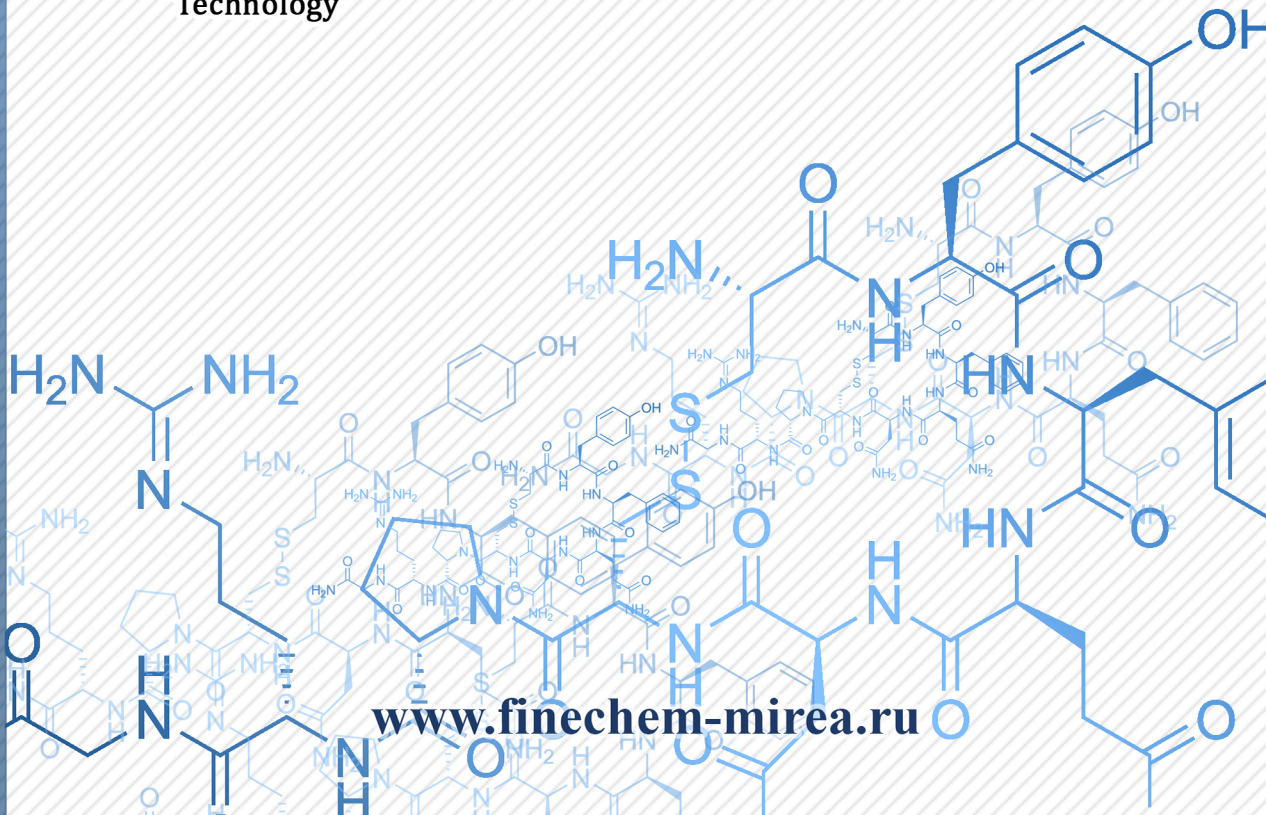

19(1)
2024

www.finechem-mirea.ru

ISSN 2686-7575 (Online)

ТОНКИЕ ХИМИЧЕСКИЕ ТЕХНОЛОГИИ

Fine Chemical Technologies

- Theoretical Bases of Chemical Technology
- Chemistry and Technology of Organic Substances
- Chemistry and Technology of Medicinal Compounds and Biologically Active Substances
- Biochemistry and Biotechnology
- Synthesis and Processing of Polymers and Polymeric Composites
- Chemistry and Technology of Inorganic Materials
- Analytical Methods in Chemistry and Chemical Technology
- Mathematical Methods and Information Systems in Chemical Technology

Tonkie Khimicheskie Tekhnologii =
Fine Chemical Technologies.
Vol. 19, No. 1, 2024

Тонкие химические технологии =
Fine Chemical Technologies.
Том 19, № 1, 2024

https://doi.org/10.32362/2410-6593-2024-19-1
www.finechem-mirea.ru

**Tonkie Khimicheskie Tekhnologii =
Fine Chemical Technologies
2024, Vol. 19, No. 1**

The peer-reviewed scientific and technical journal Fine Chemical Technologies highlights the modern achievements of fundamental and applied research in the field of fine chemical technologies, including theoretical bases of chemical technology, chemistry and technology of medicinal compounds and biologically active substances, organic substances and inorganic materials, biochemistry and biotechnology, synthesis and processing of polymers and polymeric composites, analytical and mathematical methods and information systems in chemistry and chemical technology.

Founder and Publisher

Federal State Budget
Educational Institution of Higher Education
"MIREA – Russian Technological University"
78, Vernadskogo pr., Moscow, 119454, Russian Federation.
Publication frequency: bimonthly.
The journal was founded in 2006. The name was Vestnik MITHT until 2015 (ISSN 1819-1487).

The journal is included into the List of peer-reviewed science press of the State Commission for Academic Degrees and Titles of the Russian Federation.

The journal is indexed: SCOPUS, DOAJ, Chemical Abstracts, Science Index, RSCI, Ulrich's International Periodicals Directory

86, Vernadskogo pr., Moscow, 119571, Russian Federation.
Phone: +7 (499) 600-80-80 (#31288)
E-mail: *seredina@mirea.ru*

The registration number ПИ № ФС 77–74580 was issued in December 14, 2018 by the Federal Service for Supervision of Communications, Information Technology, and Mass Media of Russia

The subscription index of *Pressa Rossii*: **36924**

**Тонкие химические технологии =
Fine Chemical Technologies
2024, том 19, № 1**

Научно-технический рецензируемый журнал «Тонкие химические технологии» освещает современные достижения фундаментальных и прикладных исследований в области тонких химических технологий, включая теоретические основы химической технологии, химию и технологию лекарственных препаратов и биологически активных соединений, органических веществ и неорганических материалов, биохимию и биотехнологию, синтез и переработку полимеров и композитов на их основе, аналитические и математические методы и информационные системы в химии и химической технологии.

Учредитель и издатель

федеральное государственное бюджетное
образовательное учреждение высшего образования
«МИРЭА – Российский технологический университет»
119454, РФ, Москва, пр-т Вернадского, д. 78.
Периодичность: один раз в два месяца.
Журнал основан в 2006 году. До 2015 года издавался под названием «Вестник МИТХТ» (ISSN 1819-1487).

Журнал входит в Перечень ведущих рецензируемых научных журналов ВАК РФ.

Индексируется: SCOPUS, DOAJ, Chemical Abstracts, РИНЦ (Science Index), RSCI, Ulrich's International Periodicals Directory

119571, Москва, пр. Вернадского, 86, оф. Л-119.
Тел.: +7 (499) 600-80-80 (#31288)
E-mail: *seredina@mirea.ru*

Регистрационный номер и дата принятия решения о регистрации СМИ: ПИ № ФС 77-74580 от 14.12.2018 г. СМИ зарегистрировано Федеральной службой по надзору в сфере связи, информационных технологий и массовых коммуникаций (Роскомнадзор)

Индекс по Объединенному каталогу «Пресса России»: **36924**

EDITORIAL BOARD

РЕДАКЦИОННАЯ КОЛЛЕГИЯ

19(1) 2024 | Tonkie Khimicheskie Tekhnologii
Fine Chemical Technologies

Contents

СОДЕРЖАНИЕ

Tonkie Khimicheskie Tekhnologii = Fine Chemical Technologies.
2024;19(1):7–16
ISSN 2686-7575 (Online)

Theoretical bases of chemical technology
Теоретические основы химической технологии

UDC 544.726
https://doi.org/10.32362/2410-6593-2024-19-1-7-16

RESEARCH ARTICLE

Sorption of picolinic acid by Cu(II)-containing sulfocationite KU-2-8

Heinrich N. Altshuler[1],✉, Vladimir N. Nekrasov[1], Sergey Yu. Lyrshchikov[1], Olga H. Altshuler[1,2]

[1] *Federal Research Center of Coal and Coal Chemistry, Siberian Branch, Russian Academy of Sciences, Kemerovo, 650000 Russia*

[2] *Kemerovo State University, Kemerovo, 650000 Russia*

✉ *Corresponding author, e-mail: altshulerh@gmail.com*

Abstract

Objectives. To study the equilibrium distribution of components between KU-2-8 sulfocationite and an aqueous solution containing picolinic acid and Cu(II); to show the possibility of immobilization of cations of picolinic acid and Cu^{2+} in sulfonic cation exchanger KU-2-8; to calculate the component compositions of the equilibrium solution, in order to obtain the required ionic composition of the KU-2-8 sulfonic cation exchanger according to the selectivity coefficients of binary ion exchange, and the constants of formation of such complexes in water.

Methods. The concentrations of the individual components in multicomponent solutions were calculated using the HySS 2009 program (Hyperquad Simulaton and Speciation). The calculation of the equilibrium ionic compositions of KU-2-8 sulfocationite was performed using the selectivity coefficients of binary ion exchanges and the formation constants of complexes of picolinic acid with Cu^{2+} and H^+ cations. Experimental study of the equilibrium distribution of components between aqueous solutions of picolinic acid, copper nitrate, and KU-2-8 sulfocationite was carried out by means of the dynamic method at a temperature of 298 K. Fourier-transform infrared spectroscopy and electron paramagnetic resonance spectroscopy were used, in order to determine the ionic forms of the components contained in the sulfocationite.

Results. It was shown that the equilibrium solution contains H^+ protons, Cu^{2+} cations, LH picolinic acid molecules, protonated picolinic acid cations $[H_2L]^+$, deprotonated picolinic acid anions L^-, Cu^{2+} complexes with the deprotonated picolinic acid anion $[CuL]^+$, and Cu^{2+} complexes with two anions of deprotonated picolinic acid $[CuL_2]$. The concentration of H^+, Cu^{2+}, and $[H_2L]^+$ cations in the solution significantly exceeds the concentration of other components at pH values from 0 to 0.5. The content of $[CuL]^+$ cations and neutral complexes $[CuL_2]$ increases significantly in the solution, while the $[H_2L]^+$ cations disappear at pH greater than 1. It was experimentally established that the concentrations of picolinic acid and copper in the polymer phase are many times higher than the concentrations of these components in an aqueous solution. The partition coefficients are about 24 and 210 for picolinic acid and Cu(II), respectively. The calculated dependencies of the concentrations of Cu^{2+}, $[H_2L]^+$, H^+, $[CuL]^+$ cations in the polymer *vs* pH of an equilibrium solution containing picolinic acid were obtained. The experimental data on the concentrations of all cations in the ion exchanger is in the intervals of the calculated compositions within the limits of measurement errors.

Conclusions. KU-2-8 sulfocationite is proposed as a container for obtaining drugs based on picolinic acid and Cu^{2+} cations. It was shown that the selectivity coefficients of binary ion exchanges and the formation constants of $[H_2L]^+$, $[CuL]^+$ complexes can be used to precalculate the ionic compositions of the equilibrium solution, in order to obtain the required compositions of the sulfocationite.

Keywords

KU-2-8 sulfocationite, picolinic acid, copper(II) cations, sorption

Submitted: 12.12.2022
Revised: 31.03.2023
Accepted: 22.01.2024

For citation

Altshuler H.N., Nekrasov V.N., Lyrshchikov S.Yu., Altshuler O.H. Sorption of picolinic acid by Cu(II)-containing sulfocationite KU-2-8. *Tonk. Khim. Tekhnol. = Fine Chem. Technol*. 2024;19(1):7–16. https://doi.org/10.32362/2410-6593-2024-19-1-7-16

НАУЧНАЯ СТАТЬЯ

Сорбция пиколиновой кислоты Cu(II)-содержащим сульфокатионитом КУ-2-8

Г.Н. Альтшулер[1,✉], В.Н. Некрасов[1], С.Ю. Лырщиков[1], О.Г. Альтшулер[1,2]

[1] *Федеральный исследовательский центр угля и углехимии Сибирского отделения РАН, Кемерово, 650000 Россия*

[2] *Кемеровский государственный университет, Кемерово, 650000 Россия*

✉ *Автор для переписки, e-mail: altshulerh@gmail.com*

Аннотация

Цели. Изучить равновесное распределение компонентов между сульфокатионитом КУ-2-8 и водным раствором, содержащим пиколиновую кислоту и Cu(II); показать возможность иммобилизации катионов пиколиновой кислоты и Cu^{2+} в сульфокатионите КУ-2-8. Выполнить предрасчет компонентного состава равновесного раствора для получения необходимого ионного состава сульфокатионита КУ-2-8 по коэффициентам селективности бинарных ионных обменов и константам образования комплексов в воде.

Методы. Концентрации индивидуальных компонентов в многокомпонентных растворах рассчитывали с помощью программы HySS 2009 (Hyperquad Simulaton and Speciation). Расчет равновесных ионных составов сульфокатионита КУ-2-8 выполнен по коэффициентам селективности бинарных ионных обменов и константам образования комплексов пиколиновой кислоты с катионами Cu^{2+} и H^+. Экспериментальное исследование равновесного распределения компонентов между водными растворами пиколиновой кислоты, нитрата меди и сульфокатионитом КУ-2-8 проведено динамическим методом при температуре 298 К. Для определения ионных форм компонентов, содержащихся в сульфокатионите, использованы инфракрасная спектроскопия с преобразованием Фурье и спектроскопия электронного парамагнитного резонанса.

Результаты. Показано, что в равновесном растворе содержатся протоны H^+, катионы Cu^{2+}, молекулы пиколиновой кислоты LH, катионы протонированной пиколиновой кислоты $[H_2L]^+$, анионы депротонированной пиколиновой кислоты L^-, комплексы Cu^{2+} с анионом депротонированной пиколиновой кислоты $[CuL]^+$, комплексы Cu^{2+} с двумя анионами депротонированной пиколиновой кислоты $[CuL_2]$. При значениях pH от 0 до 0.5 в растворе концентрация катионов H^+, Cu^{2+}, $[H_2L]^+$ существенно превышает концентрацию других компонентов, при pH больше 1 в растворе значительно увеличивается содержание катионов $[CuL]^+$, нейтральных комплексов $[CuL_2]$ и практически исчезают катионы $[H_2L]^+$. Экспериментально установлено, что концентрация пиколиновой кислоты и меди в полимерной фазе во много раз превышает концентрацию этих компонентов в водном растворе. Коэффициенты распределения составляют примерно 24 и 210 для пиколиновой кислоты и Cu(II) соответственно. Получены расчетные зависимости концентрации катионов Cu^{2+}, $[H_2L]^+$, H^+, $[CuL]^+$ в полимере от pH равновесного раствора, содержащего пиколиновую кислоту. Экспериментальные данные о концентрациях всех катионов в ионите в пределах ошибок измерений попадают в интервалы расчетных составов.

Выводы. Сульфокатионит КУ-2-8 предложен в качестве контейнера для получения лекарственных препаратов на основе пиколиновой кислоты и катионов Cu^{2+}. По коэффициентам селективности бинарных ионных обменов и константам образования комплексов $[H_2L]^+$, $[CuL]^+$ выполнен предрасчет компонентного состава равновесного раствора для получения необходимого ионного состава сульфокатионита КУ-2-8.

Ключевые слова

сульфокатионит КУ-2-8, пиколиновая кислота, катионы меди, сорбция

Поступила: 12.12.2022
Доработана: 31.03.2023
Принята в печать: 22.01.2024

Для цитирования

Альтшулер Г.Н., Некрасов В.Н., Лырщиков С.Ю., Альтшулер О.Г. Сорбция пиколиновой кислоты Cu(II)-содержащим сульфокатионитом КУ-2-8. *Тонкие химические технологии*. 2024;19(1):7–16. https://doi.org/10.32362/2410-6593-2024-19-1-7-16

INTRODUCTION

Pyridine carboxylic acids are an object of interest to researchers. Picolinic acid (2-pyridinecarboxylic acid) is known for its antibacterial activity against *S. aureus*, *S. epidermidis*, *E. coli* [1]. Fusaric acid, a picolinic acid derivative, possesses antibacterial, insecticidal, bactericidal activity [2], while picolinic acid amides possess anti-inflammatory and analgesic activity [3]. Copper is widely used in medicine as an anti-inflammatory, styptic, antibacterial and antipyretic agent [4, 5]. In pharmacology, Ehrlich's idea of the feasibility of targeted drug delivery to the focus of disease is becoming increasingly relevant [6]. The use of nanocontainers [7] helps to achieve the desired pharmacokinetics, opening up significant opportunities for the preservation and storage of dosage forms. They also enable the vector delivery of drug substance to the focus of the disease. Studies on the creation of polymer and biocomposite matrices as carriers of target pharmaceutical substances [8] and nanocontainers on matrices of mesh polymers are of topical relevance [9].

In the food industry and medicine, the deep desalination of water, as well as purification of vitamins and pharmaceuticals, is achieved with the help of sulfonated copolymer of styrene with divinylbenzene (industrial KU-2-8 cationite or Dowex 50) [10]. A known property is its complementarity to pyridinecarboxylic acids, possessing the highest capacity among other sulfocationites [11]. It was shown [11] that the elementary link of sulfonated styrene copolymer with divinylbenzene is a nanocarrier for pyridinecarboxylic acid (Fig. 1).

We previously studied the sorption of nicotinic and isonicotinic acids by Dowex-50 sulphocationite in Ni(II)- and Cu(II)-form and Ag-containing KU-2-4 sulphocationite [12, 13].

The objectives of this study were:

- To study the equilibrium distribution of components between KU-2-8 sulphocationite and aqueous solution containing picolinic acid and Cu(II); and to show the possibility of immobilization of picolinic acid and Cu^{2+} cations in KU-2-8 sulphocationite;
- To precalculate the component composition of the equilibrium solution, in order to obtain the required ionic composition of KU-2-8 sulphocationite according to the selectivity coefficients of binary ionic exchanges and constants of complex formation in water.

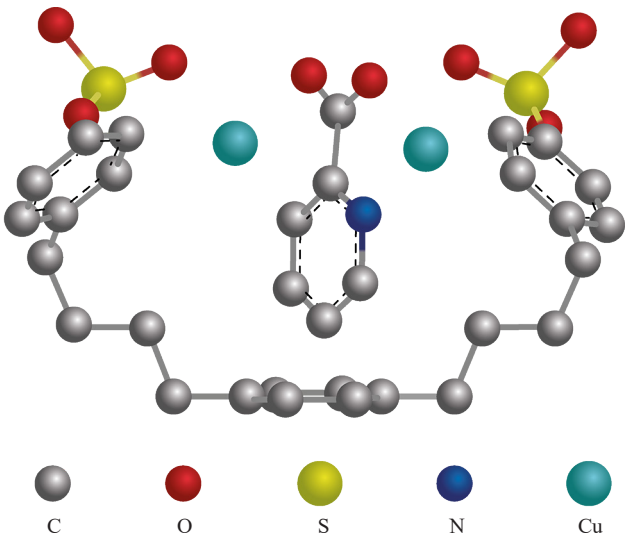

Fig. 1. Structure of a nanocontainer (an elementary unit of sulfonated copolymer of styrene with divinylbenzene) containing pyridinecarboxylic acid [11], minimized in terms of internal energy using the MOPAC 2016 program[1]

MATERIALS AND METHODS

Strong-acid KU-2-8 cationite (sulfonated copolymer of styrene with 8% divinylbenzene) has a gel structure, and contains SO_3H-groups as ionogenic groups. The total ion exchange capacity is 5.0 mEq per 1 g of H-form of the dry polymer (2.0 mol per 1 L of native volume of the swollen ion exchanger phase). Picolinic (2-pyridinecarboxylic) acid (*Kiev plant RIAP*, Ukraine) contained at least 98.0% of the basic substance. The electrolyte solutions were prepared from $Cu(NO_3)_2$ (*Ural Plant of Chemical Reagents*, Russia), HNO_3, $NaNO_3$ (*Mikhailovsky Plant of Chemical Reagents*, Russia), chemically pure grade.

The equilibrium distribution of components between aqueous solutions of picolinic acid, copper nitrate and KU-2-8 sulfocationite was studied by means of the dynamic method at 298 K. The working interval of pH of equilibrium solutions was chosen in the range of 2.0–2.5. This was based on the content of components in the solution, and their ability to participate in the cation exchange reaction. The multicomponent aqueous solutions were passed through an ion-exchange column filled with the Cu^{2+}-form of polymer (5 mL of swollen ionite) until equilibrium was established (until the compositions and pH of the initial solution and filtrate coincided). The equimolar concentrations of picolinic acid and

[1] MOPAC (Molecular Orbital PACkage) is the semi-empirical quantum chemistry program developed by James J. P. Stewart, Stewart Computational Chemistry, Colorado Springs, Colorado, USA, http://openmopac.net/. Accessed December 12, 2023.

copper nitrate in the solutions were maintained near 0.005 mol/L (at picolinic acid concentrations above 0.01 mol/L, a precipitate of complexes containing Cu(II) and picolinic acid forms in the solution). After reaching the equilibrium state, desorption of picolinic acid and copper was carried out using a 0.1 M $NaNO_3$ solution. The concentration of picolinic acid in the solutions was measured using a spectrophotometer SF-46 (*LOMO*, Russia) at λ = 262.7 nm and pH = 6.86.

The total copper concentration in the multicomponent solutions ($\sum C_{Cu}$) was determined by means of complexometric titration. The concentrations of the individual components C_i in solutions were calculated using HySS 2009 software[2]. The concentration of components in the polymer ($\overline{C}_i$) was calculated in moles per liter of the native volume of the swollen ionite phase. Infrared (IR) spectra were obtained using an Infralum FT-801 FTIR spectrometer (*SIMEX*, Russia) in KBr tablets. The electron paramagnetic resonance spectra were recorded on a Bruker EMX micro 6/1 electron spin resonance (ESR) spectrometer (*Bruker EMX*, Germany) at room temperature (20°C). The number of paramagnetic centers was calculated by comparison with a standard sample (Mn^{2+} in MgO). The spectra were processed using the WinEPR software package[3].

RESULTS AND DISCUSSION

The experimental data thus obtained is presented in Table 1.

Table 1. Equilibrium compositions of KU-2-8 sulfocationite and aqueous solutions containing $Cu(NO_3)_2$ and picolinic acid at 298 K

Solution			Sulfocationite	
pH	$\sum C_{Cu}$	$\sum C_{HL}$	$\sum \overline{C}_{Cu}$	$\sum \overline{C}_{HL}$
	mol/L			
2.00	0.005	0.0053	1.04	0.144
2.13	0.005	0.0052	1.04	0.104
2.20	0.005	0.0053	1.06	0.144
2.28	0.005	0.0053	1.05	0.097
2.39	0.005	0.0054	1.05	0.145

Table 1 shows that the concentration of picolinic acid and Cu(II) in the polymer phase is many times higher than that of the same components in aqueous solution. The distribution ratios ($\overline{C}_i / C_i$) are approximately 24 and 210 for picolinic acid and Cu(II), respectively.

Let us consider the reasons of occurrence of high distribution ratios. The following reactions take place in the solution being studied:

$$L^- + H^+ = HL, \quad (1)$$

$$HL + H^+ = [H_2L]^+, \quad (2)$$

$$Cu^{2+} + L^- = [CuL]^+, \quad (3)$$

$$[CuL]^+ + L^- = [CuL_2]. \quad (4)$$

These reactions can be characterized by the constants of complex formation as presented in Table 2.

Table 2. Stability constants β[4]

Substance	lgβ
HL (picolinic acid)	5.184
$[H_2L]^+$	6.066
$[CuL]^+$	7.9
$[CuL_2]$	14.75

The equilibrium solution contains protons H^+, cations Cu^{2+}, molecules of picolinic acid LH, cations of protonated picolinic acid $[H_2L]^+$, anions of deprotonated picolinic acid L^-, Cu^{2+} complexes with an anion of deprotonated picolinic acid $[CuL]^+$, and Cu^{2+}complexes with two anions of deprotonated picolinic acid $[CuL_2]$. Figure 2 shows the equilibrium ratio of components in solution as calculated using the HySS 2009 software. At pH values from 0 to 0.5 in the solution the concentration of cations H^+, Cu^{2+}, $[H_2L]^+$ significantly exceeds the concentration of other components. The concentration of H^+ exceeds the concentration of Cu^{2+}, $[H_2L]^+$ by more than 2 orders of magnitude. At a pH level from 0.5 to 1.5, the content of $[CuL]^+$ cations, $[CuL_2]$ neutral complexes and $[H_2L]^+$ cations practically disappear in the solution. At pH > 1.8 the concentration of H^+ decreases significantly. The concentrations of Cu^{2+} and $[CuL]^+$ cations attain values ≈0.001 and ≈0.003 mol/L, respectively. In the pH range from 1.8 to 2.5

[2] HySS 2009. Hyperquad Simulation and Speciation, Protonic Software, Leeds (UK), Universita di Firenze, Firenze (Italy), 2009.

[3] Software for the Bruker EMX micro 6/1 spectrometer (*Bruker Corporation*, USA).

[4] IUPAC Stability Constants Database. http://www.acadsoft.co.uk/scdbase/scdbase.htm. Accessed December 03, 2019.

the calculated ratio $C_{[CuL]^+} / C_{Cu^{2+}}$ remains constant and equal to 3.5. It is clearly in this range of solution pH, that it is reasonable to consider the equilibrium ionic composition of the cationite.

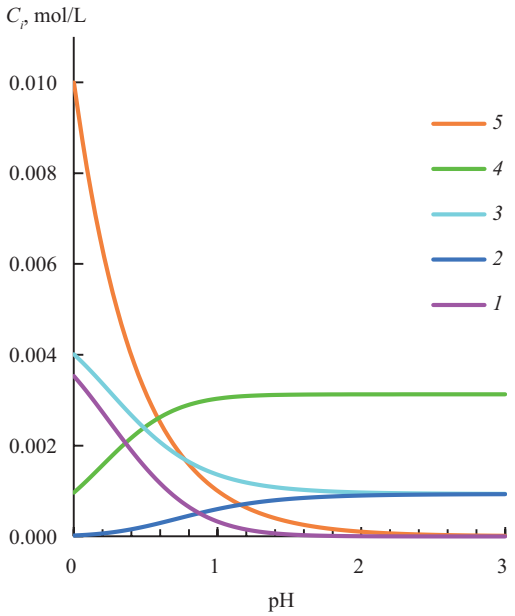

Fig. 2. Dependencies of the concentration of individual components (C_i) on pH of aqueous solutions containing 0.005 mol/L $Cu(NO_3)_2$ and 0.005 mol/L picolinic acid:
(*1*) $C_{[H_2L]^+}$;
(*2*) $C_{[CuL_2]}$;
(*3*) $C_{Cu^{2+}}$;
(*4*) $C_{[CuL]^+}$;
(*5*) $C_{H^+} \cdot 10^{-2}$

Fourier transform infrared (FTIR) spectroscopy and ESR spectroscopy were performed, in order to determine the ionic forms of the components contained in the polymer. A clear signal of Cu^{2+} ions is observed in the ESR spectrum of the sample containing copper and picolinic acid. The free radical concentration is $1.65 \cdot 10^{17}$ spin/g, the g-factor is 2.1811 and the line width is 17.5 mTL.

Table 3 shows the wave numbers and the attribution of absorption bands in the FTIR spectra of picolinic acid. It also shows salt $(C_6H_6NO_2)_2SO_4$ containing $[H_2L]^+$ cations, as well as KU-2-8 sulfocationite in Cu^{2+}-form and sulfocationite in mixed Cu^{2+}, $[CuL]^+$-form (brought into equilibrium with a solution containing Cu^{2+} and picolinic acid at pH 2.20, Table 1). A band at 1574 cm^{-1} appears in the spectrum of KU-2-8 sulfocationite in the mixed Cu^{2+}, $[CuL]^+$-form. This corresponds to vibrations of the C=C bond of the pyridine ring [14, 15] according to theoretical calculations [15] by the B3PW91/6-311++G** method. The band at 1377 cm^{-1} corresponds to deformation vibrations of the CH bond [14] and the band at 1297 cm^{-1} to symmetric stretching vibrations of CO [14].

The intense bands at 1724, 1741 cm^{-1} corresponding to the stretching vibrations of the C=O bond in COOH [16, 17], observed in the spectra of picolinic acid and its salt $(C_6H_6NO_2)_2SO_4$, are absent in the spectrum of its complex with Ni(II) and sulfocationite KU-2-8 containing Cu^{2+} and complex $[CuL]^+$.

Thus, analysis of ESR and FTIR spectra confirms that the counterionic composition of KU-2-8 sulfocationite, brought into equilibrium with the solution containing Cu^{2+} and picolinic acid, is represented by Cu^{2+} and $[CuL]^+$ cations. The Cu^{2+} cation in the polymer phase of KU-2-8 sulfocationite, as in aqueous solution [18], interacts with the nitrogen atom of picolinic acid to form $[CuL]^+$ cations.

In the heterogeneous system containing KU-2-8 sulfocationite, aqueous solution of picolinic acid, copper nitrate, and protons, ion exchange reactions take place:

$$2\overline{H^+} + Cu^{2+} = \overline{Cu^{2+}} + 2H^+, \quad (5)$$

$$\overline{H^+} + [H_2L]^+ = \overline{[H_2L]^+} + H^+, \quad (6)$$

$$\overline{H^+} + [CuL]^+ = \overline{[CuL]^+} + H^+. \quad (7)$$

The line above the cations shows that they are part of the polymer phase.

Let us consider the possibility of calculating the composition of the ion exchanger phase. Based on the content of components in the solution, their sorption capacity, and the above-mentioned reactions, we can assume that four competing cations participate in ion exchange on the sulphocationite: Cu^{2+}, $[H_2L]^+$, H^+, $[CuL]^+$. In order to calculate the equilibrium composition of the sulphocationite phase, we used the following system of equations (8):

$$\begin{cases} \dfrac{\overline{C}_{Cu^{2+}}}{\left(\overline{C}_{H^+}\right)^2} = k_{Cu/H} \cdot \dfrac{C_{Cu^{2+}}}{\left(C_{H^+}\right)^2} \\ \dfrac{\overline{C}_{[H_2L]^+}}{\overline{C}_{H^+}} = k_{H_2L/H} \cdot \dfrac{C_{[H_2L]^+}}{C_{H^+}} \\ \dfrac{\overline{C}_{[CuL]^+}}{\overline{C}_{H^+}} = k_{CuL/H} \cdot \dfrac{C_{[CuL]^+}}{C_{H^+}} \\ 2\overline{C}_{Cu^{2+}} + \overline{C}_{[H_2L]^+} + \overline{C}_{[CuL]^+} + \overline{C}_{H^+} = E, \end{cases} \quad (8)$$

where $k_{Cu/H}$, $k_{H_2L/H}$, $k_{CuL/H}$ are equilibrium constants (selectivity coefficients of binary ion exchanges) of processes (5), (6), and (7) on KU-2-8 sulfocationite according to [19, 20]. The dimension of component concentration and capacity (E) in the system of equations (8) is mol/L.

Table 3. Wavenumbers of absorption bands in FTIR spectra of picolinic acid, its sulfate $(H_2L)_2SO_4$, complex with Ni(II), and KU-2-8 sulfocationite containing Cu^{2+} and complex $[CuL]^+$, cm^{-1}

Picolinic acid			KU-2-8 in counterionic form		Assignments
HL	$(H_2L)_2SO_4$	$[Ni(II)L_2 \cdot 2H_2O]$ [14]	Cu^{2+}	Cu^{2+}, $[CuL]^+$	
1724s	1741s	–	–	–	Stretching vibrations of the C=O bond in COOH [16, 17]
–	–	1568 FTIR 1575.36 Calculation 1573.44 Calculation	–	1574w	Vibrations of the C=C bond of the pyridine ring [14, 15]
–	–	1374 FTIR 1409 Calculation	–	1377w	Deformation in plane of CH [14]
–	–	1299 FTIR 1291 Calculation	–	1297m	Symmetric CO stretching vibrations [14]
–	–	no data	499s	501s, 490s Doublet	Deformation vibrations of C–H and CCC bonds [15]

Note: s is a strong band, w is a weak band, m is a medium intensity band.

By resolving this system of equations, the calculated dependences of the concentration of cations Cu^{2+}, $[H_2L]^+$, H^+, $[CuL]^+$ in the polymer on the pH of the equilibrium solution containing picolinic acid were obtained at a constant value of $k_{H_2L/H}$, equal to 3.2 (Fig. 3).

Figure 3 shows that as the pH of the solution increases from 1.8 to 2.5, the concentration of Cu^{2+} cations in the polymer slightly increases from 0.87 to 0.93 mol/L. The concentration of $[CuL]^+$ cations remains constant at 0.1 mol/L. The concentration of H^+ decreases from 0.15 to 0.03 mol/L, while the concentration of $[H_2L]^+$ cations is almost zero in the above pH range. The ratio $C_{[CuL]^+} / C_{Cu^{2+}}$ in the polymer, equal to 0.11, remains unchanged. The ratio $C_{[CuL]^+} / C_{Cu^{2+}}$ in the polymer cannot be increased either by increasing the concentration of picolinic acid in solution because of the low solubility of its complexes, or by decreasing the concentration of copper nitrate in solution. The latter will lead to a decrease in the total concentration of Cu^{2+} and $[CuL]^+$ cations in the polymer due to an increase in the concentration of H^+. This is because the concentration of $[H_2L]^+$ cations is practically equal to zero, and the total capacity of the cationite is a constant value. This explains the choice of the concentration of picolinic acid and copper nitrate in solution (0.005 mol/L) in the experiment.

Experimental data on the concentrations of all cations in the cationite within the measurement errors fall within the intervals of calculated compositions (Fig. 3).

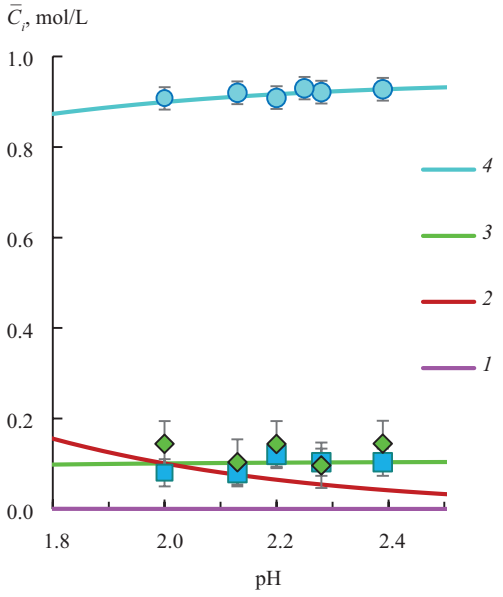

Fig. 3. Dependencies of cations concentration in the polymer on pH of the equilibrium solution: (*1*) $\bar{C}_{[H_2L]^+}$; (*2*) $\bar{C}_{H^+}$; (*3*) $\bar{C}_{[CuL]^+}$; (*4*) $\bar{C}_{Cu^{2+}}$. The lines are the calculations according to the system of equations (8), while the markers are the experiment. The concentrations of Cu^{2+} and $[CuL]^+$ cations in the polymer (blue circle and green rhombus) were obtained from data on the material balance of sorption processes. The concentration of $[CuL]^+$ cations in the polymer (blue square) was obtained from experimental data on the change of the concentration of Cu(II) in the polymer, taking into account the material balance according to the reaction $\overline{Cu^{2+}} + 2[CuL]^+ = 2\overline{[CuL]^+} + Cu^{2+}$

CONCLUSIONS

Thus, equilibrium reactions (1)–(7) do occur in multicomponent heterophase systems consisting of KU-2-8 sulfocationite and aqueous solutions of picolinic acid and copper nitrate. Consequently, it is possible to precalculate the equilibrium ionic compositions of the solution and KU-2-8 sulfocationite by the selectivity coefficients of binary ionic exchanges and the constants of formation of $[H_2L]^+$, $[CuL]^+$ complexes. It is probable that KU-2-8 sulphocationite can be considered as a container for the preparation of drugs based on picolinic acid and Cu^{2+} cations.

Acknowledgments

This work was performed as part of the State Task for the Institute of Coal Chemistry and Chemical Materials Science, project No. 121031500194-5.

Authors' contributions

H.N. Altshuler – development of the concept and management of scientific work, writing the text of the article.

V.N. Nekrasov – performing an experiment to determine the composition of phases, writing the text of the article.

S.Yu. Lyrshchikov – IR-Fourier spectroscopic study of the polymer phase.

O.H. Altshuler – calculation of equilibrium compositions of the sulfocationite and aqueous solutions, writing the text of the article.

The authors declare no conflicts of interest.

REFERENCES

1. Narui K., Noguchi N., Saito A., Kakimi K., Motomura N., Kubo K., Takamoto S., Sasatsu M. Anti-infectious activity of tryptophan metabolites in the L-triptophan – L-kynurenine pathway. *Biol. Pharm. Bull*. 2009;32(1):41–44. https://doi.org/10.1248/bpb.32.41
2. Stipanovic R.D., Wheeler M.H., Puckhaber L.S., Liu J., Bell A.A., Williams H.J. Nuclear magnetic resonance (NMR) studies on the biosynthesis of fusaric acid from *Fusarium oxysporum* f. sp. *vasinfectum*. *J. Agric. Food Chem.* 2011;59(10):5351–5356. https://doi.org/10.1021/jf200628r
3. Godin A.M., Ferreira W.C., Rocha L.T.S., Seniuk J.G.T., Paiva A.L.L., Merlo L.A., Nascimento E.B., Bastos L.F.S., Coelho M.M. Antinociceptive and anti-inflmmatory activites of nicotinamide and isomers in different experimental models. *Pharmacol. Biochem. Behav*. 2011;99(4):782–788. https://doi.org/10.1016/j.pbb.2011.07.003
4. Weder J.E., Dillon C.T., Hambley T.W., Kennedy B.J., Lay P.A., Biffin J.R., Regtop H.L., Davies N.M. Copper complexes of non-steroidal anti-inflammatory drugs: an opportunity yet to be realized. *Coord. Chem. Rev*. 2002;232(1–2):95–126. https://doi.org/10.1016/S0010-8545(02)00086-3
5. Iakovidis I., Delimaris I., Piperakis S.M. Copper and its complexes in medicine: a biochemical approach. *Mol. Biol. Int*. 2011;2011:594529. https://doi.org/10.4061/2011/594529
6. Himmelweit F. (Ed.) *The Collected Papers of Paul Ehrlich: in Four Volumes Including a Complete Bibliography*. London: Pergamon Press; 1960. P. 95.
7. Tarakhovskii Yu.S. *Intellektual'nye lipidnye nanokonteinery v adresnoi dostavke lekarstvennykh veshchestv* (*Smart Lipid Nanocontainers for Targeted Drug Delivery*). Moscow: URSS; 2011. 280 p. (in Russ.).
8. Lykoshin D.D., Zaitsev V.V., Kostromina M.A., Esipov R.S. New-generation osteoplastic materials based on biological and synthetic matrices. *Tonk. Khim. Tekhnol. = Fine Chem. Technol.* 2021;16(1):36–54 (Russ., Eng.). https://doi.org/10.32362/2410-6593-2021-16-1-36-54

СПИСОК ЛИТЕРАТУРЫ

1. Narui K., Noguchi N., Saito A., Kakimi K., Motomura N., Kubo K., Takamoto S., Sasatsu M. Anti-infectious activity of tryptophan metabolites in the L-triptophan – L-kynurenine pathway. *Biol. Pharm. Bull*. 2009;32(1):41–44. https://doi.org/10.1248/bpb.32.41
2. Stipanovic R.D., Wheeler M.H., Puckhaber L.S., Liu J., Bell A.A., Williams H.J. Nuclear magnetic resonance (NMR) studies on the biosynthesis of fusaric acid from *Fusarium oxysporum* f. sp. *vasinfectum*. *J. Agric. Food Chem.* 2011;59(10):5351–5356. https://doi.org/10.1021/jf200628r
3. Godin A.M., Ferreira W.C., Rocha L.T.S., Seniuk J.G.T., Paiva A.L.L., Merlo L.A., Nascimento E.B., Bastos L.F.S., Coelho M.M. Antinociceptive and anti-inflmmatory activites of nicotinamide and isomers in different experimental models. *Pharmacol. Biochem. Behav*. 2011;99(4):782–788. https://doi.org/10.1016/j.pbb.2011.07.003
4. Weder J.E., Dillon C.T., Hambley T.W., Kennedy B.J., Lay P.A., Biffin J.R., Regtop H.L., Davies N.M. Copper complexes of non-steroidal anti-inflammatory drugs: an opportunity yet to be realized. *Coord. Chem. Rev*. 2002;232(1–2):95–126. https://doi.org/10.1016/S0010-8545(02)00086-3
5. Iakovidis I., Delimaris I., Piperakis S.M. Copper and its complexes in medicine: a biochemical approach. *Mol. Biol. Int*. 2011;2011:594529. https://doi.org/10.4061/2011/594529
6. Himmelweit F. (Ed.) *The Collected Papers of Paul Ehrlich: in Four Volumes Including a Complete Bibliography*. London: Pergamon Press; 1960. P. 95.
7. Тараховский Ю.С. *Интеллектуальные липидные наноконтейнеры в адресной доставке лекарственных веществ*. М.: URRS; 2017. 280 с. ISBN 978-5-382-01752-5
8. Лыкошин Д.Д., Зайцев В.В., Костромина М.А., Есипов Р.С. Остеопластические материалы нового поколения на основе биологических и синтетических матриксов. *Тонкие химические технологии*. 2021;16(1):36–54. https://doi.org/10.32362/2410-6593-2021-16-1-36-54

9. Shkurenko G.Yu., Lyrshchikov S.Yu., Gorlov A.A., Al'tshuler O.G., Al'tshuler G.N. Immobilization of benzocaine in polymeric nanocontainers, pharmacokinetic modeling. *Pharm. Chem. J.* 2018;52(5):464–466. https://doi.org/10.1007/s11094-018-1840-3
[Original Russian Text: Shkurenko G.Yu., Lyrshchikov S.Yu., Gorlov A.A., Al'tshuler O.G., Al'tshuler G.N. Immobilization of benzocaine in polymeric nanocontainers, pharmacokinetic modeling. *Khimiko-Farmatsevticheskii Zhurnal.* 2018;52(5): 46–48 (in Russ.). https://doi.org/10.30906/0023-1134-2018-52-5-46-48]
10. *Ionity. Katalog* (*Ionites. Catalog*). Cherkassy: NIITEKhIM; 1980. 33 p. (in Russ.).
11. Altshuler H., Ostapova E., Altshuler O., Shkurenko G., Malyshenko N., Lyrschikov S., Parshkov R. Nicotinic acid in nanocontainers. Encapsulation and release from ion exchangers. *ADMET DMPK*. 2019;7(1):76–87. https://doi.org/10.5599/admet.626
12. Altshuler H.N., Malyshenko N.V., Nekrasov V.N., Altshuler O.H. Sorption of pyridine-3-carboxylic acid by the Dowex-50 sulfonic cation-exchange resin in the Ni^{II} and Cu^{II} forms. *Russ. Chem. Bull.* 2021;70(8):1421–1428. https://doi.org/10.1007/s11172-021-3235-y
[Original Russian Text: Altshuler H.N., Malyshenko N.V., Nekrasov V.N., Altshuler O.H. Sorption of pyridine-3-carboxylic acid by the Dowex-50 sulfonic cation-exchange resin in the Ni^{II} and Cu^{II} forms. *Izvestiya Akademii Nauk. Seriya Khimicheskaya.* 2021;(8):1421–1428 (in Russ.).]
13. Altshuler G.N., Shkurenko G.Yu., Nekrasov V.N., Altshuler O.G. Sorption of nicotinic and isonicotinic acids by Ag-containing sulfocationite KU-2–4. *Russ. J. Phys. Chem. A*. 2022;96(7): 1535–1540. https://doi.org/10.1134/S0036024422070032
[Original Russian Text: Altshuler G.N., Shkurenko G.Yu., Nekrasov V.N., Altshuler O.G. Sorption of nicotinic and isonicotinic acids by Ag-containing sulfocationite KU-2–4. *Zhurnal Fizicheskoi Khimii.* 2022;96(7):1062–1067 (in Russ.).]
14. Tamer O., Avcı D., Atalay Y. Synthesis, X-ray structure, spectroscopic characterization and nonlinear optical properties of Nickel (II) complex with picolinate: A combined experimental and theoretical study. *J. Mol. Struct*. 2015;1098(15):12–20. https://doi.org/10.1016/j.molstruc.2015.05.035
15. Koczon P., Dobrowolski J.Cz., Lewandowski W., Mazurekd A.P. Experimental and theoretical IR and Raman spectra of picolinic, nicotinic and isonicotinic acids. *J. Mol. Struct.* 2003;655(1): 89–95. https://doi.org/10.1016/S0022-2860(03)00247-3
16. Smith A. *Applied IR Spectroscopy: Fundamentals, Techniques, Analytical problem-solving:* transl. from Engl. Moscow: Mir; 1982. P. 301–308 (in Russ.).
[Smith A. *Applied IR Spectroscopy: Fundamentals, Techniques, Analytical problem-solving*. New York/Chichester/Brisbane/Toronto: John Wiley & Sons; 1979. 336 p.]
17. Nakanishi *K. Infrared Absorption Spectroscopy*: transl. from Engl. Moscow: Mir; 1965. P. 51–54 (in Russ.).
[Nakanishi *K. Infrared Absorption Spectroscopy.* San Francisco: Holden-Day; 1962. 216 p.]
18. Rajhi Y., Ju Y.-H., Angkawijaya A.E., Fazary A.E. Complex formation equilibria and molecular structure of divalent metal ions–vitamin B3–glycine oligopeptides systems. *J. Solution Chem*. 2013;42(12):2409–2442. https://doi.org/10.1007/s10953-013-0116-5
19. Ostapova E.V., Lyrshchikov S.Yu., Altshuler G.N. Equilibrium constants of pyridinecarboxylic acids sorption from aqueous solutions by DOWEX 50 cation exchangers. *Russ. J. Appl. Chem*. 2022;95(8):1223–1231. https://doi.org/10.1134/S1070427222080195
9. Шкуренко Г.Ю., Лырщиков С.Ю., Горлов А.А., Альтшулер О.Г., Альтшулер Г.Н. Иммобилизация бензокаина в полимерных наноконтейнерах. Моделирование фармакокинетики. *Хим.-фарм. журнал.* 2018;52(5):46–48. https://doi.org/10.30906/0023-1134-2018-52-5-46-48
10. *Иониты. Каталог*. Черкассы: НИИТЭХИМ; 1980. 33 с.
11. Altshuler H., Ostapova E., Altshuler O., Shkurenko G., Malyshenko N., Lyrschikov S., Parshkov R. Nicotinic acid in nanocontainers. Encapsulation and release from ion exchangers. *ADMET DMPK*. 2019;7(1):76–87. https://doi.org/10.5599/admet.626
12. Альтшулер Г.Н., Малышенко Н.В., Некрасов В.Н., Альтшулер О.Г. Сорбция пиридин-3-карбоновой кислоты сульфокатионитом Dowex-50 в Ni(II)- и Cu(II)-форме. *Известия Академии наук. Серия химическая*. 2021;(8):1421–1428.
13. Альтшулер Г.Н., Шкуренко Г.Ю., Некрасов В.Н., Альтшулер О.Г. Сорбция никотиновой и изоникотиновой кислот Ag-содержащим сульфокатионитом КУ-2-4. *Журн. физ. химии*. 2022;96(7):1062–1067.
14. Tamer O., Avcı D., Atalay Y. Synthesis, X-ray structure, spectroscopic characterization and nonlinear optical properties of Nickel (II) complex with picolinate: A combined experimental and theoretical study. *J. Mol. Struct*. 2015;1098(15):12–20. https://doi.org/10.1016/j.molstruc.2015.05.035
15. Koczon P., Dobrowolski J.Cz., Lewandowski W., Mazurekd A.P. Experimental and theoretical IR and Raman spectra of picolinic, nicotinic and isonicotinic acids. *J. Mol. Struct.* 2003;655(1): 89–95. https://doi.org/10.1016/S0022-2860(03)00247-3
16. Смит А. *Прикладная ИК-спектроскопия: Основы, техника, аналитическое применение*. М.: Мир; 1982. С. 301–308.
17. Наканиси К. *Инфракрасные спектры и строение органических соединений*. М.: Мир; 1965. С. 51–54.
18. Rajhi Y., Ju Y.-H., Angkawijaya A.E., Fazary A.E. Complex formation equilibria and molecular structure of divalent metal ions–vitamin B3–glycine oligopeptides systems. *J. Solution Chem*. 2013;42(12): 2409–2442. https://doi.org/10.1007/s10953-013-0116-5
19. Остапова Е.В., Лырщиков С.Ю., Альтшулер Г.Н. Константы равновесия сорбции пиридинкарбоновых кислот из водных растворов сульфокатионитами типа DOWEX 50. *Журн. прикл. химии*. 2022;95(8):1059–1067.
20. Bonner O.D., Smith L.L. The Effect of Temperature on Ion-exchange Equilibria. I. The Sodium–Hydrogen and Cupric–Hydrogen Exchanges. *J. Phys. Chem.* 1957;61(12): 1614–1617. https://doi.org/10.1021/j150558a009

[Original Russian Text: Ostapova E.V., Lyrshchikov S.Yu., Altshuler G.N. Equilibrium constants of pyridinecarboxylic acids sorption from aqueous solutions by DOWEX 50 cation exchangers. *Zhurnal Prikladnoi Khimii*. 2022;95(8):1059–1067 (in Russ.).]

20. Bonner O.D., Smith L.L. The Effect of Temperature on Ion-exchange Equilibria. I. The Sodium–Hydrogen and Cupric–Hydrogen Exchanges. *J. Phys. Chem.* 1957;61(12): 1614–1617. https://doi.org/10.1021/j150558a009

About the authors

Heinrich N. Altshuler, Dr. Sci. (Chem.), Professor, Chief Researcher, The Federal Research Center of Coal and Coal Chemistry of Siberian Branch of the Russian Academy of Sciences (18, Sovetskii pr., Kemerovo, 650000, Russia). E-mail: altshulerh@gmail.com. Scopus Author ID 7003773015, 7006601157, ResearcherID B-5132-2014, https://orcid.org/0000-0003-1733-7649

Vladimir N. Nekrasov, Postgraduate Student, The Federal Research Center of Coal and Coal Chemistry of Siberian Branch of the Russian Academy of Sciences (18, Sovetskii pr., Kemerovo, 650000, Russia). E-mail: graybadwolf@gmail.com. Scopus Author ID 57240889000, https://orcid.org/0000-0002-8479-1529

Sergey Yu. Lyrshchikov, Cand. Sci. (Chem.), Researcher, The Federal Research Center of Coal and Coal Chemistry of Siberian Branch of the Russian Academy of Sciences (18, Sovetskii pr., Kemerovo, 650000, Russia). E-mail: serstud@mail.ru. Scopus Author ID 54879375200, ResearcherID B-2673-2014, https://orcid.org/0000-0002-4570-7160

Olga H. Altshuler, Dr. Sci. (Chem.), Researcher, The Federal Research Center of Coal and Coal Chemistry of Siberian Branch of the Russian Academy of Sciences (18, Sovetskii pr., Kemerovo, 650000, Russia). E-mail: alt_og@bk.ru. Scopus Author ID 6507108263, ResearcherID B-5223-2014, https://orcid.org/0000-0001-7035-673X

Об авторах

Альтшулер Генрих Наумович, д.х.н., профессор, главный научный сотрудник, ФГБНУ «Федеральный исследовательский центр угля и углехимии Сибирского отделения Российской академии наук» (650000, Россия, г. Кемерово, пр-т Советский, д. 18). E-mail: altshulerh@gmail.com. Scopus Author ID 7003773015, 7006601157, ResearcherID B-5132-2014, https://orcid.org/0000-0003-1733-7649

Некрасов Владимир Николаевич, аспирант, ФГБНУ «Федеральный исследовательский центр угля и углехимии Сибирского отделения Российской академии наук» (650000, Россия, г. Кемерово, пр-т Советский, д. 18). E-mail: graybadwolf@gmail.com. Scopus Author ID 57240889000, https://orcid.org/0000-0002-8479-1529

Лырщиков Сергей Юрьевич, к.х.н., научный сотрудник, ФГБНУ «Федеральный исследовательский центр угля и углехимии Сибирского отделения Российской академии наук» (650000, Россия, г. Кемерово, пр-т Советский, д. 18). E-mail: serstud@mail.ru. Scopus Author ID 54879375200, ResearcherID B-2673-2014, https://orcid.org/0000-0002-4570-7160

Альтшулер Ольга Генриховна, д.х.н., научный сотрудник, ФГБНУ «Федеральный исследовательский центр угля и углехимии Сибирского отделения Российской академии наук» (650000, Россия, г. Кемерово, пр-т Советский, д. 18). E-mail: alt_og@bk.ru. Scopus Author ID 6507108263, ResearcherID B-5223-2014, https://orcid.org/0000-0001-7035-673X

Translated from Russian into English by H. Moshkov
Edited for English language and spelling by Dr. David Mossop

Tonkie Khimicheskie Tekhnologii = Fine Chemical Technologies.
2024;19(1):17–27 ISSN 2686-7575 (Online)

UDC 66.048.625
https://doi.org/10.32362/2410-6593-2024-19-1-17-27

RESEARCH ARTICLE

Effect of glucose–citric acid deep eutectic solvent on the vapor–liquid equilibrium of an aqueous ethanol solution

Alexander V. Klinov, Alina R. Khairullina ✉
Kazan National Research Technological University, Kazan, 420015 Republic of Tatarstan, Russia
✉ *Corresponding author, e-mail: khalina@kstu.ru*

Abstract

Objectives. To study the effect of a deep eutectic solvent (DES) based on glucose and citric acid on the vapor–liquid equilibrium of an aqueous solution of ethanol.

Methods. A qualitative and quantitative analysis of the conditions of vapor–liquid equilibrium in an ethanol–water–DES ternary mixture was performed based on the open evaporation method and the measurement of *TPxy* data using a Świętosławski ebulliometer. Since the volatility of the DES is negligible in comparison with that of water and ethanol, the composition of the vapor phase was measured by means of Karl Fischer titration. The conditions of vapor–liquid phase equilibrium were modeled using the UNIFAC model.

Results. The open evaporation method was used to determine the curves of residual concentrations for the ethanol–water–DES mixture at various DES concentrations and compositions (glucose–citric acid ratios). *TPxy* data was obtained for the mixture produced by adding 30 wt % DES to an aqueous solution of ethanol at atmospheric pressure. Studies show that DES based on glucose and citric acid has a significant effect on the relative volatility of ethanol in aqueous solution, leading to the disappearance of the azeotropic point. This effect is due to only the presence of glucose. Citric acid does not change the composition of the equilibrium phases, but rather increases the solubility of glucose in aqueous ethanol solutions. This is especially important at high ethanol concentrations, since glucose is poorly soluble in ethanol.

Conclusions. Addition of DES based on glucose and citric acid to an aqueous solution of ethanol leads to the disappearance of the azeotropic point. DES can thus be considered as a promising entrainer for extracting ethanol from aqueous solutions using extractive distillation. Modeling of the conditions of vapor–liquid equilibrium in the ethanol–water–DES system using the UNIFAC model showed a satisfactory level of accuracy. The error in the calculated data increases with increasing the glucose concentration, while remaining acceptable for practical use.

Keywords

vapor–liquid equilibrium, glucose, citric acid, ethanol–water mixture, glucose solubility

Submitted: 03.07.2023
Revised: 17.10.2023
Accepted: 19.01.2024

For citation

Klinov A.V., Khairullina A.R. Effect of glucose–citric acid deep eutectic solvent on the vapor–liquid equilibrium of an aqueous ethanol solution. *Tonk. Khim. Tekhnol. = Fine Chem. Technol.* 2024;19(1):17–27. https://doi.org/10.32362/2410-6593-2024-19-1-17-27

НАУЧНАЯ СТАТЬЯ

Влияние глубоко эвтектического растворителя глюкоза–лимонная кислота на парожидкостное равновесие водного раствора этанола

А.В. Клинов, А.Р. Хайруллина ✉

Казанский национальный исследовательский технологический университет, Казань, 420015 Республика Татарстан, Россия

✉ *Автор для переписки, e-mail: khalina@kstu.ru*

Аннотация

Цели. Исследовать влияние глубоко эвтектического растворителя (ГЭР) на основе глюкозы и лимонной кислоты на парожидкостное равновесие водного раствора этанола.

Методы. Для качественного и количественного анализа условий парожидкостного равновесия в трехкомпонентной смеси этанол–вода–ГЭР использовались метод открытого испарения и измерение *TPxy* данных в эбулиометре Свентославского. Так как летучесть ГЭР пренебрежимо мала по сравнению с летучестью воды и этанола, состав паровой фазы измерялся титрованием по методу Карла Фишера. Моделирование условий фазового парожидкостного равновесия проводилось на основе модели UNIFAC.

Результаты. Методом открытого испарения получены линии остаточных концентраций в смеси этанол–вода–ГЭР при разных концентрациях ГЭР и различном составе ГЭР (глюкоза–лимонная кислота). Получены *TPxy* данные при добавлении 30 мас. % ГЭР к водному раствору этанола при атмосферном давлении. Проведенные исследования показали, что ГЭР на основе глюкозы и лимонной кислоты оказывает существенное влияние на относительную летучесть этанола в водном растворе, что приводит к исчезновению азеотропной точки. Это влияние связано только с наличием глюкозы. Лимонная кислота не изменяет состава равновесных фаз, но позволяет увеличить растворимость глюкозы в водных растворах этанола. Это особенно важно при высоких концентрациях этанола, так как глюкоза плохо растворима в этаноле.

Выводы. Добавление ГЭР на основе глюкозы и лимонной кислоты к водному раствору этанола приводит к исчезновению азеотропной точки. Это позволяет рассматривать данный ГЭР в качестве перспективного экстрактивного агента для извлечения этанола из водных растворов с помощью экстрактивной ректификации. Моделирование условий парожидкостного равновесия в системе этанол–вода–ГЭР с использованием модели UNIFAC показали удовлетворительную точность. Ошибка расчетных данных возрастает с увеличением концентрации глюкозы, однако остается приемлемой для практического использования.

Ключевые слова

парожидкостное равновесие, глюкоза, лимонная кислота, этанол-вода, растворимость глюкозы

Поступила: 03.07.2023
Доработана: 17.10.2023
Принята в печать: 19.01.2024

Для цитирования

Клинов А.В., Хайруллина А.Р. Влияние глубоко эвтектического растворителя глюкоза–лимонная кислота на парожидкостное равновесие водного раствора этанола. *Тонкие химические технологии*. 2024;19(1):17–27. https://doi.org/10.32362/2410-6593-2024-19-1-17-27

INTRODUCTION

Ethanol is an important organic solvent. It is used in many industries: as a reactant in the synthesis of ethers and esters; a solvent in the paint and varnish industry; and as a raw material in the production of household chemicals, medicines, and food products. Ethanol is also one of the most commonly used biofuel components [1–3]. In industrial technologies, ethanol is often present in mixtures with water which are azeotropic. In this regard, the problem arises of separating these mixtures into individual substances.

The separation of azeotropic mixtures is an important requirement in many technological processes. It can be addressed by various methods including: overpressure or vacuum distillation; special distillation methods (azeotropic and extractive distillation)[1] [4];

[1] Hilmen E.K. *Separation of Azeotropic Ixtures: Tools for Nalysis and Tudies on Batch Distillation Operation*. PhD Thesis. Norwegian Univ. of Science and Technology; 2000. 288 p.

as well as membrane and extraction processes. At the present time, industrial technologies mainly use various distillation methods. For example, in extractive distillation, the mixture to be separated is supplemented with an additional component, or entrainer, which changes the relative volatility of the components of the mixture by interacting with them. The selection of the optimal entrainer from both economic and environmental points of view is an important stage in the development of this technology [5].

Today, four classes of entrainers for separating ethanol–water mixtures exist: organic solvents, solid salts, mixtures of organic solvents with solid salts, and ionic liquids (ILs). Organic solvents used as entrainers may remain in the ethanol obtained, thereby contaminating it. ILs are more environmentally friendly (green) solvents and a promising alternative to conventional organic solvents [6]. The disadvantage of ILs is the complexity of synthesis and separation of the target component with the required purity, thus determining the high cost of the product. Therefore, the search for alternative solvents for the separation of azeotropic mixtures is a challenge. At the present time, research has begun on the use of deep eutectic solvents (DESs) as entrainers. DESs are a new class of environmentally friendly solvents which have many properties similar to ILs [7, 8]. The main advantages of DESs when compared to ILs are the ease of preparation and, as a consequence, their low cost. They also possess the ability to vary the physicochemical properties depending on the nature of the components, their molar ratio, and water content. DESs have virtually zero vapor pressure and are viscous liquids. By increasing the temperature or adding a small amount of water, the viscosity of DESs can be significantly reduced [9–11].

DESs are obtained by mixing two or more components, some of which act as hydrogen bond donors, while others act as hydrogen bond acceptors. The resultant eutectic mixture has a melting point lower than the melting point of pure components [9, 10]. The eutectic point of a mixture is reached at the molar ratio of the mixture components at which the melting point is the lowest[2]. A striking example of a eutectic mixture is the combination of choline chloride and urea. They are solids at room temperature, but when mixed in a certain ratio, they form a liquid solution [12].

In this work, glucose-containing mixtures were studied as DESs for the separation of an ethanol–water mixture.

Glucose, or dextrose (D-glucose), $C_6H_{12}O_6$, is an organic compound. It is a monosaccharide, one of the most common sources of energy in living organisms: a C_6 sugar containing six carbon atoms, an aldehyde group, and five hydroxyl groups [13]. The large number of hydroxyl groups leads to the significant effect of glucose on the relative volatility of the components of an ethanol–water mixture. This gives grounds to consider glucose as an efficient entrainer for the extractive distillation of an ethanol–water mixture. At the same time, glucose under normal conditions is in a solid state and is slightly soluble in ethanol. These circumstances limit the possibility of using glucose as an entrainer. The purpose of this work is to show that the use of the properties of glucose as an entrainer for an ethanol–water azeotropic mixture is possible in its DES with citric acid (CA).

SYNTHESIS OF DES FROM GLUCOSE WITH CA

In order to prepare a DES, glucose monohydrate (*LenReaktiv*, Russia) with a water content of 9.12 wt % was mixed with CA monohydrate (*LenReaktiv*, Russia) with a water content of 8.34 wt % in a round-bottomed flask. This was placed in a thermostated medium of silicone oil (*Solins*, Russia) and continuously rotated. The mixing process was carried out for 2 h until a yellow homogeneous liquid was formed [14]. The temperature of the thermostated medium was maintained at 85–95°C, depending on the ratio of the components. The studies showed that a DES in the liquid phase is formed at various molar ratios of components. In our experiments, the components (glucose and CA) were mixed in the following molar ratio: 0.25 : 0.75; 1 : 1; 0.75 : 0.25; and 0.90 : 0.10. At all ratios, the mixture was in the liquid state. Since the monohydrates were mixed, the water content in the resulting DES was about 9 wt %. An attempt to remove water from the mixture by evaporating it under vacuum resulted in caramelization.

The synthesized DES was stored in glass bottles in a desiccator.

EXPERIMENTAL

In order to assess the effect of the DES mixture on the relative volatility of ethanol in solutions, data on the vapor–liquid phase equilibrium (VLE) in the ethanol–water–DES ternary system is required. The VLE was studied by means of the open evaporation method and the measurement of *TPxy*[3] data using a Świętosławski ebulliometer [15]. In comparison with other methods

[2] Harris R.C. *Physical Properties of Alcohol Based Deep Eutectic Solvents*. PhD Thesis. University of Leicester; 2009. 188 p.

[3] *T* is temperature, *P* is pressure, *x* is the concentration of the volatile component in the liquid phase, and *y* is the concentration of the volatile component in the vapor phase.

of measuring equilibrium, the open evaporation method is less labor-intensive and enables the rapid qualitative and quantitative assessment of the effect of adding solvents on the conditions of phase equilibrium in an azeotropic mixture in a certain concentration range [16]. The experimental setup and experimental procedure have previously been described in detail [17–19]. Based on the results of the experiment, the dependence of the composition x of the boiling mixture on its weight L (curve of residual concentration [19]) was calculated according to the following material balance equation:

$$x_i = \frac{\left(L_0 - \sum_{k=1}^{i-1} D_k\right) x_{i-1} + D_i y_i}{L_0 - \sum_{k=1}^{i} D_k} = \frac{\left(1 - \sum_{k=1}^{i-1} e_k\right) x_{i-1} + e_i y_i}{1 - \sum_{k=1}^{i} e_k}, \quad i = 1 \ldots n, \tag{1}$$

where L_0 and x_0 (at $I = 1$, $x_0 = x_{i-1}$) are the initial weight of the mixture and its initial composition (mass fractions); D_i and D_k are the weights of the ith and kth samples of the distillate, respectively; y_i is the composition of the distillate (mass fractions); n is the number of samples of the distillate; and $e_i = \frac{D_i}{L_0}$ and $e_k = \frac{D_k}{L_0}$ are the relative weights of the ith and kth samples of the distillate, respectively.

Since the volatility of the DES can be neglected, the distillate contains only volatile components. In our case, these are ethanol and water. Therefore, for the convenience of analyzing the results, x and L were taken to be the mass fraction of ethanol in the mixture and the mass of the boiling mixture without taking into the DES into account.

TPxy data in the mixture with DES were measured using a Świętosławski ebulliometer (*Khimlaborpribor*, Russia) [15] (Fig. 1). The temperature was measured with an LT-300-N electronic thermometer (*Termeks*, Russia) with an error of ±0.05°C. The thermometer was installed into pocket *3* filled with electrocorundum. The initial mixture was poured into boiler *1* through condenser *5*. The test mixture was heated with a flexible electric heater wrapped around the outer surface of boiler *1*. The mixture was brought to the boil and maintained for 2.5 h, in order to reach equilibrium of the system. At the same time, samples of the vapor phase were taken, in order to refine the composition of distillate *6*, Samples of the liquid phase were taken, in order to refine the composition of the boiling mixture from the bottom of overflow tube *7*.

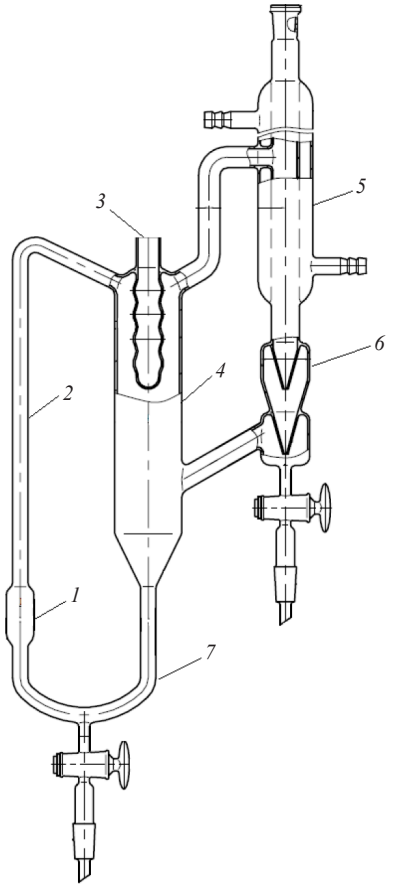

Fig. 1. Świętosławski ebulliometer:
(*1*) boiler,
(*2*) Cottrell pump,
(*3*) thermometer pocket,
(*4*) separation space,
(*5*) condenser,
(*6*) drop counter, and
(*7*) overflow tube [15]

The reliability of the results obtained using this experimental setup was checked by comparing the *TPxy* data on the ethanol–water binary system at an atmospheric pressure of 760 mmHg with experimental results from literature sources in the work [17].

The water content in the initial reagents and in the selected samples of the distillate and the liquid phase from the boiler was determined using a V20 Compact Karl Fischer volumetric titrator (*MettlerToledo*, USA) by means of the Karl Fischer method (with a relative measurement error of ±3%).

MODELING OF THE CONDITIONS OF VAPOR–LIQUID PHASE EQUILIBRIUM

Mathematically, the process of open evaporation of a binary mixture is described by means of the following differential equation:

$$(\bar{e} - 1)\frac{d\bar{x}}{d\bar{e}} = \bar{y}^*(\bar{x}) - \bar{x}, \tag{2}$$

where $\bar{x}$ [4] and $\bar{y}^*$ is the liquid composition and its equilibrium vapor composition (mole fractions), respectively; $\bar{e}$ is the mole fraction of the distillate. The VLE condition at moderate pressures has the following form:

$$\bar{y}^* = \frac{P^S(T)\bar{x}\gamma(x,T)}{P}, \quad (3)$$

where P^S and γ are the saturated vapor pressure of the pure component and its activity coefficient in the mixture respectively, while P is the pressure in the system.

By solving Eq. (2) simultaneously with the equilibrium model $\bar{y}^* = f(\bar{x},T,P)$, curves of residual concentrations can be calculated. These are experimentally determined using Eq. (1).

The equilibrium distribution of components between the vapor and liquid phases is often characterized by relative volatility:

$$\alpha = \frac{\bar{y}(1-\bar{x})}{\bar{x}(1-\bar{y})}. \quad (4)$$

Given the assumption that α = const, which is acceptable, then if during the open evaporation process, the concentrations in the liquid phase vary within a narrow range, the equilibrium condition (3) takes the following form:

$$\bar{y}^* = \frac{\alpha\bar{x}}{1+(\alpha-1)\bar{x}}. \quad (5)$$

The substitution of condition (5) into Eq. (2) gives the following solution:

$$\bar{e} = 1 - \left[\frac{\bar{x}}{\bar{x}_0}\left(\frac{1-\bar{x}_0}{1-\bar{x}}\right)^{\alpha}\right]^{\frac{1}{\alpha-1}}, \quad (6)$$

where $\bar{x}_0$ is the composition of the initial mixture.

By comparing solution (6) with experimental data on the curves of residual concentrations (1), the relative volatilities of ethanol and water after adding a certain amount of the DES can be determined. Thus, based on the results of the open evaporation method, the effect of the DES on the relative volatility of the components of the mixture being separated can be quantified. For the needs of such a comparison, in solution (6), the molar concentrations need to converted into mass concentrations, taking into account that $\bar{e} = e\frac{M(\bar{x})}{M(\bar{x}_0)}$, where M is the molecular mass of the mixture.

The *TPxy* phase equilibrium conditions in the ethanol–water–DES ternary system were modeled using the UNIFAC model[5] [20]. In this case, the activity coefficients are calculated from the parameters of group components of the molecules of the mixture.

The UNIFAC model divides molecules of substances into group components. The logarithm $\ln\gamma_i$ of the activity coefficient of the ith component is the sum of the combinatorial component $\ln\gamma_i^C$ and the residual component $\ln\gamma_i^R$:

$$\ln\gamma_i = \ln\gamma_i^C + \ln\gamma_i^R, \quad (7)$$

which characterize the differences in the sizes of molecules and in the energies on intermolecular interactions, respectively.

In order to determine the combinatorial contribution to the activity coefficient, data needs to entered regarding the parameters of the group volume R and group surface area Q. This data is related to the van der Waals group volume V_k and the surface area A_k of the kth functional group [20, 21]:

$$R_k = \frac{V_k}{15.17}, \quad (8)$$

$$Q_k = \frac{A_k}{2.5\cdot10^9}. \quad (9)$$

The residual (energy) component of the activity coefficient in group models is represented by the sum of group contributions, characterized by the group interaction parameter a_{mn}:

$$\psi_{mn} = \exp\left(\frac{-a_{mn}}{T}\right). \quad (10)$$

The energy group parameter a_{mn} shows the difference in the energies of interactions of groups n–m and m–n. Each of the group–group interactions is described by two parameters, a_{mn} and a_{nm}.

The UNIFAC model distinguishes between main groups and subgroups. The subgroups of a main group are energetically identical: i.e., they have the same energy parameters of interaction with other groups

[4] In this article, a lowercase variable with an overline is mole fraction, a lowercase variable without an overline is mass fraction.

[5] UNIFAC stands for UNIQUAC (**uni**versal **qua**si**c**hemical) Functional-group Activity Coefficients, a semi-empirical system for the prediction of nonelectrolyte activity in nonideal mixtures.

and differ only in geometric characteristics. For example, one main group CH_2 includes subgroups CH_3, CH_2, CH, and C of aliphatic hydrocarbons, and so on.

Forwater molecules and various alcohols, such a partition has already been proposed in the UNIFAC model [20]. The partitions of glucose and CA molecules (Table 1) were taken from the most complete database of group interaction parameters for the UNIFAC model in the form of UNIFAC Matrix 2020, as presented in the Dortmund Data Bank[6]. Thus, glucose consists of the following subgroups: CH_2, 2; C, 1; OH, 1; and COOH, 3. CA consists of the following subgroups: CH_2, 1; CH, 4; OH, 5; and CHO, 1. Table 1 presents the group interaction parameters.

The conformity of the UNIFAC model with the parameters shown in Table 1 was verified by comparing calculated and available experimental data. In the case of an ethanol–water mixture, a satisfactory level of accuracy has previously been shown [17]. With regard to aqueous solutions of glucose and CA, Fig. 2 presents the calculated and experimental [22–24] concentration dependences of boiling points. The average error for the glucose–water mixture was 0.35%, and for the CA–water mixture was 5.2%. This indicates a satisfactory level of accuracy. In addition, Figs. 3 and 4 show the experimental curves of residual concentrations calculated using Eq. (2) for the ethanol–water–DES mixture, the agreement of which is also satisfactory.

Table 1. Group interaction parameters a_{mn}, K

Substance	Formula
D-Glucose	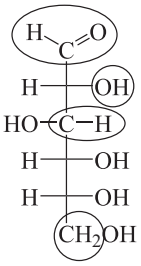
CA	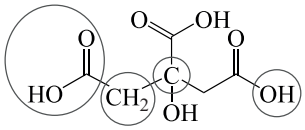
Ethanol	
Water	

n \ *m*	CH_2	COOH	CHO	OH	H_2O
CH_2	–	315.3	505.7	156.4	300
COOH	663.5	–	497.5	199	−14.09
CHO	677	−165.5	–	−203.6	−116
OH	986.5	−151	529	–	−229.1
H_2O	1318	−66.17	480.8	353.5	–

Note: *n* and *m* are group interaction parameters.

6 https://www.ddbst.com/ddb-search.html. Accessed July 03, 2023.

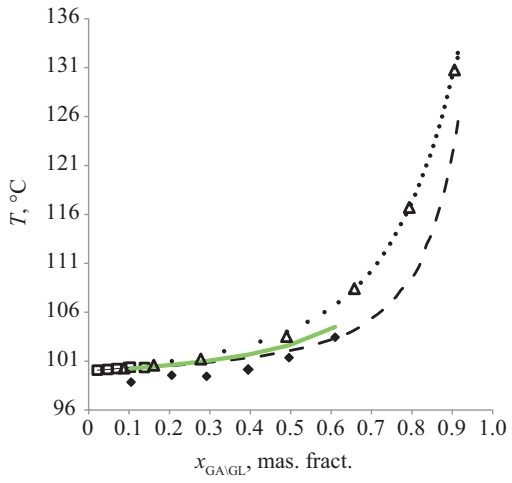

Fig. 2. Boiling points of aqueous solutions of glucose and CA. Glucose–water system (P = 93.6 kPa). The solid line represents the results of calculation using the UNIFAC model. The diamonds represent the experimental data [22]. CA–water system (P = 101.3 kPa). The dotted line represents the results of calculation using the UNIFAC model. The experimental data is represented by the bullets, squares [23], and triangles [24]

Solubility of DES components in aqueous ethanol solutions

Data on the solubility of glucose in water, ethanol, and their solutions, depending on temperature is available in the literature [25, 26]. The solubility of glucose in water increases linearly with increasing temperature, regardless of ethanol concentration. However, this solubility decreases with increasing ethanol concentration. Thus, the solubility of glucose in water equals 74.1 g glucose/100 g mixture at 60°C, while the solubility of glucose in an 80 wt % aqueous ethanol solution equals 36.2 and 4.2 g glucose/100 g mixture at 60 and 20°C, respectively [25].

Such low solubility of glucose in ethanol does not allow it to be used in its pure form, in order to break up the azeotrope of an ethanol–water mixture.

This work offers an assessment of the changes in the solubility of glucose in an aqueous solution of ethanol in the form of DES in various ratios with CA at 20°C. Solutions at two concentrations of ethanol in water, 80 and 70 wt %, were studied. The solutions were prepared at a given ethanol concentration and various glucoses content by dissolving DES in molar ratios of glucose to CA of 50 : 50, 75 : 25, and 90 : 10. The glucose concentration varied in increments from the solubility concentration of pure glucose to its fivefold value. For example, for the 80 wt % aqueous solution of ethanol, solutions with glucose concentrations of 4, 8, 12, 16, and 20 wt % were prepared. Next, the prepared solutions were heated to 60°C in sealed containers using a magnetic stirrer. The temperature was controlled by a temperature sensor. After complete dissolution, the solutions were cooled to a temperature of 20°C and left for several days. Solubility was determined by the presence or absence of a white crystalline phase in solutions. The studies showed that the use of glucose in the form of DES together with CA enables its solubility to be almost tripled. The effect of the amount of CA was detected only for the 90 : 10 DES (10 mol % CA). In this case, the solubility doubles.

RESULTS AND DISCUSSION

Since the DES consists of two components, one of which (CA) is highly soluble in an ethanol–water mixture, the effect of CA on the VLE of this mixture was studied. The experimental results obtained using the open evaporation method (Fig. 3) and the ebulliometrically measured compositions of the equilibrium phases showed an insignificant effect of CA on the relative volatility of the components of the ethanol–water mixture. Figure 3 demonstrates the curves of residual concentrations after adding 60 wt % CA monohydrate to an aqueous ethanol solution. In its absence they coincide.

The curves of residual concentrations calculated using Eq. (2) and the UNIFAC model also predict an insignificant, although slightly greater in comparison with the experimental data, effect of CA on the volatility of water and ethanol.

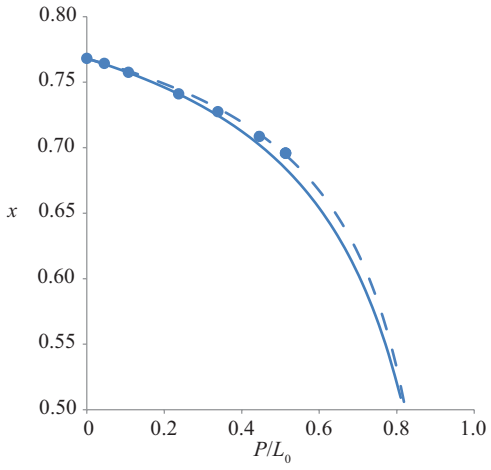

Fig. 3. Curves of residual concentrations of an ethanol–water mixture after adding 60 wt % CA. P is the mass of the ith portion of the distillate P_i; L_0 is the initial mass of the mixture. The points represent experimental data; the solid line, the results of calculation using the UNIFAC model; and the dotted line, the results of calculation without CA

Next, the effect of DES on the relative volatility of ethanol in aqueous solution was studied. Figure 4 illustrates the effect of DES added in an amount of 60 wt % at various glucose and CA contents.

The behavior of the curves of residual concentrations shows that the addition of the DES (Fig. 4) increases the relative volatility of ethanol. This leads to its more rapid depletion in the boiler due to the disappearance of the azeotropic point. Increase in the concentration of glucose in the mixture leads to an increase in the relative volatility of ethanol. Table 2 presents the relative volatilities calculated by comparing formulas (6) and (1). In comparison with the ethanol–water binary mixture, the addition of DES almost doubles the volatility.

Table 2. Relative volatility of ethanol in an aqueous solution with the addition of DES

Glucose : CA ratio	α
0 : 1	2.0
25 : 75	2.6
50 : 50	2.9
75 : 25	3.0
90 : 10	3.7

Note: α is the relative volatility determined using Eq. (4).

Figure 4 also shows the curves of residual concentrations calculated using Eq. (6) and the UNIFAC model. Discrepancy with the experimental data increases with increased glucose concentration. Since the UNIFAC model satisfactorily describes the VLE in aqueous solutions of glucose (Fig. 4), the discrepancy is most likely due to an error in the description of the energy of interaction of ethanol with glucose.

In this work, *TPxy* data on the ethanol–water system was obtained. The addition of 30 wt % DES in a molar ratio of glucose and CA of 50 : 50 (Figs. 5, 6, and Table 3) leads to the disappearance of the azeotropic point. In this case, the equilibrium compositions of the phases are noticeably affected in the range of ethanol concentrations above 50%. The *TPxy* dependencies calculated using the UNIFAC model showed a satisfactory level of accuracy. Figure 6 also presents the compositions of equilibrium phases after adding 30 wt % CA, coinciding with the data in its absence. This confirms the previously made conclusion about the weak influence of CA on the relative volatility of the components in the ethanol–water mixture.

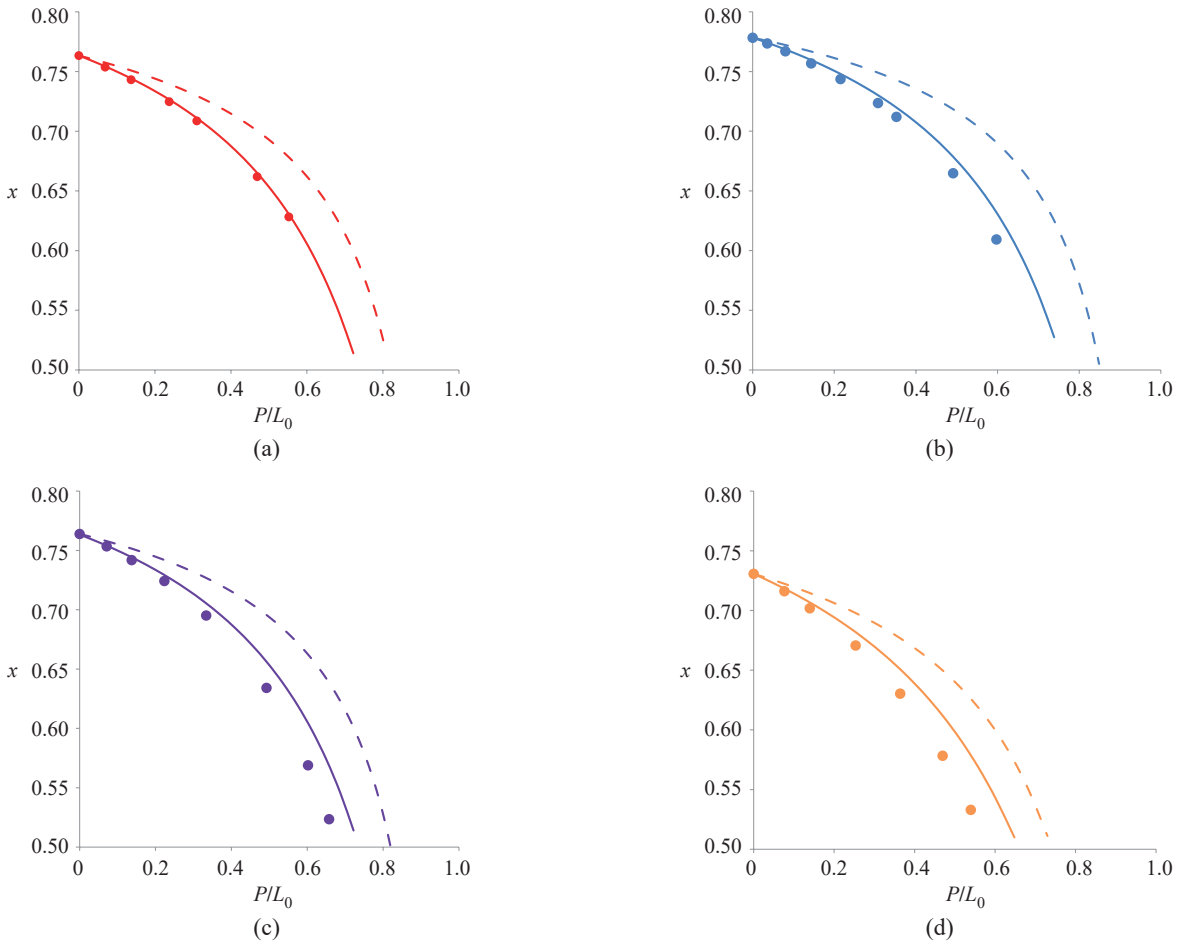

Fig. 4. Curves of residual concentrations of an ethanol–water mixture after adding 60 wt % DES at various ratios of glucose and CA, mol %: (a) 25 : 75, (b) 50 : 50, (c) 75 : 25, and (d) 90 : 10. The points represent experimental data; the solid line, the results of calculation using the UNIFAC model; and the dotted line, the results of calculation without the DES

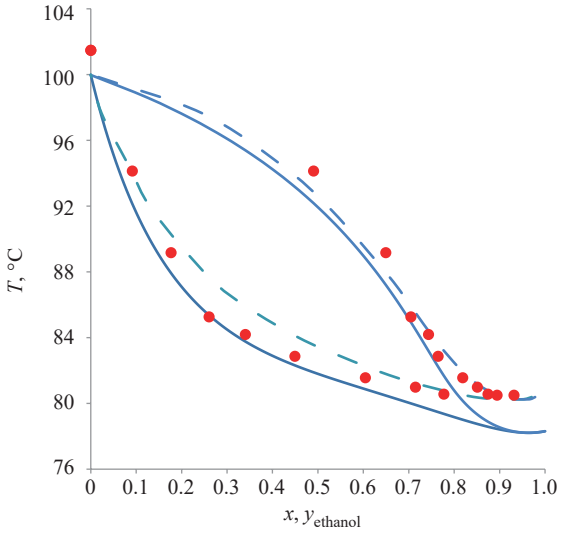

Fig. 5. Phase diagram of the ethanol–water–DES ternary mixture at an atmospheric pressure of 760 mm Hg. The solid line represents the data on the ethanol–water binary mixture; the points, experimental data; and the dotted line, the results of calculation using the UNIFAC model (30 wt % DES)

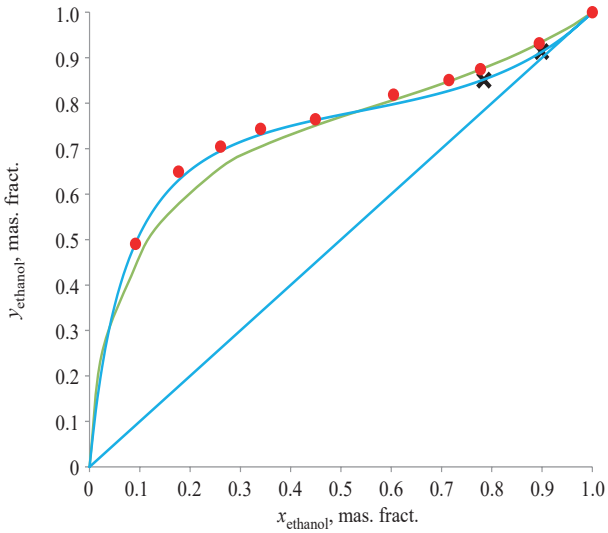

Fig. 6. Liquid–vapor equilibrium in the ethanol–water–DES system at an atmospheric pressure of 760 mm Hg. The blue line represents the data on the binary mixture; the bullets, on the mixture containing 30 wt % DES; and the crosses, on the mixture containing 30 wt % CA. The green line represents the results of calculation using the UNIFAC model

Table 3. Experimental data

T, °C	Mass fraction $x_{ethanol}$	Mass fraction $y_{ethanol}$	α	α (without DES)
80.49	0.8945	0.9315	1.60	1.21
80.55	0.7773	0.8746	1.99	1.66
80.98	0.7145	0.8510	2.28	1.91
81.55	0.6043	0.8189	2.96	2.49
82.86	0.4493	0.7645	3.97	3.81
84.19	0.3401	0.7436	5.62	5.11
85.26	0.2604	0.7046	6.77	6.47
89.17	0.1767	0.6493	8.62	8.54
94.13	0.0913	0.4905	9.57	10.99

Note: $x_{ethanol}$ and $y_{ethanol}$ are the ethanol concentrations in the liquid and vapor phases, respectively.

CONCLUSIONS

The studies showed that DES based on glucose and CA has a significant effect on the relative volatility of ethanol in an aqueous solution. This effect is due to only the presence of glucose. CA does not change the composition of equilibrium phases but increases the solubility of glucose in aqueous ethanol solutions. This is especially important at high ethanol concentrations, since glucose is poorly soluble in ethanol. In order to assess the effect of the amount of CA on glucose solubility, the composition of the DES varied from 25 to 90 mol % glucose. However, no such dependence was detected in this concentration range. In most probability, this is not strong.

The *TPxy* data obtained after adding 30 wt % DES to an aqueous solution of ethanol showed the disappearance of the azeotropic point. This allows us to consider DES based on glucose and CA as a promising entrainer for extracting ethanol from aqueous solutions from both environmental and economic points of view. Modeling of the experimental data on VLE using the UNIFAC model showed a satisfactory level of agreement. The error in the calculated data increases with increasing glucose concentration while remaining acceptable for practical use.

Authors' contributions

A.V. Klinov – guidance and scientific advice, analysis of research materials.

A.R. Khairullina – conducting research, analysis of research materials.

The authors declare no conflicts of interest.

REFERENCES

1. Xu K.X. *Handbook of Fine Organic Chemical Raw Materials and Intermediates*, 2nd ed. Beijing, China: Chemical Industry Press; 2002.
2. Mahdi T., Ahmad A., Nasef M.M., Ripin A. State-of-the-Art Technologies for Separation of Azeotropic Mixtures. *Sep. Purif. Rev*. 2014;44(4):308–330. https://doi.org/10.1080/15422119.2014.963607
3. Bajpai P. *Developments in Bioethanol. Green Energy and Technology*. Springer; 2021. 222 p. https://doi.org/10.1007/978-981-15-8779-5
4. Lei Z., Chen B., Ding Z. *Special Distillation Processes*. Elsevier; 2005. 370 p.
5. Laroche L., Andersen H.W., Morari M., Bekiaris N. Homogeneous azeotropic distillation: Comparing entrainers. *The Canadian J. Chem. Eng*. 1991;69(6):1302–1319. https://doi.org/10.1002/cjce.5450690611
6. Pereiro A.B., Araújo J.M.M., Esperança J.M.S.S., Marrucho I.M., Rebelo L.P.N. Ionic liquids in separations of azeotropic systems – A review. *J. Chem. Thermodyn*. 2012;46:2–28. https://doi.org/10.1016/j.jct.2011.05.026
7. Abbott A.P., Capper G., Davies D.L., Rasheed R.K., Tambyrajah V. Novel solvent properties of choline chloride/urea mixtures. *Chem. Commun*. 2002;(1):70–71. https://doi.org/10.1039/B210714G
8. Abbott A.P., Boothby D., Capper G., Davies D.L., Rasheed R.K. Deep Eutectic Solvents Formed between Choline Chloride and Carboxylic Acids: Versatile Alternatives to Ionic Liquids. *J. Am. Chem. Soc.* 2004;126(29):9142–9147. https://doi.org/10.1021/ja048266j
9. Neubauer M., Wallek N., Lux S. Deep eutectic solvents as entrainers in extractive distillation – A review. *Chem. Eng. Res. Des*. 2022;184:402–418. https://doi.org/10.1016/j.cherd.2022.06.019
10. Hansen B.B., Spittle S., Chen B., Poe D., Zhang Y., Klein J.M., *et al*. Deep Eutectic Solvents: A Review of Fundamentals and Applications. *Chem. Rev*. 2021;121(3):1232–1285. https://doi.org/10.1021/acs.chemrev.0c00385
11. Smith E.L., Abbott A.P., Ryder K.S. Deep Eutectic Solvents (DESs) and Their Applications. *Chem. Rev*. 2014;114(21):11060–11082. https://doi.org/10.1021/cr300162p
12. Paiva A., Craveiro R., Aroso I., Martins M., Reis R.L., Duarte A.R.C. Natural deep eutectic solvents – solvents for the 21st century. *ACS Sustain. Chem. Eng*. 2014;2(5):1063–1071. https://doi.org/10.1021/sc500096j
13. Stepanenko B.N., Gorodetsky V.K., Kovalev G.V. (farm.). Glucose. In: Petrovsky B.V. (Ed.). *Bol'shaya meditsinskaya entsiklopediya* (*Big Medical Encyclopedia*): in 30 v. V. 6. Moscow: Sov. Entsiklopediya; 1977.
14. Troter D.Z., Zlatkovic M., Đokić-Stojanović D.R. Konstantinović S.S., Todorović Z.B. Citric acid-based deep eutectic solvents: Physical properties and their use as cosolvents in sulphuric acid-catalysed ethanolysis of oleic acid. *Adv. Technol*. 2016;5(1):53–65. https://doi.org/10.5937/savteh1601053T
15. Świetoslawski W. *Azeotropy and Polyazeotropy*. NY, USA: Macmillan Company; 1963. 226 p.
16. Gmehling J., Kleiber M., Kolbe B., Rarey J. *Chemical Thermodynamics for Process Simulation*. WILEY-VCH; 2019. 808 p.
17. Davletbaeva I.M., Klinov A.V., Khairullina A.R., *et al*. Organoboron ionic liquids as extractants for distillation process of binary ethanol+ water mixtures. *Processes*. 2020;8(5):628. https://doi.org/10.3390/pr8050628
18. Klinov A.V., Malygin A.V., Khairullina A.R., *et al*. Alcohol Dehydration by Extractive Distillation with Use of Aminoethers of Boric Acid. *Processes*. 2020;8(11):1466. https://doi.org/10.3390/pr8111466
19. Davletbaeva I.M., Klinov A.V., Khairullina A.R., *et al*. Vapor–Liquid Equilibrium in Binary and Ternary Azeotropic Solutions Acetonitrile-Ethanol-Water with the Addition of Amino Esters of Boric Acid. *Processes*. 2022;10(10):2125. https://doi.org/10.3390/pr10102125
20. Reid R.C., Prausnitz J.M., Poling B.E. *The Properties of Gases and Liquids*. McGraw-Hill Publisher; 1987. 753 p.
21. Abrams D.S., Prausnitz J.M. Statistical thermodynamics of liquid mixtures: A new expression for the excess Gibbs energy of partly or completely miscible systems. *AIChE J*. 1975;21(1):116–128. https://doi.org/10.1002/aic.690210115

22. Maximo G.J., Meirelles A.J.A., Batista E.A.C. Boiling point of aqueous D-glucose and D-fructose solutions: Experimental determination and modeling with group-contribution method. *Fluid Phase Equilib*. 2010;299(1):32–41. https://doi.org/10.1016/j.fluid.2010.08.018
23. Timmermans J. *The Physico-Chemical Constants of Binary Systems in Concentrated Solutions.* V. IV. *Systems with Inorganic + Organic or Inorganic Compounds* (*Excepting Metallic Derivatives*). NY: Interscience Publishers; 1960. 1347 p.
24. Hall R.E., Sherill M.S. Freezing point lowering of aqueous solutions. In: Washburn E.W. (Ed.). *International Critical Tables of Numerical Data Physics. Chemistry and Technology*. V. IV. NY: McGraw-Hill; 1926.
25. Alves L.A., Almeida e Silva J.B., Giulietti M. Solubility of d-Glucose in Water and Ethanol/Water Mixtures. *J. Chem. Eng. Data*. 2007;52(6):2166–2170. https://doi.org/10.1021/je700177n
26. Bockstanz J.G.L., Buffa M., Lira C.T. Solubility of anhydrous-glucose in ethanol/water mixture. *J. Chem. Eng. Data*. 1989;34(4):426–429. https://doi.org/10.1021/je00058a016

About the authors

Alexander V. Klinov, Dr. Sci. (Eng.), Professor, Head of the Chemical Process Engineering Department, Kazan National Research Technological University (68, Karla Marksa ul., Kazan, 420015, Russia). E-mail: alklin@kstu.ru. Scopus Author ID 36907475500, ResearcherID K-8270-2017, RSCI SPIN-code 2116-4141, https://orcid.org/0000-0002-7833-8330

Alina R. Khairullina, Cand. Sci. (Eng.), Assistant, Chemical Process Engineering Department, Kazan National Research Technological University (68, Karla Marksa ul., Kazan, 420015, Russia). E-mail: khalina@kstu.ru. Scopus Author ID 57278592000, RSCI SPIN-code 4262-7100, https://orcid.org/0000-0003-3789-5904

Об авторах

Клинов Александр Вячеславович, д.т.н., зав. кафедрой процессов и аппаратов химической технологии, ФГБОУ ВО «Казанский национальный исследовательский технологический университет» (420015, Россия, Казань, ул. Карла Маркса, д. 68). E-mail: alklin@kstu.ru. Scopus Author ID 36907475500, ResearcherID K-8270-2017, SPIN-код РИНЦ 2116-4141, https://orcid.org/0000-0002-7833-8330

Хайруллина Алина Ришатовна, к.т.н., ассистент кафедры процессов и аппаратов химической технологии, ФГБОУ ВО «Казанский национальный исследовательский технологический университет» (420015, Россия, Казань, ул. Карла Маркса, д. 68). E-mail: khalina@kstu.ru. Scopus Author ID 57278592000, SPIN-код РИНЦ 4262-7100, https://orcid.org/0000-0003-3789-5904

Translated from Russian into English by V. Glyanchenko
Edited for English language and spelling by Dr. David Mossop

Tonkie Khimicheskie Tekhnologii = Fine Chemical Technologies.
2024;19(1):28–38 ISSN 2686-7575 (Online)

UDC 661.11+547.326
https://doi.org/10.32362/2410-6593-2024-19-1-28-38

RESEARCH ARTICLE

Kinetic regularities of neopentyl glycol esterification with acetic and 2-ethylhexanoic acids

D.S. Chicheva, E.L. Krasnykh✉, V.A. Shakun
Samara State Technical University, Samara, 443100 Russia
✉ *Corresponding author, e-mail: kinterm@samgu.ru*

Abstract

Objectives. Development of a domestic technology for producing environmentally friendly non-phthalate plasticizers, lubricants and transformer fluids based on neopentyl glycol (NPG), an oxo-synthesis product.

Methods. The methodology of the work was to study the kinetic laws of NPG esterification with acetic and 2-ethylhexanoic acids under self-catalysis conditions with an 8-fold molar excess of monocarboxylic acids. The production of NPG esters was carried out by azeotropic esterification in the presence of solvents—benzene and *m*-xylene. The resulting diesters were isolated from the reaction mass by vacuum rectification. The purity of the obtained NPG diesters was no less than 99.7 wt %. Analysis of the qualitative and quantitative composition of reaction samples was carried out using infrared spectroscopy, gas chromatography–mass spectrometry and gas–liquid chromatography.

Results. The paper presents the results of kinetic studies on NPG esterification of with acetic and 2-ethylhexanoic acids. It compares the reaction rates and reactivity of the acids used. Under the given conditions, NPG diesters were produced, and some of their physicochemical properties were determined. This enabled the data obtained to be used for the development of industrial technology in the production of NPG diesters.

Conclusions. It was established that with an eightfold molar excess of acid under self-catalysis conditions, a yield of NPG diacetate equal to 95% is achieved within 20–22 h at an optimal process temperature of 100–110°C; NPG di(2-ethylhexanoate)—within 26–28 h at 160–170°C. The activation energies and pre-exponential factors for the formation of NPG mono- and diesters with acetic and 2-ethylhexanoic acids were established. The paper presents the kinetic models of esterification.

Keywords

neopentyl glycol, neopolyols, esterification, self-catalysis, esters, acetic acid, 2-ethylhexanoic acid, plasticizer

Submitted: 17.05.2023
Revised: 12.07.2023
Accepted: 22.12.2023

For citation

Chicheva D.S., Krasnykh E.L., Shakun V.A. Kinetic regularities of neopentyl glycol esterification with acetic and 2-ethylhexanoic acids. *Tonk. Khim. Tekhnol. = Fine Chem. Technol.* 2024;19(1):28–38. https://doi.org/10.32362/2410-6593-2024-19-1-28-38

НАУЧНАЯ СТАТЬЯ

Кинетические закономерности этерификации неопентилгликоля уксусной и 2-этилгексановой кислотами

Д.С. Чичева, Е.Л. Красных✉, В.А. Шакун

Самарский государственный технический университет, Самара, 443100 Россия

✉ *Автор для переписки, e-mail: kinterm@samgtu.ru*

Аннотация

Цели. Разработка отечественной технологии получения экологически чистых нефталатных пластификаторов, смазывающих и трансформаторных жидкостей на основе продукта оксосинтеза — неопентилгликоля (НПГ).

Методы. Методология работы заключалась в исследовании кинетических закономерностей реакции этерификации НПГ уксусной и 2-этилгексановой кислотами в условиях самокатализа при восьмикратном мольном избытке монокарбоновых кислот. Наработку сложных эфиров НПГ вели методом азеотропной этерификации в присутствии растворителей — бензола и *м*-ксилола. Полученные диэфиры выделяли из реакционной массы вакуумной ректификацией. Чистота полученных диэфиров НПГ составляла не менее 99.7 мас. %. Качественный и количественный состав реакционных проб проводили методами инфракрасной спектроскопии, газовой хромато-масс-спектрометрией и газожидкостной хроматографией.

Результаты. В работе представлены результаты кинетических исследований реакций этерификации НПГ уксусной и 2-этилгексановой кислотами. Проведено сравнение скоростей реакции и реакционной способности используемых кислот. В заданных условиях наработаны диэфиры НПГ и определены их некоторые физико-химические свойства, позволяющие рекомендовать полученные данные для разработки промышленной технологии получения сложных диэфиров НПГ.

Выводы. Установлено, что при восьмикратном мольном избытке кислоты в условиях самокатализа выход диацетата НПГ, равный 95%, достигается в течение 20–22 ч при оптимальной температуре процесса 100–110°С; ди(2-этилгексаноата) НПГ — в течение 26–28 ч при 160–170°С. Определены энергии активации и предэкспоненциальные множители реакций образования моно- и диэфиров НПГ с уксусной и 2-этилгексановой кислотами. Представлены кинетические модели этерификации.

Ключевые слова

неопентилгликоль, неополиолы, этерификация, самокатализ, сложные эфиры, уксусная кислота, 2-этилгексановая кислота, пластификатор

Поступила: 17.05.2023
Доработана: 12.07.2023
Принята в печать: 22.12.2023

Для цитирования

Чичева Д.С., Красных Е.Л., Шакун В.А. Кинетические закономерности этерификации неопентилгликоля уксусной и 2-этилгексановой кислотами. *Тонкие химические технологии*. 2024;19(1):28–38. https://doi.org/10.32362/2410-6593-2024-19-1-28-38

INTRODUCTION

In the current environmental situation, the production of phthalate plasticizers is strictly regulated by environmentalists. This requires modern manufacturers of plasticizers to actively develop and create alternative raw materials and options for their production. Thus, the synthesis gas required for the synthesis of olefins by oxo-synthesis can be obtained by steam reforming or partial oxidation of methane. As a result, natural gas is an accessible raw material for the production of alcohols and carboxylic acids which are the starting components in esterification reactions. Carboxylic acids are obtained by low-temperature oxidation of the products of lower olefins hydroformylation (aldehydes) in oxygen or air, while alcohols are obtained by catalytic hydrogenation.

Oxosynthesis processes are primarily aimed at producing oxygen-containing products of linear structure. However, 30–35% of the products are aldehydes of iso structure [1]. Regioisomeric isobutyraldehyde is among them. Its aldol condensation with formaldehyde followed by catalytic hydrogenation produces one of the most important neo alcohols: neopentyl glycol (NPG, 2,2-dimethyl-1,3-propanediol).

Due to the structural features of NPG (i.e., the presence of a quaternary carbon atom in the molecule), NPG esters can be characterized by their good ability to biodegrade under aerobic and anaerobic conditions [2]. They are thermostable and have low melting points [3]. They have a reduced potential for oxidation and hydrolysis when compared to natural esters [4]. For this

reason, they are considered as potential environmentally friendly insulating liquids [5].

A significant part of industrially produced NPG is used to produce esters of various structures, used in the cosmetic and polymer industries, as well as plasticizers and synthetic oils [6]. Plasticizers based on NPG belong to hazard class IV [7] and are environmentally safer compared to phthalate plasticizers, which belong to hazard class II [7].

The global NPG market was worth USD 1346 mln in 2020, and its average annual growth rate over the forecast period of 2021–2027 will be 4.1%[1]. NPG production is not currently carried out in Russia, although Russia possesses all the prerequisites for mastering modern oxo-synthesis processes and their improvement. This will allow domestic production of environmentally friendly plasticizing materials to be established and the amount of natural gas burned to be reduced.

The main industrial method for producing esters is esterification reaction using acidic homogeneous and heterogeneous catalysts: sulfuric and orthophosphoric acids; and sulfonic cation exchangers. The use of mineral acids as catalysts leads to tarring and a decrease in the color stability of the reaction mass, thus increasing the cost of isolating and purifying the target product. There is a tendency to use heterogeneous catalysts (ion exchange resins) in esterification reactions due to the ease of separation of the reaction mass from the catalyst and the absence of wastewater [8].

The carboxylic acids used for esterification are weak acylating reagents capable of autoprotolysis [9]. This enables the process to be carried out without the use of a catalyst: under conditions of self-catalysis. The pK values of carboxylic acids do not differ greatly from the pK of the catalyst [the pK values of acetic acid (AA) and the H_3PO_4 catalyst (in the first group) are 4.76 and 2.12, respectively]. Despite the longer reaction time under self-catalysis conditions, the problem of side reactions occurring in the system is resolved. This makes it possible to obtain esters which require minimal additional purification, if necessary.

The literature devoted to studies on NPG esterification contains practically no information about conducting kinetic studies of the esterification reaction under self-catalysis conditions. Therefore, we conducted studies of the kinetics of NPG esterification with acetic and 2-ethylhexanoic (2EH) acids under conditions of self-catalysis, in order to create a theoretical basis for the development of domestic technology for the production of environmentally friendly non-phthalate plasticizers.

EXPERIMENTAL

Materials

Two monocarboxylic acids—AA and 2EH—with a purity of at least 97 wt % and NPG with a purity of at least 99.8 wt % were used as reagents in the study of NPG etherification.

Synthesis of NPG esters

NPG is a diatomic alcohol. The esterification reaction with its participation is equilibrium, and proceeds sequentially through the formation of a monoester, ending with the formation of a diester (Fig. 1). In addition, a disproportionation reaction of monoesters is also possible. However, this reaction occurs to a very small extent, and its contribution to the process kinetics is insignificant [10].

The production of NPG diesters was carried out by means of azeotropic esterification at an acid/alcohol molar ratio of 8 : 1, under conditions of self-catalysis using a Dean–Stark trap to separate reaction water. Benzene (*Reaktiv*, Russia) was used as an azeotrope-forming agent in the synthesis of NPG diacetate, and *m*-xylene (*EKOS-1*, Russia) in the synthesis of NPG di(2-ethylhexanoate). The choice of acylating reagents is determined by the difference in the lengths of their alkyl chains. This allows for evaluation of the influence of the length of the acid carbon chain on the reaction rate, on the time of ester synthesis, on some physicochemical properties, and, as a consequence, on the scope of application of the resulting NPG diesters. The completion of the reaction was determined by the cessation of water formation. Next, the excess carboxylic acid was distilled off under vacuum. The resulting diesters were washed with a 5% $NaHCO_3$ solution to remove traces of the acid. In the case of NPG diacetate, purification from by-products was carried out by means of vacuum rectification. In the case of NPG di(2-ethylhexanoate), purification was carried out by treatment with bleached clay, in order to remove resins. Then the product was washed with an aqueous solution of sodium hypochlorite for clarification [11]. The purity of the obtained esters was no less than 99 wt % (determined by gas–liquid chromatography, GLC).

Identification and analysis

Identification of the components of the reaction mixtures was carried out by means of gas chromatography–mass spectrometry using an Agilent 6850 gas chromatograph (*Agilent Technologies*, USA) equipped with an Agilent 19091S-433E capillary column (30 m × 250 μm × 0.25 μm) on an HP-5MS

[1] Global neopentyl glycol market 2021 – industry statistics. Gen Consulting. 2020.

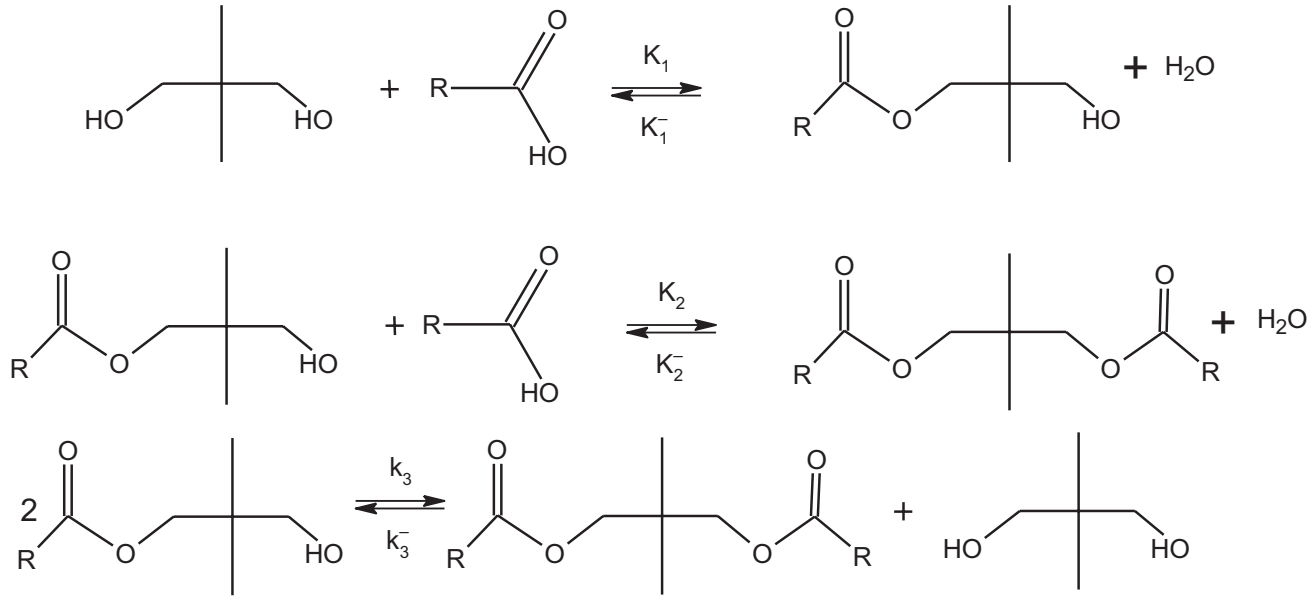

Fig. 1. Scheme of NPG esterification with monocarboxylic acids

chromatographic column (stationary phase: 5% diphenylpolysiloxane + 95% dimethylpolysiloxane) and an Agilent 5975C VL MSD mass selective detector at an ionizing voltage of 70 eV.

Furthermore, the structure of the NPG diesters obtained was confirmed by infrared (IR) spectrometry using an FSM 2201 IR Fourier spectrometer (*Infraspek*, Russia) equipped with a multiple attenuated total internal reflection horizontal type MNPVO36 attachment with a zinc selenide-based prism.

The reaction samples were analyzed by GLC using a Kristall-2000M chromatograph (*Chromatec*, Russia) equipped with a flame ionization detector and a capillary column measuring 100 m × 0.2 mm × 0.5 μm with a grafted stationary liquid phase DB-1 (dimethylpolysiloxane). The masses of the components were determined by GLC using an internal standard. Analysis modes are presented in Table 1.

Table 1. Modes of reaction mass analysis using GLC

Parameter	NPG + AA	NPG + 2EH
Column temperature, °C	100–170*	250
Evaporator temperature, °C	350	330
Detector temperature, °C	300	300
Carrier gas	Helium	
Flow rate, mL/min	0.7	
Split ratio	1/100	

* The temperature was maintained at 100°C for 10 min, then the column temperature was raised to 170°C at a heating rate of 20°C/min.

Kinetic studies

Kinetic studies were carried out under conditions of self-catalysis in the absence of an azeotrope-forming agent at an acid/alcohol molar ratio of 8 : 1 under nonequilibrium conditions (with distillation of reaction water) with intense stirring. The choice of the acid/alcohol molar ratio was determined by achieving the optimal equilibrium conversion of NPG based on the thermodynamic analysis of the system. The reactions were carried out under thermostatting in an open ideal mixing reactor system: a three-neck round-bottom flask equipped with a stirrer and a Liebig refrigerator. NPG is a crystalline substance, so the start time of the kinetic experiment was counted from the moment of its dissolution in the acid at the reaction temperature.

Under the conditions of kinetic studies, reverse hydrolysis reactions did not occur, since water was removed from the system [4]. This allowed the account the water concentration not to be taken into account in the kinetic equations, also allowing the rate constant values to be calculated only for direct reactions.

As a result, the system of kinetic equations looks as follows:

$$\frac{\partial C_{\text{ME}}}{\partial \tau} = k[\text{NPG}][\text{A}] - k_2[\text{DE}][\text{A}], \quad (1)$$

$$\frac{\partial C_{DE}}{\partial \tau} = k_2 [ME][A], \quad (2)$$

where A is monocarboxylic acid; ME is NPG monoester; DE is NPG diester; C_{ME} and C_{DE} are concentrations of monoester and diester, respectively; τ is time.

Based on the available literature data, the reaction order for each component was taken to be equal to 1 [10–13]. The rate constants k_1 and k_2 were determined by jointly solving kinetic Eqs. (1) and (2) for each temperature under the assumption that $\frac{\partial C_i}{\partial \tau} \approx \frac{\Delta C_i}{\Delta \tau}$ at $\Delta\tau$ = 10 min. Optimization of values was carried out using the Euler method.

RESULTS AND DISCUSSION

Table 2 presents the characteristics of the mass spectra of the samples of the NPG diacetate and di(2-ethylhexanoate) obtained. The data shows that the mass spectrum of NPG diacetate can be characterized by 100% relative intensity of the $C_2H_3O^+$ ion, and in the case of di-2-ethylhexanoate, of the *tert*-$C_4H_9^+$ ion. The maximum intensity of the latter is due to energetically favorable pathways of decomposition of the *n*-butyl fragment of the ester molecule acidic part followed by its isomerization into the *tert*-butyl cation [14]. One notable feature of the NPG esters fragmentation is the elimination of the $CH_3^\bullet$ radical from the quaternary carbon atom of the ester molecule alcohol part.

Besides, IR spectra of the synthesized esters were obtained. They are presented in Figs. 2 and 3.

All the spectra contain characteristic intense absorption bands in the region of 2860–2975 cm^{-1} indicating the presence of stretching vibrations of C–H bonds related to the alkyl moiety of the acidic part of the molecule. Absorption bands in the region of 1750–1735 cm^{-1} are characteristic of the C=O bond of the ester group. The band in the range of 1000–1260 cm^{-1} represents bending vibrations of the C–O bond. A small band in the region of 3550–3450 cm^{-1} characterizes the presence of an OH group, confirming the presence of NPG monoesters (up to 0.1 wt %) in the resulting diesters.

Determination of kinetic characteristics

The study of the kinetics of NPG diacetate formation was carried out in the temperature range of 70–110°C with steps of 10°C and a time interval of 0–300 min. The initial concentrations of the reagents in all the experiments were: NPG — 1.8 mol/L; and AA — 14.2 mol/L. Experiments involving 2EH acid were carried out at temperatures of 140–170°C with steps of 10°C and a time interval of 0–160 min. The initial concentrations of the reagents in all the experiments were: NPG — 0.8 mol/L; and 2EH — 6.1 mol/L. In order to control the experiment, material balance was calculated at each time point to assess the relative deviation of the analytically determined masses of the components from the mass of the loaded components. The average deviation did not exceed 10%.

Typical chromatograms of reaction masses are presented in Figs. 4 and 5.

Figure 6 shows the results obtained for one of the study temperatures. They indicate the concentration dependencies of the reaction mixture components on time, illustrating the sequence of NPG transformation into monoesters and of monoesters into diesters.

The dynamics of the reactions over time show that the rate of the reaction with the participation of AA is higher than in the case of 2EH. This may be due to the strength of the acids used (the dissociation constant of AA is greater than that of 2EH) and due to spatial factors.

The values of the rate constants k_1 and k_2 obtained during the experiments are presented in Table 3.

The pre-exponential factors and activation energies were determined graphically on the basis of the obtained approximation equations for the dependence of the natural logarithm of the rate constants on the inverse temperature. The resulting Arrhenius equations for a system with CM have the form:

$$k_1 = 5.74 \cdot 10^4 \cdot e^{\frac{(-57.6 \pm 2.2)}{RT}}, \quad (3)$$

$$k_2 = 1.94 \cdot 10^3 \cdot e^{\frac{(-49.9 \pm 12.1)}{RT}}, \quad (4)$$

Table 2. Characterization of the main series of ions in mass spectra of synthesized NPG diesters

NPG ester	Main mass spectrum ion series 70 eV, *m/z*, (structure, % rel.)
Diacetate	**188** ($M^{+\bullet}$, 0); **145** ($[M^{+\bullet}–C_2H_3O^\bullet]^+$, 1); **115** ($[M^{+\bullet}–C_3H_5O_2^\bullet]^+$, 20); **86** ($[M^{+\bullet}–C_2H_3O_2^\bullet$; $–C_2H_3O^\bullet]^+$, 15); **56** ($[M^{+\bullet}–2C_2H_3O_2^\bullet$; $–CH_3^\bullet]^+$, 25); **43** ($C_2H_3O^+$, 100)
Di(2-ethylhexanoate)	**356** ($M^{+\bullet}$, 0); **341** ($[M^{+\bullet}–CH_3^\bullet]^+$, 1); **328** ($[M^{+\bullet}–C_2H_4]^{+\bullet}$, 3); **300** ($[M^{+\bullet}–C_4H_8]^{+\bullet}$, 8); **213** ($[M^{+\bullet}–C_8H_{15}O_2^\bullet]^+$, 45); **156** ($[M^{+\bullet}– C_8H_{15}O_2^\bullet$;$–C_4H_9^\bullet$, 35$]^{+\bullet}$); **127** ($[M^{+\bullet}–C_4H_9^\bullet$; $–C_8H_{15}O_2^\bullet$; $–2CH_3^\bullet]^+$, 85); **99** (*sec*-$C_7H_{15}O^+$, 43); **57** (*tert*-$C_4H_9^+$, 100)

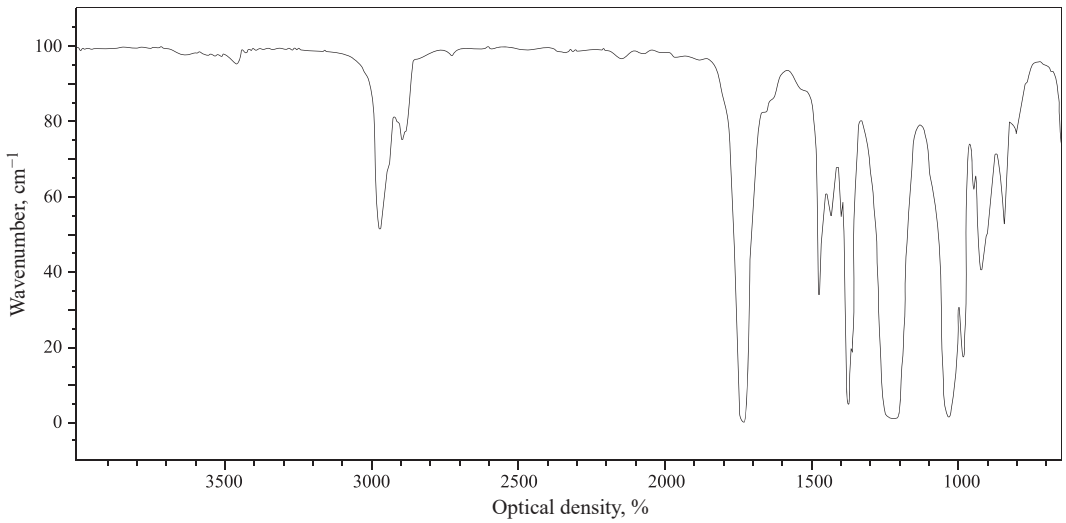

Fig. 2. IR spectrum of NPG diacetate

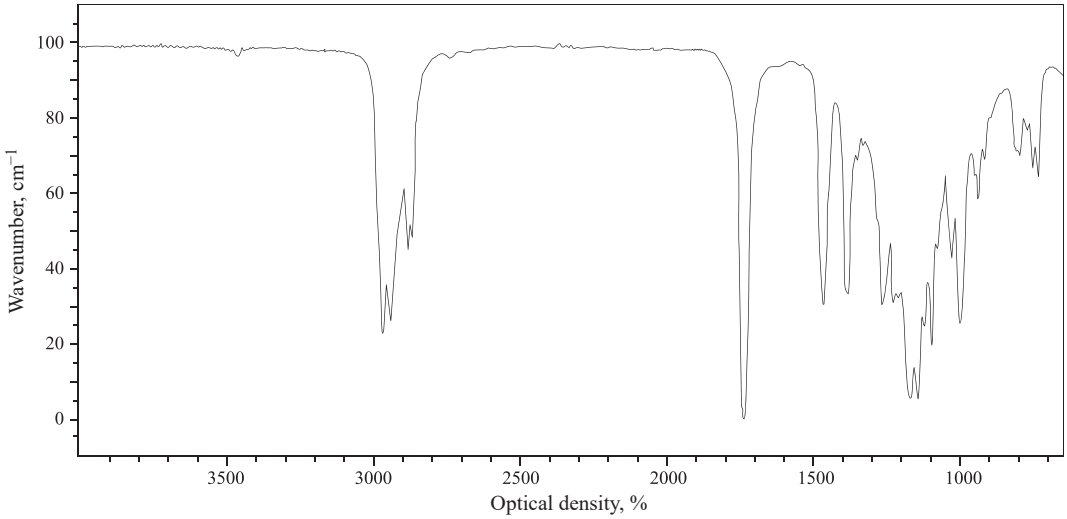

Fig. 3. IR spectrum of NPG di(2-ethylhexanoate)

where R is the gas constant, T is the absolute temperature. In case of esterification with 2EH acid:

$$k_1 = 5.94 \cdot 10^3 \cdot e^{\frac{(-57.5 \pm 6.2)}{RT}}, \quad (5)$$

$$k_2 = 4.16 \cdot 10^2 \cdot e^{\frac{(-50.9 \pm 5.2)}{RT}}. \quad (6)$$

It can be seen from Eqs. (3)–(6) that the activation energies for each stage are almost the same. However, at the same time there is a strong difference in the values of the pre-exponential factors. This can be explained by a change in the reactivity of carboxylic acids with increasing length and branching of the main carbon chain. This creates spatial obstacles to interaction due to the shielding of the active centers by the alcohol molecules. Thus, the ethyl radical at the α-carbon atom of 2EH acid reduces the acid strength and complicates the nucleophilic attack of the nearby carbon atom of the carboxyl group [15]. This significantly affects the rate of esterification in the case of isomeric acids with similar dissociation constants [13].

The viability of the proposed kinetic model (Eqs. (3)–(6)) is confirmed by comparison of experimental and calculated data, as presented in Fig. 7. The average deviation of the calculated values from the experimental values does not exceed 6%.

The time to reach 95% yield of NPG di(2-ethylhexanoate) is 26–28 h; in the case of NPG diacetate, 20–22 h (Fig. 8).

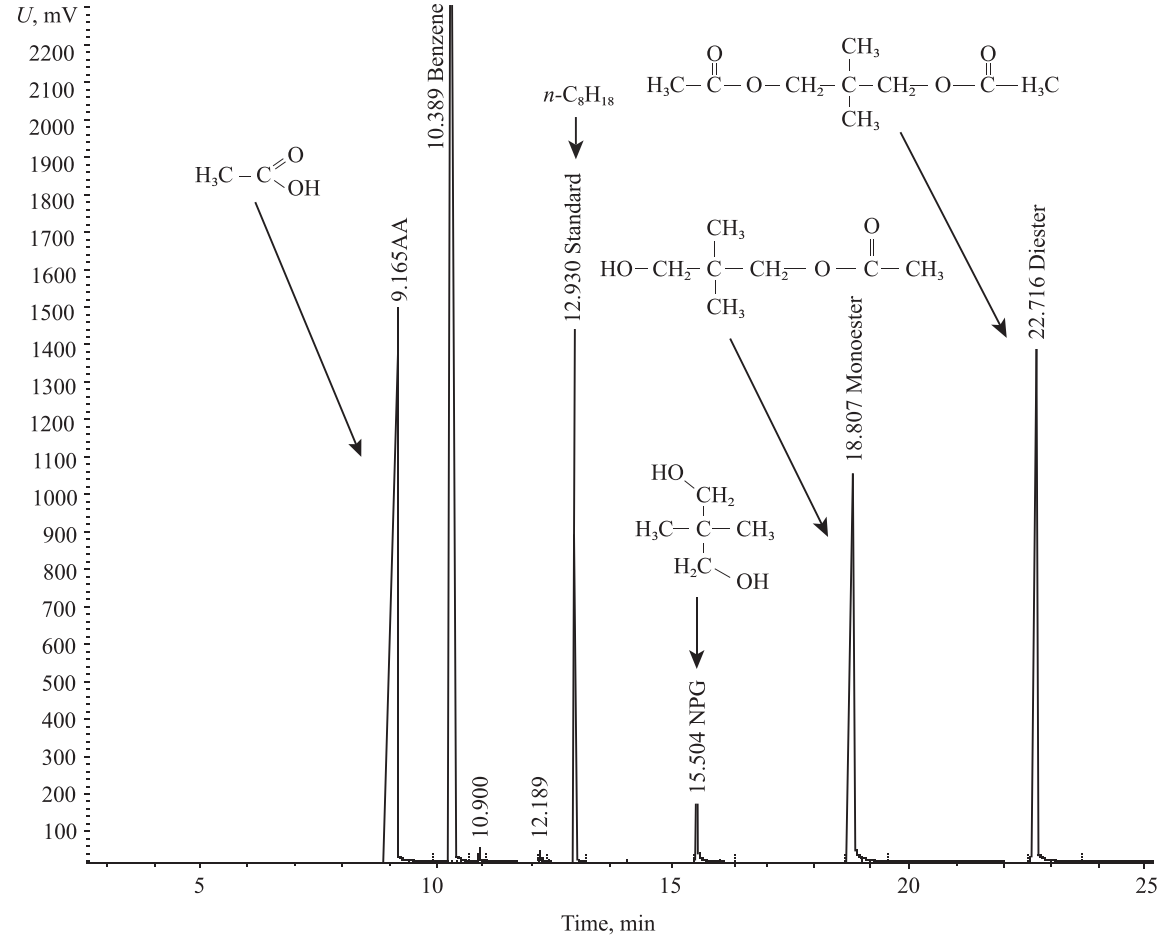

Fig. 4. Chromatogram of the reaction mass of NPG diacetate synthesis

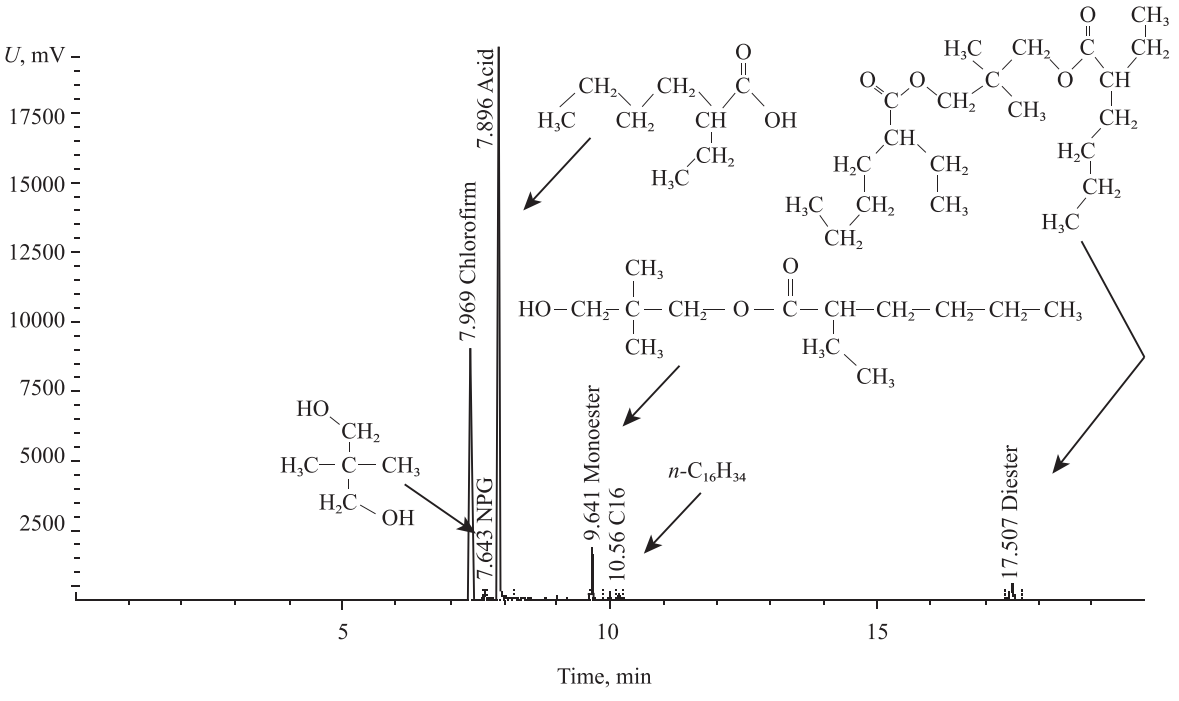

Fig. 5. Chromatogram of the reaction mass of NPG di(2-ethylhexanoate) synthesis

Table 3. Values of rate constants of NPG esterification by AA and 2EH acid

AA			2EH		
t, °C	$k_1 \cdot 10^4$, L/(mol·min)	$k_2 \cdot 10^4$, L/(mol·min)	t, °C	$k_1 \cdot 10^4$, L/(mol·min)	$k_2 \cdot 10^4$, L/(mol·min)
70	0.9	0.3	–	–	–
80	1.9	1.2	140	3.0	1.4
90	2.9	1.7	150	5.2	2.3
100	5.0	1.9	160	6.3	2.8
110	8.1	2.6	170	9.9	4.2

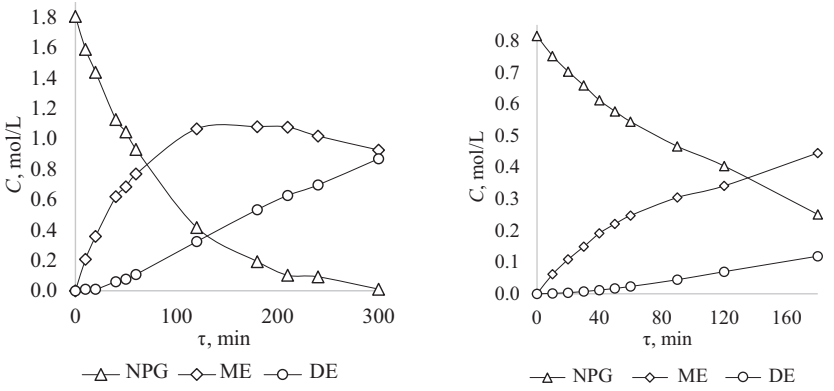

Fig. 6. Kinetic dependencies of NPG consumption, accumulation of mono- and diesters.
(a) AA + NPG at 110°C;
(b) 2EH acid + NPG at 170°C

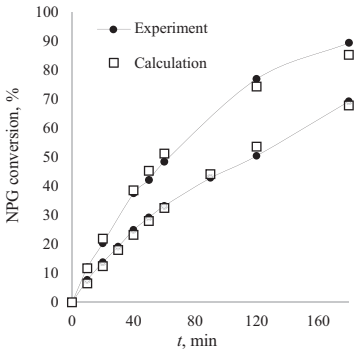

Fig. 7. Comparison of experimental and calculated values of the NPG conversion change in time. (a) AA + NPG at 110°C; (b) 2EH acid + NPG at 170°C

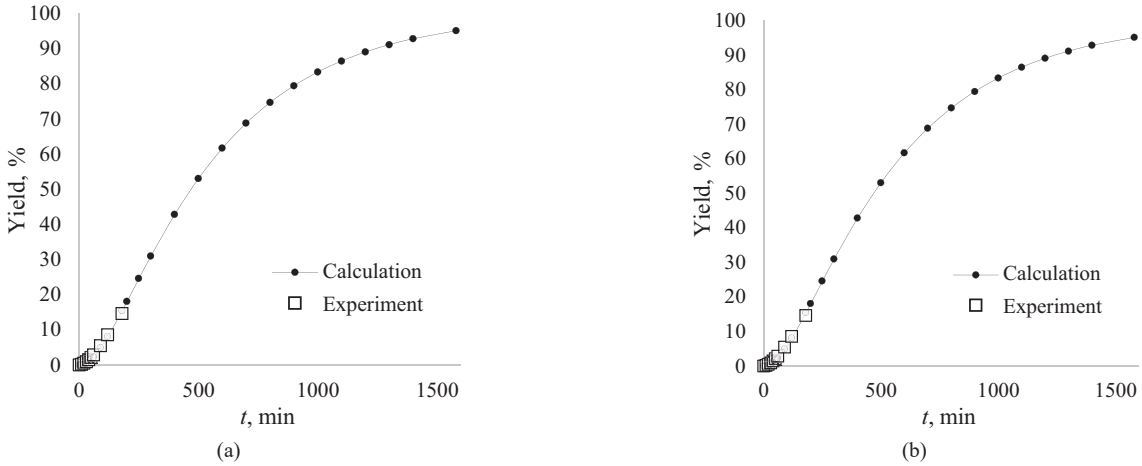

Fig. 8. Dependence of the yield of diesters on the reaction time.
(a) AA + NPG at 110°C;
(b) 2EH acid + NPG at 170°C.

Table 4. Comparison of a number of physicochemical properties of the obtained NPG esters and industrial phthalate plasticizer

Substance	Flash point in open crucible, °C	Mass fraction of volatiles, %	Density at 20°C, g/cm^3	Hazard class
NPG diacetate	100 ± 5	44.9	1.018	IV
NPG di(2-ethylhexanoate)	173 ± 2	0.4	0.918	IV
DOP (dioctyl phthalate) (GOST 8728-88)	205	up to 0.1	0.982–0.986	II

NPG esters with a content of the main substance of at least 99.7 wt % were produced under the given conditions. Their physicochemical parameters were determined in accordance with the methods of GOST 8728-88[2] (Table 4).

The data presented in Table 4 indicate that NPG diacetate is a more volatile compound due to the low molecular weight of AA used. When using NPG diacetate as a plasticizer, it will diffuse and evaporate from the polymer material, which, under high-temperature processing conditions, can lead to the ether boiling. Therefore, NPG diacetate can be recommended for use as a viscosity regulator for plastisols and provide improved resistance to staining of vinyl floor coverings. This is due to its volatility [12]. NPG di(2-ethylhexanoate) has a high boiling point and a low volatility, which makes it possible to use it as a plasticizer.

CONCLUSIONS

The study established that the optimal conditions for NPG esterification with monocarboxylic acids include a temperature range of 100–170°C with an 8-fold molar excess of the acid without the use of a catalyst. This helps prevent tarring and darkening of the reaction mass. The observed activation energies for the formation of NPG diacetate and di(2-ethylhexanoate) are similar and amount to 53.7 ± 7.2 kJ/mol and 54.2 ± 5.7 kJ/mol, respectively. This is consistent with the literature data on the esterification of propionic acid with NPG: 55.3 kJ/mol. Any differences in the values of pre-exponential factors, in the ester synthesis time and in the physicochemical parameters are due to the influence of the reactivity of the acids used and spatial hindrance. The research results obtained can be used to create domestic technology for the production of NPG esters applied as plasticizers, bases or components of lubricants.

Authors' contribution

All authors equally contributed to the research work.

The authors declare no conflicts of interest.

[2] GOST 8728-88. Interstate standard. Plasticizers. Specifications. Moscow: IPK Izd. standartov; 2003 (in Russ.).

REFERENCES

1. Marochkin D.V., Noskov Yu.G., Kron T.E., Karchevskaya O.G., Korneeva G.A. Products of oxo-process in the production of ester lubricating oils. *Nauchno-tekhnicheskii vestnik OAO "NK Rosneft."* 2016;4(45):74–81 (in Russ.).
2. Åkerman C.O., Gaber Y., Abd Ghani N., Lämsa M., Hatti-Kaul R. Clean synthesis of biolubricants for low temperature applications using heterogeneous catalysts. *J. Mol. Catal. B-Enzym*. 2011;72(3–4): 263–269. https://doi.org/10.1016/j.molcatb.2011.06.014
3. Knothe G., Dunn R.O., Shockley M.W., Bagby M.O. Synthesis and characterization of some long-chain diesters with branched or bulky moieties. *J. Am. Oil Chem. Soc.* 2000;77(8):865–871. https://doi.org/10.1007/s11746-000-0138-x
4. Serrano-Arnaldos M., García-Martínez J.J., Ortega-Requena S., Bastida J., Máximo F., Montiel M.C. Reaction strategies for the enzymatic synthesis of neopentylglycol diheptanoate. *Enzyme Microb. Technol.* 2020;132:109400. https://doi.org/10.1016/j.enzmictec.2019.109400
5. Raof N.A., Yunus R., Rashid U., Azis N., Yaakub Z. Palm-based neopentyl glycol diester: a potential green insulating oil. *Protein Pept. Lett.* 2018;25(2):171–179. https://doi.org/10.2174/0929866525666180122095056
6. Krasnykh E.L., Lukina O.D., Emelyanov V.V., Portnova S.V. Saturated vapor pressure and enthalpies of vaporization of diesters of neopentyl glycol and linear C_2–C_6 acids. *Russ. J. Phys. Chem. A.* 2021;95(10):1975–1980. https://doi.org/10.1134/S0036024421100137
[Original Russian Text: Krasnykh E.L., Lukina O.D., Emelyanov V.V., Portnova S.V. Saturated vapor pressure and enthalpies of vaporization of diesters of neopentyl glycol and linear C_2–C_6 acids. *Zhurnal fizicheskoi khimii*. 2021;95(10): 1458–1463 (in Russ.). https://doi.org/10.31857/S0044453721100137]
7. Sushkova S.V., Levanova S.V., Glazko I.L. Identification and quantitative determination of esters of citric acid. *Izv. Vyssh. Uchebn. Zaved. Khim. Khim. Tekhnol. = ChemChemTech*. 2019;62(10):110–117 (in Russ.). https://doi.org/10.6060/ivkkt.20196210.6036
8. Shmid R., Sapunov V.N. *Neformal'naya kinetika*. *V poiskakh putei khimicheskikh reaktsii* (*Non-Formal Kinetics*: *In Search for Chemical Reaction Pathways*): transl. from Engl. Moscow: Mir; 1985. 264 p. (in Russ.).
9. Ovezova M., Savin G.A. Synthesis of esters by thermal esterification. *Elektronnyi nauchno-obrazovatel'nyi zhurnal VGSPU* "*Grani Poznaniya*." 2021;3(74):66–68 (in Russ.). URL: https://sciup.org/148322077
10. Vahteristo K., Laari A., Haario H., Solonen A. Estimation of kinetic parameters in neopentyl glycol esterification with propionic acid. *Chem. Eng. Sci*. 2008;63(3):587–598. https://doi.org/10.1016/j.ces.2007.09.023
11. Abdrakhmanova L.K., Rysaev D.U., Aminova G.K., Mazitova A.K. Clarification of di-(2-ethylhexyl)phthalate plasticizer with an aqueous solution of sodium hypochlorite. *Bashkirskii khimicheskii zhurnal = Bashkir Chem. J*. 2008;15(4):38–40 (in Russ.).
12. Aleksandrov A.Yu., Krasnykh E.L., Levanova S.V., Glazko I.L., Lukina O.D. Development of technology for production of plasticizers on the basis of trimethylolpropane. *Tonk. Khim. Tekhnol. = Fine Chem. Technol*. 2019;14(1):66–74 (in Russ.). https://doi.org/10.32362/2410-6593-2019-14-1-66-74
13. Sun L., Zhu L., Xue W., Zeng Z. Kinetics of p-toluene-sulfonic acid catalyzed direct esterification of pentaerythritol with acrylic acid for pentaerythritol diacrylate production. *Chem. Eng. Commun*. 2020;207(3):331–338. https://doi.org/10.1080/00986445.2019.1592750

СПИСОК ЛИТЕРАТУРЫ

1. Марочкин Д.В., Носков Ю.Г., Крон Т.Е., Карчевская О.Г., Корнеева Г.А. Продукты оксосинтеза в производстве сложноэфирных смазочных масел. *Научно-технический вестник ОАО «НК «Роснефть»*. 2016;4(45):74–81.
2. Åkerman C.O., Gaber Y., Abd Ghani N., Lämsa M., Hatti-Kaul R. Clean synthesis of biolubricants for low temperature applications using heterogeneous catalysts. *J. Mol. Catal. B-Enzym*. 2011;72(3–4):263–269. https://doi.org/10.1016/j.molcatb.2011.06.014
3. Knothe G., Dunn R.O., Shockley M.W., Bagby M.O. Synthesis and characterization of some long-chain diesters with branched or bulky moieties. *J. Am. Oil Chem. Soc.* 2000;77(8):865–871. https://doi.org/10.1007/s11746-000-0138-x
4. Serrano-Arnaldos M., García-Martínez J.J., Ortega-Requena S., Bastida J., Máximo F., Montiel M.C. Reaction strategies for the enzymatic synthesis of neopentylglycol diheptanoate. *Enzyme Microb. Technol.* 2020;132:109400. https://doi.org/10.1016/j.enzmictec.2019.109400
5. Raof N.A., Yunus R., Rashid U., Azis N., Yaakub Z. Palm-based neopentyl glycol diester: a potential green insulating oil. *Protein Pept. Lett.* 2018;25(2):171–179. https://doi.org/10.2174/0929866525666180122095056
6. Красных Е.Л., Лукина О.Д., Емельянов В.В., Портнова С.В. Давления насыщенных паров и энтальпии испарения сложных диэфиров неопентилгликоля и линейных кислот C_2–C_6. *Журн. физ. химии*. 2021;95(10):1458–1463. https://doi.org/10.31857/S0044453721100137
7. Сушкова С.В., Леванова С.В., Глазко И.Л. Идентификация и количественное определение сложных эфиров лимонной кислоты. *Изв. вузов. Химия и хим. технология*. 2019;62(10): 110–117. https://doi.org/10.6060/ivkkt.20196210.6036
8. Шмид Р., Сапунов В.Н. *Неформальная кинетика*. *В поисках путей химических реакций*: пер. с англ. М.: Мир; 1985. 264 с.
9. Овезова М., Савин Г. А. Синтез сложных эфиров термической этерификацией. *Электронный научно-образовательный журнал ВГСПУ «Грани познания»*. 2021;3(74):66–68. URL: https://sciup.org/148322077
10. Vahteristo K., Laari A., Haario H., Solonen A. Estimation of kinetic parameters in neopentyl glycol esterification with propionic acid. *Chem. Eng. Sci*. 2008;63(3):587–598. https://doi.org/10.1016/j.ces.2007.09.023
11. Абдрахманова Л.К., Рысаев Д.У., Аминова Г.К., Мазитова А.К. Осветление ди-(2-этилгексил) фталатного пластификатора водным раствором гипохлорита натрия. *Башкирский химический журнал*. 2008;15(4):38–40.
12. Александров А.Ю., Красных Е.Л., Леванова С.В., Глазко И.Л., Лукин О.Д. Разработка технологии производства пластификаторов на основе триметилолпропана. *Тонкие химические технологии*. 2019;14(1):66–74. https://doi.org/10.32362/2410-6593-2019-14-1-66-74
13. Sun L., Zhu L., Xue W., Zeng Z. Kinetics of p-toluene-sulfonic acid catalyzed direct esterification of pentaerythritol with acrylic acid for pentaerythritol diacrylate production. *Chem. Eng. Commun*. 2020;207(3):331–338. https://doi.org/10.1080/00986445.2019.1592750
14. Емельянов В.В., Красных Е.Л., Фетисов Д.А., Леванова С.В., Шакун В.А. Особенности синтеза сложных эфиров пентаэритрита и алифатических карбоновых кислот изомерного строения. *Тонкие химические технологии*. 2022;17(1):7–17. https://doi.org/10.32362/2410-6593-2022-17-1-7-17
15. Агрономов А.Е. *Избранные главы органической химии*. М.: Химия; 1990. 560 с.

14. Emelyanov V.V., Krasnykh E.L., Fetisov D.A., Levanova S.V., Shakun V.A. Features of the synthesis of pentaerythritol esters and carboxylic acids of aliphatic isomeric structure. *Tonk. Khim. Tekhnol.* = *Fine Chem. Technol*. 2022;17(1):7–17 (Russ., Eng.). https://doi.org/10.32362/2410-6593-2022-17-1-7-17
15. Agronomov A.E. *Izbrannye glavy organicheskoi khimii* (*Selected Chapters of Organic Chemistry*). Moscow: Khimiya; 1990. 560 p. (in Russ).

About the authors

Daria S. Chicheva, Master Student, Samara State Technical University (244, Molodogvardeiskaya ul., Samara, 443100, Russia). E-mail: dasha00529@gmail.com. https://orcid.org/0000-0002-3243-5346

Eugen L. Krasnykh, Dr. Sci. (Chem.), Professor, Head of the Technology of Organic and Petrochemical Synthesis Department, Samara State Technical University (244, Molodogvardeiskaya ul., Samara, 443100, Russia). E-mail: ekras73@mail.ru, kinterm@samgtu.ru. Scopus Author ID 6602271562, ResearcherID I-6314-2013, RSCI SPIN-code 4691-1955, http://orcid.org/0000-0002-3886-1450

Vladimir A. Shakun, Cand. Sci. (Chem.), Associate Professor, Technology of Organic and Petrochemical Synthesis Department, Samara State Technical University (244, Molodogvardeiskaya ul., Samara, 443100, Russia). E-mail: shakyh@mail.ru, kinterm@samgtu.ru. Scopus Author ID 56829536300, RSCI SPIN-code 5091-8110, http://orcid.org/0000-0003-2682-3024

Об авторах

Чичева Дарья Сергеевна, магистрант, ФГБОУ ВО «Самарский государственный технический университет» (443100, Россия, г. Самара, ул. Молодогвардейская, д. 244). E-mail: dasha00529@gmail.com. https://orcid.org/0000-0002-3243-5346

Красных Евгений Леонидович, д.х.н., профессор, заведующий кафедрой «Технология органического и нефтехимического синтеза», ФГБОУ ВО «Самарский государственный технический университет» (443100, Россия, г. Самара, ул. Молодогвардейская, д. 244). E-mail: ekras73@mail.ru, kinterm@samgtu.ru. Scopus Author ID 6602271562, ResearcherID I-6314-2013, SPIN-код РИНЦ 4691-1955, http://orcid.org/0000-0002-3886-1450

Шакун Владимир Андреевич, к.х.н., доцент, кафедра «Технология органического и нефтехимического синтеза», ФГБОУ ВО «Самарский государственный технический университет» (443100, Россия, г. Самара, ул. Молодогвардейская, д. 244). E-mail: shakyh@mail.ru, kinterm@samgtu.ru. Scopus Author ID 56829536300, SPIN-код РИНЦ 5091-8110, http://orcid.org/0000-0003-2682-3024

Translated from Russian into English by M. Povorin
Edited for English language and spelling by Dr. David Mossop

Tonkie Khimicheskie Tekhnologii = Fine Chemical Technologies.
2024;19(1):39–51 ISSN 2686-7575 (Online)

Chemistry and technology of organic substances
Химия и технология органических веществ

UDC 54.057+547.791+544.478+66.095.261.4
https://doi.org/10.32362/2410-6593-2024-19-1-39-51

RESEARCH ARTICLE

Synthesis and application of chromium complexes based on 4,5-bis(diphenylphosphanyl)-*H*-1,2,3-triazole ligands to obtain higher C_{10}–C_{18} olefins

Aleksey A. Senin[1,✉], Kirill B. Polyanskii[1], Aleksey M. Sheloumov[1], Vladimir V. Afanasiev[1], Tatiana M. Yumasheva[1], Konstantin B. Rudyak[1], Stepan V. Vorobyev[2]

[1] *United Research and Development Center, Moscow, 119333 Russia*

[2] *National University of Oil and Gas (Gubkin University), Moscow, 119991 Russia*

✉ *Corresponding author, e-mail: SeninAA@rdc.rosneft.ru*

Abstract

Objectives. To synthesize 4,5-bis(diphenylphosphanyl)-*H*-1,2,3-triazole ligands and new chromium complexes based on them, in order to obtain a fraction of higher C_{10}–C_{18} alpha-olefins from ethylene.

Methods. The Schlenk technique was used to obtain the target chromium complexes. Diphenylphosphanyl triazole ligands can be characterized by nuclear magnetic resonance spectroscopy. The composition of the final products was confirmed by elemental analysis. The liquid phase of the oligomerization reaction was studied by gas chromatography.

Results. **L1**–**L9** ligands were obtained, and **K1**–**K9** chromium complexes were synthesized based on the correspondent ligands using commercially available chromium (III) trichloride tris(tetrahydrofuran). The **K1**–**K9** complexes thus obtained were tested in the process of ethylene oligomerization.

Conclusions. Chromium complexes based on 4,5-bis(diphenylphosphanyl)-*H*-1,2,3-triazoles **K1**–**K9** were produced in high yields using the Schlenk technique. It was found that systems based on the **K4**–**K7** and **K9** complexes enable the ethylene oligomerization process to be carried out with a sufficiently high level of productivity. It was shown that the introduction of a dialkyl zinc derivative increases the performance and selectivity of the catalytic system for the target fraction.

Keywords

chromium complexes, 4,5-bis(diphenylphosphanyl)-*H*-1,2,3-triazoles, olefins, catalytic system, ethylene oligomerization

Submitted: 28.07.2023
Revised: 06.12.2023
Accepted: 25.01.2024

For citation

Senin A.A., Polyanskii K.B., Sheloumov A.M., Afanasiev V.V., Yumasheva T.M., Rudyak K.B., Vorobyev S.V. Synthesis and application of chromium complexes based on 4,5-bis(diphenylphosphanyl)-*H*-1,2,3-triazole ligands to obtain higher C_{10}–C_{18} olefins. *Tonk. Khim. Tekhnol. = Fine Chem. Technol.* 2024;19(1):39–51. https://doi.org/10.32362/2410-6593-2024-19-1-39-51

НАУЧНАЯ СТАТЬЯ

Синтез комплексных соединений хрома на основе 4,5-бис(дифенилфосфанил)-*H*-1,2,3-триазольных лигандов и их применение для получения высших олефинов C_{10}–C_{18}

А.А. Сенин[1,✉], К.Б. Полянский[1], А.М. Шелоумов[1], В.В. Афанасьев[1], Т.М. Юмашева[1], К.Б. Рудяк[1], С.В. Воробьев[2]

[1] *Объединенный центр исследований и разработок (РН-ЦИР), Москва, 119333 Россия*

[2] *Российский государственный университет нефти и газа им. И.М. Губкина, Москва, 119991 Россия*

✉ *Автор для переписки, e-mail: SeninAA@rdc.rosneft.ru*

Аннотация

Цели. Синтезировать 4,5-бис(дифенилфосфанил)-*H*-1,2,3-триазольные лиганды и на их основе новые комплексы хрома для получения фракции высших альфа-олефинов C_{10}–C_{18} из этилена.

Методы. Для получения целевых комплексов хрома использовали методы работы в инертной атмосфере (техника Шленка). Дифенилфосфанил триазольные лиганды охарактеризованы методами спектроскопии ядерного магнитного резонанса. Состав конечных продуктов подтвержден с помощью элементного анализа. Жидкая фаза реакции олигомеризации охарактеризована методом газовой хроматографии.

Результаты. Получены лиганды **L1**–**L9** и из них с помощью коммерчески доступного трихлоридтрис(тетрагидрофуран) хрома(III) синтезированы комплексы хрома **К1**–**К9**. Полученные комплексы **К1**–**К9** испытаны в процессе олигомеризации этилена.

Выводы. С высокими выходами получены новые комплексы хрома на основе 4,5-бис(дифенилфосфанил)-*H*-1,2,3-триазолов **К1**–**К9**. Обнаружено, что системы на основе комплексов **К4**–**К7** и **К9** позволяют проводить процесс олигомеризации этилена с достаточно высокой производительностью. Показано, что введение диалкильного производного цинка повышает производительность и селективность каталитической системы по целевой фракции.

Ключевые слова

4,5-бис(дифенилфосфанил)-Н-1,2,3-триазолы, комплексы хрома, олефины, каталитическая система, олигомеризация этилена, метилалюмоксан

Поступила: 28.07.2023
Доработана: 06.12.2023
Принята в печать: 25.01.2024

Для цитирования

Сенин А.А., Полянский К.Б., Шелоумов А.М., Афанасьев В.В., Юмашева Т.М., Рудяк К.Б., Воробьев С.В. Синтез комплексных соединений хрома на основе 4,5-бис(дифенилфосфанил)-*H*-1,2,3-триазольных лигандов и их применение для получения высших олефинов C_{10}–C_{18}. *Тонкие химические технологии*. 2024;19(1):39–51. https://doi.org/10.32362/2410-6593-2024-19-1-39-51

INTRODUCTION

Higher alpha-olefins are valuable multipurpose raw materials for a range of applications. In particular, C_{10}–C_{18} fractions are used to produce poly alpha-olefins and additives for lubricants, alcohols for detergents, amines, amine oxides, nonionic surfactants, hydraulic fluids, and are also used as components of drilling fluids. C_{20+} olefins can be raw materials for the production of synthetic oils and cutting fluids, and can also be used in oilfield chemistry. As a rule, the use of individual olefins is not required in these areas, but the entire fraction of heavy linear terminal alkenes is [1, 2].

In contrast to the existing highly selective processes for the di-, tri- and tetramerization of ethylene, to date selective processes for the production of individual high-molecular-weight alpha-olefins have not been developed. According to the generally accepted mechanism [3], this can be explained by the impossibility of sequential coordination and cyclization of more than three to four ethylene molecules during the catalytic cycle. This is due to steric hindrances and thermodynamic limitations of the ethylene oligomerization process.

In modern scientific and patent literature, there are few descriptions of ethylene oligomerization processes in which the reaction products contain significant amounts of heavy olefin fractions [4–7]. Fe(II), Fe(III) complexes, as well as Cr(III) complexes containing a tridentate ligand with benzimidazole and pyridyl

fragments, activated with methylaluminoxane (MAO) or with modified MAO (MMAO), can catalyze the oligomerization of ethylene to form fractions C_{8+} and C_{10+} olefins under mild conditions [8–10]. Catalytic systems based on chromium complexes with diphosphine ligands exhibit a high level of activity in the process of trimerization of ethylene to 1-hexene [11].

The objective of our work was to synthesize 4,5-bis(diphenylphosphanyl)-*H*-1,2,3-triazole ligands and the chromium complexes based on them, in order to obtain a higher alpha-olefin fraction C_{10}–C_{18} from ethylene.

EXPERIMENTAL

The synthesis of compounds and the preparation of catalytic systems were carried out in an inert atmosphere using the Schlenk technique. The initial solvents (tetrahydrofuran (THF) (reagent grade, *Chimmed*, Russia), toluene (special purity grade, *Chimmed*), and hexane (reagent grade, *Chimmed*)) used for the synthesis were purified by boiling and distillation over sodium with benzophenone ketyl at atmospheric pressure in an argon flow. Diphenyl(chloro)phosphine (95%, *Acros Organics*, Belgium) was distilled in a vacuum (boiling point T_b = 124–126°C at 3 mm Hg). Acetone (special purity grade, *Chimmed*), chloroform (reagent grade, stabilized with 0.6–1.0% EtOH, *Chimmed*), ethyl acetate (reagent grade, *Chimmed*), methanol (Labscan, HPLC-grade), and methylene chloride (reagent grade, *Chimmed*) were used without additional purification. Chromium(III) trichloride tris(tetrahydrofuran) ($Cr(THF)_3Cl_3$) (98%, *Acros Organics*, Belgium), MAO (10% solution in toluene, *Sigma-Aldrich*, USA), diethylzinc ($ZnEt_2$) (1.5 M solution in toluene, *Sigma-Aldrich*), *n*-pentadecane (99%, *Sigma-Aldrich*), copper(I) iodide (98%, *Acros Organics*), aqueous hydrogen peroxide (35%, *Acros Organics*), sodium azide (special purity grade, *Chimmed*), trichlorosilane (99%, *Acros Organics*), methyl iodide (99%, *Sigma-Aldrich*), *n*-butyl chloride (99%, *Sigma-Aldrich*), sodium iodide (special purity grade, *Chimmed*), *n*-hexyl iodide (98%), *n*-octyl chloride (99%), silica gel (60 A, *Sigma-Aldrich*), pyridine (97%, *Acros Organics*), calcium carbide (98%, *Acros Organics*), and triethylamine (99%, *Acros Organics*) were used without any additional purification. Dibromobis(triphenylphosphine)nickel(II) ($NiBr_2(PPh_3)_2$) was obtained from nickel(II) bromide (98%, *Acros Organics*) and triphenylphosphine (99+%, *Acros Organics*) according to the published procedure [12]. Alkyl azides were obtained from the corresponding commercially available alkyl halides (*Sigma-Aldrich*). Ethylene (*Mostekhgaz*, Russia) was passed through three series-connected columns filled with activated carbon (*Chimmed*) and zeolites (3A and 13X, *Chimmed*). High-purity argon (*Moscow Gas Processing Plant*, Russia) was further purified by being passed through three series-connected columns filled with zeolites (3A and 13X), copper oxide (CuO reduced to Cu, *Chimmed*), and a CE35KF polisher (*Entegris*, USA). This ensured the residual content of oxygen, water, CO, etc. at the 1 ppb level. The purity of the resulting compounds was determined by ^1H and $^{31}P\{^1H\}$ nuclear magnetic resonance (NMR) spectroscopy.

^1H and $^{31}P\{^1H\}$ NMR spectra were recorded by means of a Bruker AVANCE 400 NMR spectrometer (*Bruker Corporation*, USA) at the A.N. Nesmeyanov Institute of Organoelement Compounds, Russian Academy of Sciences, using tetramethylsilane as an internal standard and 85% H_3PO_4 as an external standard. Elemental analysis was performed using a FLASH 2000 CHNS/O analyzer (*Thermo Fisher Scientific*, United Kingdom). The melting points were measured by the capillary method with an Electrothermal IA 9000 Series (*Thermo Fisher Scientific*) digital melting point apparatus. The studies were carried out at the Analytical Laboratory, *United Research and Development Center*, Moscow, Russia.

The liquid phase of the reaction mixture containing ethylene oligomerization products was analyzed using a Focus GC gas chromatograph (*ThermoFinnigan*, USA) with a flame ionization detector and a DB5 MS capillary column (length 50 m, diameter 0.2 mm) at a maximum operating temperature of 340°C. The contents of individual components in the mixture of ethylene oligomerization products were determined by the internal standard method using *n*-decane as an internal standard. A 0.2–0.3-μL sample was introduced using a *Hamilton* microsyringe (USA).

The column thermostat was programmed as follows: initial temperature 75°C; isothermal holding at 75°C, 12 min; heating from 75 to 290°C at a rate of 7 deg/min; isothermal holding at 290°C, 95 min. The vaporizer was programmed as follows: temperature 280°C; total carrier gas (helium) flow rate 35 mL/min; split ratio 50 : 1; constant gas flow rate through the column, 0.7 mL/min.

The general methodology for testing catalytic systems in the process of ethylene oligomerization was described earlier [13].

Synthesis of ligands

Method for the synthesis of 1,2-bis(diphenylphosphanyl)acetylene (**1**)

A solution of 50.0 g (0.23 mol) of diphenyl(chloro)-phosphine, 1.30 g (6.81 mmol) of copper(I) iodide, 57.4 g (0.568 mol) of triethylamine, and 4.0 g (5.68 mmol) of $NiBr_2(PPh_3)_2$ in 100 mL of toluene was stirred at 60°C for 18 h in an atmosphere of dry and purified acetylene obtained from 73.0 g (1.135 mol) calcium carbide. Next, the solvent was evaporated, and 1,2-bis(diphenylphosphanyl)acetylene was isolated from the residue by chromatography (silica gel; eluent: chloroform–hexane (1 : 10)).

Yield: 32.0 g (71%). ^{1}H NMR spectrum (400 MHz, $CDCl_3$): δ (ppm) 7.34–7.46 (13H, m, H_{Ar}), 7.60–7.73 (8H, m, H_{Ar}). $^{31}P\{^1H\}$ NMR spectrum (161.98 MHz, $CDCl_3$): δ (ppm) −32.13 (1P, s). ^{13}C NMR spectrum (101 MHz, $CDCl_3$): δ (ppm) 106.9, 128.7, 129.2, 132.6 132.8, 135.7. $C_{26}H_{20}P_2$. Calculated (%): C, 79.18; H ,5.11. Found (%): C, 79.13; H, 5.19.

Method for the synthesis of acetylene-1,2-diylbis(diphenylphosphine oxide) (**2**)

A 35% aqueous solution of hydrogen peroxide (6.51 mL (76.1 mmol)) was added dropwise with stirring to a solution (cooled to 5°C) of 10.0 g (25.4 mmol) of compound **1** in 100 mL of THF, and the obtained mixture was then stirred for 30 min. Next, 50 mL of a saturated aqueous solution of sodium thiosulfate was added and left to stir for 30 min, after which the obtained mixture was extracted 3 times with 50 mL of chloroform. The organic layer was dried over sodium sulfate, the solvent was evaporated, and acetylene-1,2-diylbis(diphenylphosphine oxide) was obtained in the form of a light yellow powder.

Yield: 9.30 g (86%). ^{1}H NMR spectrum (400 MHz, $CDCl_3$): δ (ppm) 7.45–7.55 (8H, m, H_{Ar}), 7.57–7.64 (4H, m, HAr), 7.73–7.85 (8H, m, HAr). $^{31}P\{^1H\}$ NMR spectrum (161.98 MHz, $CDCl_3$): δ (ppm) 9.78 (1P, s). ^{13}C NMR spectrum (101 MHz, $CDCl_3$): δ (ppm) 99.9, 129.2, 129.7, 131.0, 131.1, 132.2, 133.3. $C_{26}H_{20}P_2O_2$. Calculated (%): C, 73.24; H, 4.73. Found (%): C, 73.18; H, 4.75.

Method for the synthesis of (2*H*-1,2,3-triazole-4,5-diyl)bis(diphenylphosphine oxide) (**3**)

To a solution of 9.30 g (21.8 mmol) of compound **2** in 75 mL of THF, 1.84 g (28.3 mmol) of sodium azide was added, and the obtained mixture was stirred at a temperature of 50°C for 10 h. Then the reaction mass was evaporated to dryness, and the residue was dissolved in 100 mL of water and acidified to pH 5. The formed precipitate was filtered off, washed on the filter with water 3 times, 30 mL each, and dried in a vacuum.

Yield: 7.80 g (76%). ^{1}H NMR spectrum (400 MHz, $CDCl_3$): δ (ppm) 7.45–7.55 (8H, m, H_{Ar}), 7.57–7.66 (84H, m, H_{Ar}), 7.83 (8H, dd, J = 13.83, 8.11 Hz, H_{Ar}). $^{31}P\{^1H\}$ NMR spectrum (161.98 MHz, $CDCl_3$): δ (ppm) 9.18 (1P, s). $C_{26}H_{21}N_3P_2O_2$. Calculated (%): C, 66.53; H, 4.51; N, 8.95. Found (%): C, 66.37; H, 4.49; N, 8.74.

General procedure for the synthesis of (1-R-1*H*-1,2,3-triazol-4,5-diyl)-bis(diphenylphosphine oxides)

To a solution of 9.30 g (21.8 mmol) of compound **2** in 75 mL of THF, 28.3 mmol of azide was added, and the obtained mixture was stirred at a temperature of 50°C for 10 h. Then the reaction mass was cooled to room temperature (20°C), the solvent was evaporated, and the residue was chromatographed (silica gel; eluent: ethyl acetate–hexane (3 : 1)).

(1-hexyl-1*H*-1,2,3-triazol-4,5-diyl)-bis(diphenylphosphine oxide) (**4**)

Yield: 8.80 g (73%). ^{1}H NMR spectrum (400 MHz, dimethyl sulfoxide-d_6 (DMSO-d_6)): δ (ppm) 0.74–0.84 (3H, m, CH_3), 1.09–1.19 (6H, m, 3 x CH_2), 1.75 (2H, q, J = 7.23 Hz, CH_2), 5.05 (2H, t, J = 7.31 Hz, CH_2), 7.21–7.59 (16H, m, H_{Ar}), 7.85–7.91 (4H, m, H_{Ar}). $^{31}P\{^1H\}$ NMR spectrum (161.98 MHz, $CDCl_3$): δ (ppm) 18.05 (1P, s), 21.22 (1P, s). $C_{32}H_{33}N_3P_2O_2$. Calculated (%): C, 69.43; H, 6.01; N, 7.59. Found (%): C, 69.50; H, 6.39; N, 7.44.

(1-(2-octylthioethyl)-1*H*-1,2,3-triazol-4,5-diyl)-bis(diphenylphosphine oxide) (**5**)

Yield: 10.80 g (77%). ^{1}H NMR spectrum (400 MHz, CD_2Cl_2): δ (ppm) 0.92 (3H, t, J = 6.83 Hz, CH_3), 1.19–1.61 (12H, m, 6 x CH_2), 2.41–2.57 (2H, m, CH_2), 2.87–3.01 (2H, m, CH_2), 2.88–3.02 (2H, m, CH_2), 5.25 (2H, t, J = 7.31 Hz, CH_2), 7.27–7.58 (16H, m, H_{Ar}), 7.83–8.00 (4H, m, H_{Ar}). $^{31}P\{^1H\}$ NMR spectrum (161.98 MHz, CD_2Cl_2): δ (ppm) 17.00 (1P, s), 20.88 (1P, s). $C_{36}H_{41}N_3P_2O_2S$. Calculated (%): C, 67.38; H, 6.44; N, 6.55. Found (%): C, 67.57; H, 6.39; N, 6.45.

General procedure for the synthesis of (2-(alkyl)-2*H*-1,2,3-triazol-4,5-diyl)-bis(diphenylphosphine oxides)

To a solution of 9.30 g (21.8 mmol) of compound **2** in 75 mL of THF, 1.84 g (28.3 mmol) of sodium azide was added, and the mixture was stirred at a temperature of 50°C for 10 h. Then the reaction mass was cooled to room temperature (20°C), and the formed precipitate was filtered off. To the filtrate, 21.8 mmol of alkyl iodide was added, and the mixture was heated at 70°C with reflux and stirring for 8 h. Then the reaction mass was cooled to room temperature, the precipitate was filtered off, the filtrate was evaporated, and the residue was chromatographed (silica gel; eluent: ethyl acetate–hexane (3 : 1)). As a result, compounds **6**–**11** were obtained.

(2-(methyl)-2*H*-1,2,3-triazol-4,5-diyl)-bis(diphenylphosphine oxide) (**6**)

Yield: 6.50 g (62%). ^{1}H NMR spectrum (400 MHz, C_6D_6): δ (ppm) 4.31 (3H, s, CH_3), 7.31–7.75 (20H, m, H_{Ar}). $^{31}P\{^1H\}$ NMR spectrum (161.98 MHz, C_6D_6): δ (ppm) 18.65 (1P, s). $C_{27}H_{23}N_3P_2O_2$. Calculated (%): C, 67.08; H, 4.80; N, 8.69. Found (%): C, 67.00; H, 4.79; N, 8.64.

(2-(butyl)-2*H*-1,2,3-triazol-4,5-diyl)-bis(diphenylphosphine oxide) (**7**)

Yield: 7.60 g (66%). ^{1}H NMR spectrum (400 MHz, $CDCl_3$): δ (ppm) 0.91 (3H, t, J = 7.31 Hz, CH_3), 1.28–1.34 (2H, m, CH_2), 1.93 (2H, q, J = 7.15 Hz, CH_2), 4.50 (2H, t, J = 7.15 Hz, CH_2), 7.31–7.36 (8H, m, H_{Ar}), 7.43–7.50 (4H, m, H_{Ar}), 7.67–7.73 (8H, m, H_{Ar}). ^{31}P{^{1}H} NMR spectrum (161.98 MHz, $CDCl_3$): δ (ppm) 21.81 (1P, s). $C_{30}H_{29}N_3P_2O_2$. Calculated (%): C, 68.56; H, 5.56; N, 8.00. Found (%): C, 68.47; H, 5.60; N, 7.95.

(2-(hexyl)-2*H*-1,2,3-triazol-4,5-diyl)-bis(diphenylphosphine oxide) (**8**)

Yield: 8.60 g (71%). ^{1}H NMR spectrum (400 MHz, DMSO-d_6): δ (ppm) 0.93 (3H, t, J = 6.83 Hz, CH_3), 1.31–1.38 (4H, m, 2 x CH_2), 1.77–1.87 (2H, m, CH_2), 3.17–3.30 (2H, m, CH_2), 4.53 (2H, t, J = 6.83 Hz, CH_2), 7.33–7.46 (8H, m, H_{Ar}), 7.51–7.58 (4H, m, H_{Ar}), 7.62–7.66 (8H, m, H_{Ar}). ^{31}P{^{1}H} NMR spectrum (161.98 MHz, DMSO-d_6): δ (ppm) 17.90 (1P, s). $C_{32}H_{33}N_3P_2O_2$. Calculated (%): C, 69.43; H, 6.01; N, 7.59. Found (%): C, 69.40; H, 6.09; N, 7.57.

(2-(octyl)-2*H*-1,2,3-triazol-4,5-diyl)-bis(diphenylphosphine oxide) (**9**)

Yield: 8.50 g (67%). ^{1}H NMR spectrum (400 MHz, DMSO-d_6): δ (ppm) 0.79–0.92 (3H, m, CH_3), 1.10–1.35 (4H, m, 2 x CH_2), 1.68–1.91 (6H, m, 3 x CH_2), 3.12–3.26 (2H, m, CH_2), 4.50 (2H, t, J = 6.99 Hz, CH_2), 7.34–7.47 (8H, m, H_{Ar}), 7.45–7.55 (4H, m, H_{Ar}), 7.65–7.78 (8H, m, H_{Ar}). ^{31}P{^{1}H} NMR spectrum (161.98 MHz, DMSO-d_6): δ (ppm) 17.62 (1P, s). $C_{34}H_{37}N_3P_2O_2$. Calculated (%): C, 70.21; H, 6.41; N, 7.22. Found (%): C, 70.21; H, 6.45; N, 7.19.

(2-(allyl)-2*H*-1,2,3-triazol-4,5-diyl)-bis(diphenylphosphine oxide) (**10**)

Yield: 8.30 g (75%). ^{1}H NMR spectrum (400 MHz, CD_2Cl_2): δ (ppm) 5.40 (2H, d, J = 6.36 Hz, CH_2), 5.22–5.35 (2H, m, =CH_2), 6.0–6.13 (1H, m, =CH), 7.35–7.38 (8H, m, H_{Ar}), 7.48–7.58 (4H, m, H_{Ar}), 7.61–7.74 (12H, m, H_{Ar}). ^{31}P{^{1}H} NMR spectrum (161.98 MHz, CD_2Cl_2): δ (ppm) 18.37 (1P, s). $C_{29}H_{25}N_3P_2O_2$. Calculated (%): C, 68.37; H, 4.95; N, 8.25. Found (%): C, 68.29; H, 4.91; N, 8.23.

(2-(hex-5-en-1-yl)-2*H*-1,2,3-triazol-4,5-diyl)-bis(diphenylphosphine oxide) (**11**)

Yield: 7.85 g (65%). ^{1}H NMR spectrum (400 MHz, DMSO-d_6): δ (ppm) 1.07–1.30 (2H, m, CH_2), 1.77–1.85 (2H, m, CH_2), 1.87–1.95 (2H, m, CH_2), 4.54 (2H, t, J = 6.68 Hz, $CH_2CH{=}CH_2$), 4.89–4.96 (2H, m, $CH{=}CH_2$), 5.63–5.75 (1H, m, $CH{=}CH_2$), 7.39–7.48 (8H, m, H_{Ar}) 7.55 (12H, d, J = 11.44 Hz). ^{31}P{^{1}H} NMR spectrum (161.98 MHz, DMSO-d_6): δ (ppm) 15.82 (1P, s). $C_{32}H_{31}N_3P_2O_2$. Calculated (%): C, 69.68; H, 5.67; N, 7.62. Found (%): C, 69.67; H, 5.59; N, 7.57.

General procedure for the reduction of diphenylphosphine oxides to obtain ligands L1–L9

A 250-mL magnetically stirred three-neck round-bottom flask with an inert gas supply line and a dropping funnel was charged with 0.014 mol of one of compounds **3**–**11** and 75 mL of absolute toluene. To the obtained solution, 11.5 g (0.085 mol) of trichlorosilane and then 20.1 g (0.255 mol) of pyridine were added dropwise in an argon atmosphere. The reaction mixture was stirred at 90°C for 2 h and next filtered, the filtrate was evaporated, and the residue was chromatographed (silica gel; eluent: ethyl acetate–hexane (1:10)). As a result, **L1**–**L9** ligands were obtained.

4,5-bis(diphenylphosphanyl)-2*H*-1,2,3-triazole (**L1**)

Yield: 2.50 g (41%). Retention factor R_f = 0.22 (Sorbfil); eluent: ethyl acetate–hexane (1 : 2). ^{1}H NMR spectrum (300 MHz, $CDCl_3$): δ (ppm) 7.21–7.56 (20H, m, H_{Ar}), 12.42 (1H, br. s, NH). ^{31}P{^{1}H} NMR spectrum (161.98 MHz, $CDCl_3$): δ (ppm) −36.26 (1P, s), −2.49 (1P, s). $C_{26}H_{21}N_3P_2$. Calculated (%): C, 71.39; H, 4.84; N, 9.61. Found (%): C, 71.37; H, 4.79; N, 9.64.

4,5-bis(diphenylphosphanyl)-1-hexyl-1*H*-1,2,3-triazole (**L2**)

Yield: 5.46 g (74%). R_f = 0.37 (Sorbfil); eluent: ethyl acetate–hexane (1 : 2). ^{1}H NMR spectrum (400 MHz, $CDCl_3$): δ (ppm) 0.80–0.87 (3H, m, CH_3), 1.10–1.23 (6H, m, 3 x CH_2), 1.65–1.69 (2H, m, CH_2), 4.40 (2H, t, J = 7.63 Hz, CH_2), 7.19–7.36 (20H, m, H_{Ar}). ^{31}P{^{1}H} NMR spectrum (161.98 MHz, $CDCl_3$): δ (ppm) –36.09 (1P, m). $C_{32}H_{33}N_3P_2$. Calculated (%): C, 73.69; H, 6.38; N, 8.06. Found (%): C, 73.87; H, 6.49; N, 7.94.

4,5-bis(diphenylphosphanyl)-1-((2-octylthio)-ethyl)-1*H*-1,2,3-triazole (**L3**)

Yield: 6.50 g (76%). R_f = 0.41 (Sorbfil); eluent: ethyl acetate–hexane (1 : 2). ^{1}H NMR spectrum (400 MHz, $CDCl_3$): δ (ppm) 0.84–0.97 (3H, m, CH_3), 1.23–1.55 (12H, m, 6 x CH_2), 2.38–2.47 (2H, m, CH_2), 2.76–2.85 (2H, m, CH_2), 4.66 (2H, t, J = 7.63 Hz, CH_2), 7.27–7.41 (20H, m, H_{Ar}). ^{31}P{^{1}H} NMR spectrum (161.98 MHz, $CDCl_3$): δ (ppm) −36.09 (1P, s). $C_{36}H_{41}N_3P_2S$. Calculated (%): C, 70.91; H, 6.78; N, 6.89. Found (%): C, 70.87; H, 6.79; N, 6.82.

4,5-bis(diphenylphosphanyl)-2-(methyl)-2*H*-1,2,3-triazole (**L4**)

Yield: 4.30 g (68%). R_f = 0.33 (Sorbfil); eluent: ethyl acetate–hexane (1 : 2). ^{1}H NMR spectrum (500 MHz, $CDCl_3$): δ (ppm) 4.23 (3H, m, CH_3), 7.24–7.31 (12H, m, H_{Ar}), 7.36–7.44 (8H, m, H_{Ar}). $^{31}P\{^1H\}$ NMR spectrum (202 MHz, $CDCl_3$): δ (ppm) −34.29 (1P, s). $C_{27}H_{23}N_3P_2$. Calculated (%): C, 71.83; H, 5.14; N, 9.31. Found (%): C, 71.85; H, 5.29; N, 9.34.

4,5-bis(diphenylphosphanyl)-2-(butyl)-2*H*-1,2,3-triazole (**L5**)

Yield: 4.40 g (64%). R_f = 0.35 (Sorbfil); eluent: ethyl acetate–hexane (1 : 2). ^{1}H NMR spectrum (400 MHz, CD_2Cl_2): δ (ppm) 0.90–0.96 (3H, m, CH_3), 1.25–1.35 (2H, m, CH_2), 1.88–1.96 (2H, m, CH_2), 4.47 (2H, t, J = 7.13 Hz, CH_2), 7.24–7.30 (12H, m, H_{Ar}), 7.37–7.44 (8H, m, H_{Ar}). $^{31}P\{^1H\}$ NMR spectrum (202 MHz, $CDCl_3$): δ (ppm) −34.10 (1P, s). $C_{30}H_{29}N_3P_2$. Calculated (%): C, 73.01; H, 5.92; N, 8.51. Found (%): C, 73.07; H, 5.84; N, 8.50.

4,5-bis(diphenylphosphanyl)-2-(hexyl)-2*H*-1,2,3-triazole (**L6**)

Yield: 5.53 g (75%). R_f = 0.37 (Sorbfil); eluent: ethyl acetate–hexane (1 : 2). ^{1}H NMR spectrum (400 MHz, CD_2Cl_2): δ (ppm) 0.89–0.97 (3H, m, CH_3), 1.25–1.36 (6H, m, 3 x CH_2), 1.90–2.03 (2H, m, CH_2), 4.50 (2H, t, J = 6.99 Hz, CH_2), 7.28–7.46 (20H, m, H_{Ar}). $^{31}P\{^1H\}$ NMR spectrum (161.98 MHz, CD_2Cl_2): δ (ppm) −34.02 (1P, s). $C_{32}H_{33}N_3P_2$. Calculated (%): C, 73.69; H, 6.38; N, 8.06. Found (%): C, 73.70; H, 6.39; N, 7.97.

4,5-bis(diphenylphosphanyl)-2-(octyl)-2*H*-1,2,3-triazole (**L7**)

Yield: 5.23 (68%). R_f = 0.40 (Sorbfil); eluent: ethyl acetate–hexane (1 : 2). ^{1}H NMR spectrum (400 MHz, CD_2Cl_2): δ (ppm) 0.88–0.98 (3H, m, CH_3), 1.18–1.31 (10H, m, 5 x CH_2), 1.87–1.99 (2H, m, CH_2), 4.47 (2H, t, J = 6.99 Hz, CH_2), 7.25–7.43 (20H, m, H_{Ar}). $^{31}P\{^1H\}$ NMR spectrum (161.98 MHz, CD_2Cl_2): δ (ppm) −34.14 (1P, s). $C_{34}H_{37}N_3P_2$. Calculated (%): C, 74.30; H, 6.79; N, 7.65. Found (%): C, 74.37; H, 6.89; N, 7.54.

4,5-bis(diphenylphosphanyl)-2-(allyl)-2*H*-1,2,3-triazole (**L8**)

Yield: 5.00 g (75%). R_f = 0.34 (Sorbfil); eluent: ethyl acetate–hexane (1 : 2). ^{1}H NMR spectrum (400 MHz, CD_2Cl_2): δ (ppm) 5.08–5.35 (4H, m, 2 x CH_2), 6.04–6.22 (1H, m, CH), 7.24–7.31 (12H, m, H_{Ar}), 7.28–7.69 (20H, m, H_{Ar}). $^{31}P\{^1H\}$ NMR spectrum (161.98 MHz, CD_2Cl_2): δ (ppm) −33.69 (1P, s). $C_{29}H_{25}N_3P_2$. Calculated (%): C, 72.95; H, 5.28; N, 8.80. Found (%): C, 72.94; H, 5.21; N, 8.74.

4,5-bis(diphenylphosphanyl)-2-(hex-5-en-1-yl)-2*H*-1,2,3-triazole (**L9**)

Yield: 5.24 g (71%). R_f = 0.37 (Sorbfil); eluent: ethyl acetate–hexane (1 : 2). ^{1}H NMR spectrum (400 MHz, CD_2Cl_2): δ (ppm) 1.18–1.48 (3H, m, CH_3), 1.90–2.17 (4H, m, CH_2), 4.51 (2H, t, J = 6.99 Hz, =$CHCH_2$), 4.87–5.17 (2H, m, CH_2=CH), 5.79 (1H, ddt, J = 17.05, 10.29, 6.68, 6.68 Hz, CH_2=CH), 7.24–7.53 (20H, m, H_{Ar}). $^{31}P\{^1H\}$ NMR spectrum (161.98 MHz, CD_2Cl_2): δ (ppm) −34.00 (1P, s). $C_{32}H_{31}N_3P_2$. Calculated (%): C, 73.98; H, 6.01; N, 8.09. Found (%): C, 73.97; H, 5.99; N, 8.07.

General procedure for the synthesis of chromium complexes

In a 100-mL magnetically stirred Schlenk flask, 3.39 g (9.1 mmol) of the $Cr(THF)_3Cl_3$ complex and 10.1 mmol of the corresponding **L1**–**L9** ligand were placed. The flask was evacuated and filled with argon. In a stream of argon, 50 mL of absolute THF was added, the obtained suspension was degassed and stirred at room temperature (20°C) for 18 h. The solvent was evaporated, and the residue was washed with hexane and dried in vacuum. As a result, **K1**–**K9** complexes were obtained.

(4,5-bis(diphenylphosphanyl)-2*H*-1,2,3-triazole)-P,P)-tetrahydrofurantrichlorochrome(III) (**K1**)

Yield of the final **K1** chromium complex in the form of a blue-violet powder: 4.30 g (71%). Melting point T_{melt} > 250°C. $C_{30}H_{29}Cl_3CrN_3OP_2$. Calculated (%): C, 53.97; H, 4.35; N, 6.29. Found (%): C, 53.66; H, 4.26; N, 6.44.

(4,5-bis(diphenylphosphanyl)-1-hexyl-1*H*-1,2,3-triazole)-P,P)-tetrahydrofurantrichlorochrome(III) (**K2**)

Yield of the final **K2** chromium complex, in the form of a blue-violet powder: 5.60 g (82%). T_{melt} > 250°C. $C_{36}H_{41}Cl_3CrN_3OP_2$. Calculated (%): C, 57.52; H, 5.46; N, 5.59. Found (%): C, 56.37; H, 5.29; N, 5.94.

(4,5-bis(diphenylphosphanyl)-1-(2-octylthio)ethyl)-1*H*-1,2,3-triazole-P,P)-tetrahydrofurantrichlorochrome(III) (**K3**)

Yield of the final **K3** chromium complex in the form of a blue-violet powder: 5.90 g (77%). T_{melt} > 250°C. $C_{40}H_{47}Cl_3CrN_3OP_2S$. Calculated (%): C, 57.34; H, 5.61; N, 5.02. Found (%): C, 56.88; H, 5.91; N, 5.18.

(4,5-bis(diphenylphosphanyl)-2-(methyl)-2*H*-1,2,3-triazole)-P,P)-tetrahydrofurantrichlorochrome(III) (**K4**)

Yield of the final **K4** chromium complex in the form of a dark blue powder: 4.35 g (70%). T_{melt} > 250°C. $C_{31}H_{31}Cl_3CrN_3OP_2$. Calculated (%): C, 54.62; H, 4.55; N, 6.16. Found (%): C, 53.79; H, 4.24; N, 6.12.

(4,5-bis(diphenylphosphanyl)-2-(butyl)-2*H*-1,2,3-triazole)-P,P)-tetrahydrofurantrichlorochrome(III) (**K5**)

Yield of the final **K5** chromium complex in the form of a blue powder: 4.50 g (68%). T_{melt} > 250°C. $C_{34}H_{37}Cl_3CrN_3OP_2$. Calculated (%): C, 56.43; H, 5.12; N, 5.81. Found (%): C, 55.89; H, 5.04; N, 5.88.

(4,5-bis(diphenylphosphanyl)-2-(hexyl)-2*H*-1,2,3-triazole)-P,P)-tetrahydrofurantrichlorochrome(III) (**K6**)

Yield of the final **K6** chromium complex in the form of a blue powder: 5.82 g (85%). T_{melt} > 250°C. $C_{36}H_{41}Cl_3CrN_3OP_2$. Calculated (%): C, 57.52; H, 5.46; N, 5.59. Found (%): C, 57.37; H, 5.29; N, 5.44.

(4,5-bis(diphenylphosphanyl)-2-(octyl)-2*H*-1,2,3-triazole)-P,P)-tetrahydrofurantrichlorochrome(III) (**K7**)

Yield of the final **K7** chromium complex in the form of a blue-violet powder: 5.34 g (75%). T_{melt} > 250°C. $C_{38}H_{45}Cl_3CrN_3OP_2$. Calculated (%): C, 58.53; H, 5.78; N, 5.39. Found (%): C, 58.31; H, 5.56; N, 5.54.

(4,5-bis(diphenylphosphanyl)-2-(allyl)-2*H*-1,2,3-triazole)-P,P)-tetrahydrofurantrichlorochrome(III) (**K8**)

Yield of the final **K8** chromium complex in the form of a blue powder: 5.89 g (76%). T_{melt} > 250°C. $C_{33}H_{33}Cl_3CrN_3OP_2$. Calculated (%): C, 56.01; H, 4.67; N, 5.94. Found (%): C, 56.20; H, 4.51; N, 5.98.

(4,5-bis(diphenylphosphanyl)-2-(hex-5-en-1-yl)-2*H*-1,2,3-triazole)-P,P)-tetrahydrofurantrichlorochrome(III) (**K9**)

Yield of the final **K9** chromium complex in the form of a blue-violet powder: 4.93 g (72%). T_{melt} > 250°C. $C_{36}H_{39}Cl_3CrN_3OP_2$. Calculated (%): C, 57.67; H, 5.21; N, 5.60. Found (%): C, 57.29; H, 5.16; N, 5.54.

RESULTS AND DISCUSSION

L1–**L9** ligands were synthesized according to Schemes 1 and 2. 4,5-Disubstituted 1,2,3-triazoles were obtained by reacting activated alkynes with various azides [13, 14]. Acetylene-1,2-diylbis(diphenylphosphine oxide) (**2**), a key compound for the synthesis of a whole series of ligands, was produced by reacting diphenylchlorophosphine with acetylene in the presence of copper and nickel salts. This was followed by oxidation of diphenylphosphanylacetylene with an aqueous solution of hydrogen peroxide.

To synthesize NH-triazole **L1**, the corresponding diphenylphosphine oxide was obtained from acetylene-1,2-diylbis(diphenylphosphine oxide) and sodium azide. It was then reduced in the trichlorosilane–pyridine system.

In order to obtain **L2** and **L3**, acetylene-1,2-diylbis(diphenylphosphine oxide) was reacted with alkyl azides, and then the intermediate dioxo derivative thus formed was reduced in the trichlorosilane–pyridine system.

In the synthesis of **L4**–**L9** ligands, the sodium triazole salt obtained was treated with the corresponding alkyl halide. As a result, after chromatographic separation, the resulting diphenylphosphine oxides were reduced. 4,5-disubstituted triazoles easily form complexes with various metals [14–17], due to which the reaction can occur under mild conditions.

K1–**K9** complexes were synthesized from the corresponding **L1**–**L9** ligands and a commercially available chromium source $Cr(THF)_3Cl_3$ with yields of up to 85% (Schemes 1 and 2).

K1–**K9** chromium complexes are paramagnetic compounds and NMR spectroscopy cannot directly confirm their structure. However, NMR spectroscopy data on their precursors, diphosphine ligands **L1**–**L9**, as well as elemental analysis data on **K1**–**K9** make it possible for their structure and composition to be unambiguously determined.

Chromium complexes based on polydentate heteroatomic ligands in combination with organoaluminum compounds as activators are highly efficient catalytic systems for ethylene oligomerization [18, 19]. The resulting **K1**–**K9** complexes were tested for activity in the process of ethylene oligomerization using methylaluminoxane as an initiator. Table 1 presents the characteristics of the process of oligomerization in toluene at an operating temperature of 95°C and a pressure of 2.0 MPa. It was previously shown that chromium complexes with polydentate organic ligands demonstrate the highest performance under these conditions [11]. The process of ethylene oligomerization using **K1**–**K9** complexes is nonselective. The productivity ranges from 2.0 to 51.0 kg/g_{Cr}·h, depending on the compounds

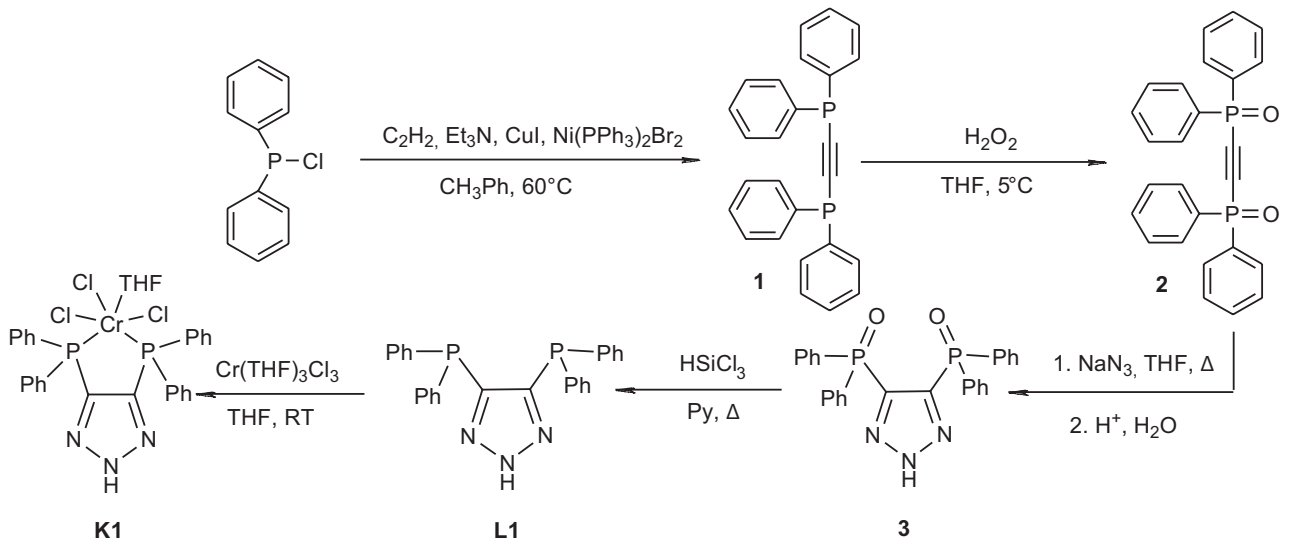

Scheme 1. Synthesis of **L1** ligand and **K1** complex

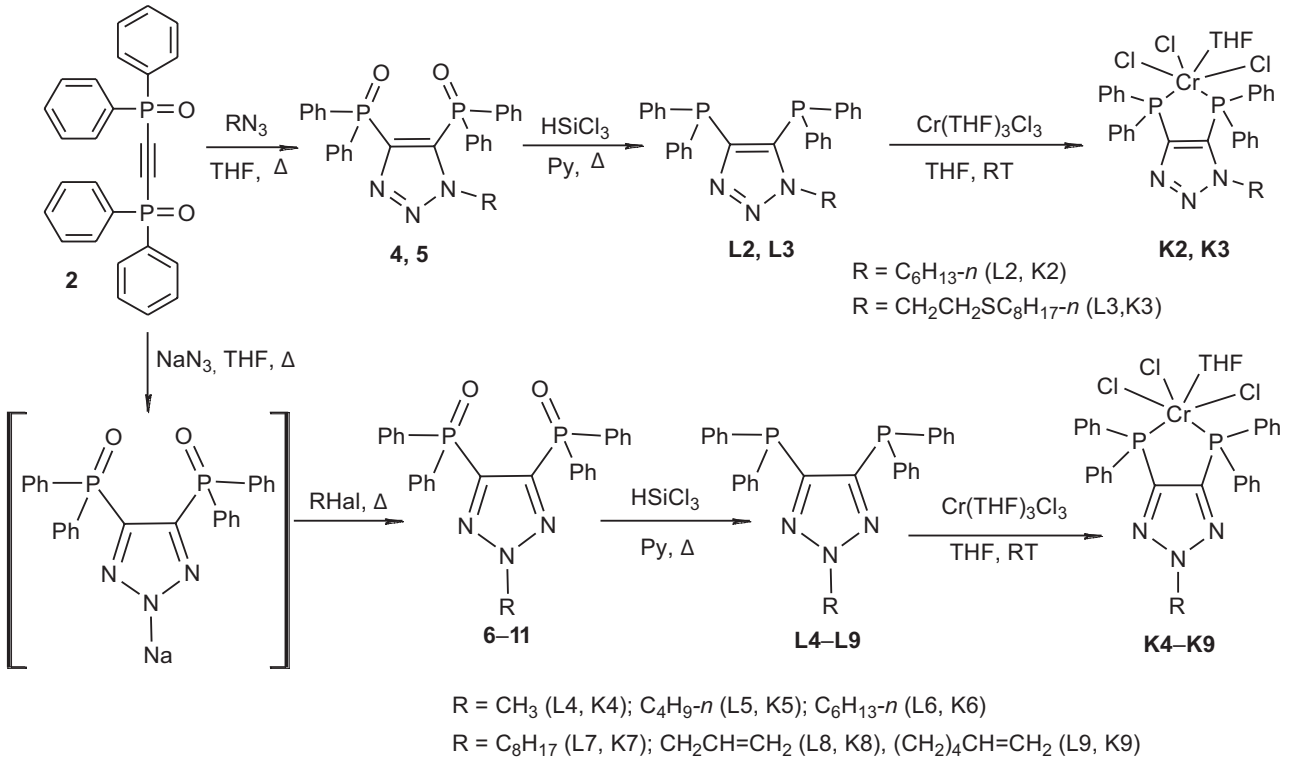

Scheme 2. Synthesis of **L2**–**L9** ligands and **K2**–**K9** complexes

used. The amount of the polymer by-product also varies significantly (Table 1). For all the systems being studied, the main olefin fraction is the C_{10}–C_{18} fraction (from 27.0 to 47.0 wt %). The content of the C_{20}–C_{30} heavy olefin fraction in the oligomerization products ranges from 4.4 to 13.0 wt %. The selectivity of the process for the final product (individual higher alpha-olefin or alpha-olefin fraction) is determined both by the process conditions and, to a large extent, by the structure and electronic properties of the organic ligands included in the metal complex catalysts. In this regard, three groups can be distinguished among the tested catalytic systems: based on **K1**–**K3**, **K4**–**K8**, and **K9** complexes. The process of ethylene oligomerization with the participation of the first group is characterized by low productivity and selectivity for C_{10}–C_{18} fractions, as

well as high polymer content, making it inefficient. Systems based on **K4**–**K8** enable the process to be carried out with a fairly high productivity from 11.0 to 43.0 kg/g_{Cr}·h and a moderate content of the polymer product (no more than 3.1 wt %). The best performance of the process is demonstrated by the system based on the **K9** complex with the ligand 4,5-bis(diphenylphosphanyl)-2-(hex-5-en-1-yl)-2*H*-1,2,3-triazole. This ensures selectivities for the C_{10}–C_{18} and C_{20}–C_{30} olefin fractions in products of 47.4 and 13.0 wt %, respectively, with a productivity of more than 50 kg/g_{Cr}·h.

The literature shows that the use of additives of organozinc compounds to the catalytic system for ethylene oligomerization, Cr(PNP)Cl_3/MAO (PNP = = $Ph_2PN(i\text{-}Pr)PPh_2$), helps to increase the productivity and selectivity of the process for the fraction of C_{10}–C_{22} oligomers (35–60 wt %). It also reduces the amount of the polyethylene by-product and its molecular weight [5]. In view of this, we used a diethylzinc solution as a coactivator for the catalytic system based on the **K7** complex and MAO (Table 2) at a temperature of 95°C and a pressure of 2.0 MPa, in order to increase the productivity of the process and reduce the yield of the polymer product. As a result, it was shown that increasing the ratio of diethylzinc in the composition of the catalytic system to the molar ratio [Cr] : [MAO] : [$ZnEt_2$] = = 1 : 850 : 300 leads to a decrease in the content of the polymer product to 0.2 wt %, and to an increase in selectivity for the C_{10}–C_{18} fraction to 49.1 wt % with an increase in productivity to 57.9 kg/g_{Cr}·h.

We studied the effect of temperature on the oligomerization process for the catalytic system with the component ratio [Cr] : [MAO] : [$ZnEt_2$] = = 1 : 850 : 300 (Table 3). As a result, it was shown that reducing the temperature to 45°C leads to an increase in the yield of the polymer by-product, as well as a decrease in selectivity for the C_{10}–C_{18} fraction to 46.3 wt %, and a drop in process productivity by a factor of 2.5. An increase in temperature to 110°C also leads to a decrease in the selectivity of the process for C_{10}–C_{18} fractions, whereas the productivity decreases to 14.4 kg/g_{Cr}·h. This shows that the optimal temperature regime for the oligomerization process using the **K7** complex activated by methylaluminoxane and diethylzinc is 95°C.

Table 1. Results of testing of catalytic systems based on **K1**–**K9** complexes activated by methylaluminoxane in the reaction of oligomerization of ethylene

Complex	Productivity, kg/g_{Cr}·h	Selectivity, wt %						
		Polymer	C_4	C_6	C_8	C_{10}–C_{18}	C_{20}–C_{30}	C_{30+}
K1	5.0	5.3	16.7	13.4	14.3	40.2	9.1	1.0
K2	2.0	10.5	28.5	13.3	13.9	29.4	4.4	–
K3	3.0	18.9	15.2	10.0	18.5	27.0	10.5	–
K4	43.0	1.4	10.4	16.6	15.5	46.8	8.8	0.5
K5	17.0	3.1	9.3	14.9	14.2	46.4	11.2	0.9
K6	28.0	1.9	10.8	17.2	16.0	46.9	6.8	0.4
K7	21.0	1.7	9.5	14.9	14.8	46.7	11.7	0.7
K8	11.0	1.6	11.4	13.9	14.6	44.7	12.2	1.6
K9	51.0	1.9	8.5	14.6	14.6	47.4	13.0	–

Experimental conditions: 75-mL autoclave with magnetic stirrer; solvent: toluene (25.0 mL); loading of chromium complexes **K1**–**K9**, 0.85 μmol; activator, MAO; molar ratio [Cr] : [MAO] = 1 : 850; temperature, 95°C; pressure, 2.0 MPa; duration of the experiment, 0.5 h.

Table 2. Effect of diethylzinc as a coactivator of the catalytic system of ethylene oligomerization based on the **K7** complex

Molar ratio [Cr] : [MAO] : [$ZnEt_2$]	Productivity, $kg/g_{Cr}·h$	Selectivity, wt %						
		Polymer	C_4	C_6	C_8	C_{10}–C_{18}	C_{20}–C_{30}	C_{30+}
1 : 850 : 0	21.0	1.7	9.5	14.9	14.8	46.7	11.7	0.7
1 : 850 : 100	54.7	1.3	9.0	16.4	15.4	50.5	7.1	0.3
1 : 850 : 300	57.9	0.2	10.0	16.7	14.7	49.1	8.8	0.5
1 : 850 : 600	44.5	–	11.5	18.2	15.1	47.5	7.3	0.4

Experimental conditions: 75-mL autoclave with magnetic stirrer; solvent, toluene (25.0 mL); loading of chromium complexes **K7**, 0.85 μmol; activator, MAO; coactivator, $ZnEt_2$; temperature, 95°C; pressure, 2.0 MPa; duration of the experiment, 0.5 h.

Table 3. Parameters of the process of ethylene oligomerization based on the **K7** complex activated by a mixture of methylaluminoxane and diethylzinc at various temperatures

Temperature, °C	Productivity, $kg/g_{Cr}·h$	Selectivity, wt %						
		Polymer	C_4	C_6	C_8	C_{10}–C_{18}	C_{20}–C_{30}	C_{30+}
45	20.9	0.7	12.8	19.1	15.5	46.3	5.5	0.1
75	44.3	0.5	11.3	17,3	15.0	48.4	7.2	0.3
95	57.9	0.2	10.0	16.7	14.7	49.1	8.8	0.5
110	14.4	–	12.8	18.8	14.3	47.1	6.8	0.2

Experimental conditions: 75-mL autoclave with magnetic stirrer; solvent, toluene (25.0 mL); loading of chromium complex **K7**, 0.85 μmol, activator, MAO; molar ratio [Cr] : [MAO] : [$ZnEt_2$] = 1 : 850 : 300; pressure, 2.0 MPa; the duration of the experiment, 0.5 h.

CONCLUSIONS

The study proposed a method for the preparation of **L1**–**L9** bis(diphenylphosphanyl)triazole ligands from commercially available compounds. This allows the introduction of alkyl and alkenyl substituents with different carbon chain lengths into the triazole fragment. This also improves the solubility of chromium complexes in the reaction medium, and affects the steric and electronic properties of ligands which control the catalytic activity and selectivity of the ethylene oligomerization process. New chromium complexes **K1**–**K9** based on 4,5-bis(diphenylphosphanyl)-*H*-1,2,3-triazoles were synthesized (with yields of 69–85%). The process of ethylene oligomerization using catalytic systems based on them was also studied. It was determined that systems based on the **K4**–**K7** and **K9** complexes enable the process of ethylene oligomerization to be carried out with a fairly high level of productivity (up to 51.0 kg/g_{Cr} h). The maximum selectivity for C_{10}–C_{18} and C_{20}–C_{30} olefins was observed for the catalytic system based on the **K9** complex with a hexenyltriazole ligand. It was shown that the introduction of diethylzinc as a coactivator of the catalytic system based on the **K7** complex leads to an increase in the productivity of the system and an increase in selectivity for the heavy olefin fraction. Further study of catalytic systems based on 4,5-bis(diphenylphosphanyl)-*H*-1,2,3-triazoles is promising with regard to determining the characteristics of the oligomerization process, as well as in creating catalysts for the production of linear alpha-olefins with a high level of selectivity for the fraction of higher alpha-olefins intended for the synthesis of synthetic oils and fuel additives.

Authors' contributions

A.A. Senin – conducting experiments on the synthesis complex compounds and oligomerization of ethylene, systematization and processing of the results obtained, and writing the text of the article.

K.B. Polyanskii – conducting experiments on the synthesis of ligands and complex compounds, systematization and processing of the results obtained, and writing the text of the article.

A.M. Sheloumov – review of publications on the topic of the article, writing the text of the article.

V.V. Afanasiev – development of the research concept and systematization of the results obtained, and preparation of materials for publication.

T.M. Yumasheva – development of the research concept and scientific guidance at all stages of the study.

K.B. Rudyak – guidance at all stages of the study.

S.V. Vorobyev – critical revision with the introduction of valuable intellectual content in the article and preparation of materials for publication.

The authors declare no conflicts of interest.

REFERENCES

1. Singh T., Naveen S.M. A review paper on production of linear alpha-olefins by undergoing oligomerization of ethylene. *Int. J. Eng. Appl. Sci. Technol.* 2017;2(4):83–86.
2. Golub' F.S., Bolotov V.A. Parmon V.N. Current Trends in the Processing of Linear Alpha Olefins into Technologically Important Products: Part 2. *Catal. Ind*. 2021;13(3):203–215. https://doi.org/10.1134/S2070050421030053
3. Bariashir C., Huang C., Solan G.A., Sun W-H. Recent advances in homogeneous chromium catalyst design for ethylene tri-, tetra-, oligo- and polymerization. *Coord. Chem. Rev*. 2019;385:208–229. https://doi.org/10.1016/j.ccr.2019.01.019
4. Ittel S.D. *Lubricant Component*: US Pat. 2013/0012675 A1. Publ. 10.01.2013.
5. Son K., Waymouth R.M. Selective Ethylene Oligomerization in the Presence of ZnR_2: Synthesis of Terminally-Functionalized Ethylene Oligomers. *Organometallics*. 2010;29(16):3515–3520. https://doi.org/10.1021/om100503v
6. Liu J., Wang J., Chen L., Zhang N., Lan T., Wang L. Ethylene Oligomerization Study Bearing Nickel(II) and Cobalt(II) Complexes with N, O-Donor Schiff Bases as Ligands. *ChemistrySelect*. 2019;4(47):13959–13963. https://doi.org/10.1002/slct.201903599
7. Tembe G.L., Pillai S.M., Satish S., Ravindranathan M. *Process for the Preparation of Low Molecular Weight Alpha Olefins*: US Pat. 6013850. Publ. 01.11.2000.
8. Xiao L., Gao R., Zhang M., Li Y., Cao X., Sun W.-H. 2-(1*H*-2-Benzimidazolyl)-6-(1-(arylimino)ethyl)pyridyl Iron(II) and Cobalt(II) Dichlorides: Syntheses, Characterizations, and Catalytic Behaviors toward Ethylene Reactivity. *Organometallics*. 2009;28(7):2225–2233. https://doi.org/10.1021/om801141n
9. Xiao L., Zhang M., Sun W.-H. Synthesis, characterization and ethylene oligomerization and polymerization of 2-(1*H*-2-benzimidazolyl)-6-(1-(arylimino)ethyl)pyridylchromium chlorides. *Polyhedron*. 2010;29(1):142–147. https://doi.org/10.1016/j.poly.2009.06.037
10. Wang Z., Mahmood Q., Zhang W., Sun W.-H. Chapter Two – Recent progress on the tridentate iron complex catalysts for ethylene oligo-/polymerization. *Advances in Organometallic Chemistry*. 2023;79:71–86. https://doi.org/10.1016/bs.adomc.2022.12.001
11. Cheredilin D.N., Sheloumov A.M., Senin A.A., Kozlova G.A., Afanas'ev V.V., Bespalova N.B. Catalytic Systems for Production of 1-Hexene by Selective Ethylene Trimerization. *Pet. Chem*. 2020;60(1):55–68. https://doi.org/10.1134/S0965544120010041 [Original Russian Text: Cheredilin D.N., Sheloumov A.M., Senin A.A., Kozlova G.A., Afanas'ev V.V., Bespalova N.B. Catalytic Systems for Production of 1-Hexene by Selective Ethylene Trimerization. *Neftekhimiya.* 2020;60(1):61–75 (in Russ.). https://doi.org/10.31857/S0028242120010049].
12. Yakhvarov D.G., Ganushevich Yu.S., Sinyashin O.G. *Novyi nikel'organicheskii sigma-kompleks-prekatalizator oligomerizatsii etilena* (*Novel Organonickel Sigma-Complex Ethylene Oligomerization Precatalyst*): RF Pat. 2400488. Publ. 27.09.2010 (in Russ.).

СПИСОК ЛИТЕРАТУРЫ

1. Singh T., Naveen S.M. A review paper on production of linear alpha-olefins by undergoing oligomerization of ethylene. *Int. J. Eng. Appl. Sci. Technol.* 2017;2(4):83–86.
2. Golub' F.S., Bolotov V.A. Parmon V.N. Current Trends in the Processing of Linear Alpha Olefins into Technologically Important Products: Part 2. *Catal. Ind*. 2021;13(3):203–215. https://doi.org/10.1134/S2070050421030053
3. Bariashir C., Huang C., Solan G.A., Sun W-H. Recent advances in homogeneous chromium catalyst design for ethylene tri-, tetra-, oligo- and polymerization. *Coord. Chem. Rev*. 2019;385:208–229. https://doi.org/10.1016/j.ccr.2019.01.019
4. Ittel S.D. *Lubricant Component*: US Pat. 2013/0012675 A1. Publ. 10.01.2013.
5. Son K., Waymouth R.M. Selective Ethylene Oligomerization in the Presence of ZnR_2: Synthesis of Terminally-Functionalized Ethylene Oligomers. *Organometallics*. 2010;29(16):3515–3520. https://doi.org/10.1021/om100503v
6. Liu J., Wang J., Chen L., Zhang N., Lan T., Wang L. Ethylene Oligomerization Study Bearing Nickel(II) and Cobalt(II) Complexes with N, O-Donor Schiff Bases as Ligands. *ChemistrySelect*. 2019;4(47):13959–13963. https://doi.org/10.1002/slct.201903599
7. Tembe G.L., Pillai S.M., Satish S., Ravindranathan M. *Process for the Preparation of Low Molecular Weight Alpha Olefins*: US Pat. 6013850. Publ. 01.11.2000.
8. Xiao L., Gao R., Zhang M., Li Y., Cao X., Sun W.-H. 2-(1*H*-2-Benzimidazolyl)-6-(1-(arylimino)ethyl)pyridyl Iron(II) and Cobalt(II) Dichlorides: Syntheses, Characterizations, and Catalytic Behaviors toward Ethylene Reactivity. *Organometallics*. 2009;28(7):2225–2233. https://doi.org/10.1021/om801141n
9. Xiao L., Zhang M., Sun W.-H. Synthesis, characterization and ethylene oligomerization and polymerization of 2-(1*H*-2-benzimidazolyl)-6-(1-(arylimino)ethyl)pyridylchromium chlorides. *Polyhedron*. 2010;29(1):142–147. https://doi.org/10.1016/j.poly.2009.06.037
10. Wang Z., Mahmood Q., Zhang W., Sun W.-H. Chapter Two – Recent progress on the tridentate iron complex catalysts for ethylene oligo-/polymerization. *Advances in Organometallic Chemistry*. 2023;79:71–86. https://doi.org/10.1016/bs.adomc.2022.12.001
11. Чередилин Д.Н., Шелоумов А.М., Сенин А.А., Козлова Г.А., Афанасьев В.В., Беспалова Н.Б. Каталитические системы процесса селективной тримеризации этилена для получения 1-гексена. *Нефтехимия*. 2020;60(1):61–75. https://doi.org/10.31857/S0028242120010049
12. Яхваров Д.Г., Ганушевич Ю.С., Синяшин О.Г. *Новый никель-органический сигма-комплекс-прекатализатор олигомеризации этилена*: Пат. 2400488 РФ. Заявка № 2009113396/04; заявл. 09.04.2009; опубл. 27.09.2010. Бюл. № 23.
13. Чередилин Д.Н., Шелоумов А.М., Сенин А.А., Козлова Г.А., Афанасьев В.В., Беспалова Н.Б. Каталитические свойства комплексов хрома на основе 1,2-бис(дифенилфосфино)-бензола в реакции олигомеризации этилена. *Нефтехимия*. 2019;59(8):918–936. https://doi.org/10.53392/00282421-2019-59-8-918

13. Cheredilin D.N., Sheloumov A.M., Senin A.A., Kozlova G.A., Afanas'ev V.V., Bespalova N.B. Catalytic Properties of Chromium Complexes Based on 1,2-Bis(diphenylphosphino)-benzene in the Ethylene Oligomerization Reaction. *Pet. Chem*. 2019;59(Suppl. 1):S72–S87. https://doi.org/10.1134/S0965544119130036
[Original Russian Text: Cheredilin D.N., Sheloumov A.M., Senin A.A., Kozlova G.A., Afanas'ev V.V., Bespalova N.B. Catalytic Properties of Chromium Complexes Based on 1,2-Bis(diphenylphosphino)benzene in the Ethylene Oligomerization Reaction. *Neftekhimiya.* 2019;59(8):918–936 (in Russ.). https://doi.org/10.53392/00282421-2019-59-8-918].
14. Rheingold A.L., Liable-Sands L.M., Trofimenko S. 4,5-Bis(diphenylthiophosphinoyl)-1,2,3-triazole, LT-S2: A new varidentate ligand containing diphenylthiophosphinoyl moieties. *Inorg. Chim. Acta.* 2002;330(1):38–43. https://doi.org/10.1016/S0020-1693(01)00706-X
15. Slutsky Smith E.A., Molev G., Botoshansky M., Gandelman M. Modifiable bidentate systems *via* N–C rearrangement in triazoles. *Chem. Commun*. 2011;47(1):319–321. https://doi.org/10.1039/c0cc02033h
16. Radhakrishna L., Kunchur H.S., Namdeo P.K., Butcher R.J., Balakrishna M.S. New 1,2,3-triazole based bis- and trisphosphine ligands: synthesis, transition metal chemistry and catalytic studies. *Dalton Trans.* 2020;49(11):3434–3449. https://doi.org/10.1039/C9DT04302K
17. Hassin A., Fridman N., Gandelman M. Bidentate Triazolate-Based Ligand System: Synthesis, Coordination Modes, and Cooperative Bond Activation. *Organometallics.* 2020;39(3):425–432. https://doi.org/10.1021/acs.organomet.9b00775
18. Zhao X., Ma X., Kong W., Zhan J. Switchable ethylene tri-/tetramerization with high catalytic performance: Subtle effect presented by P-alkyl substituent of PCCP ligands. *J. Catal.* 2022;415:95–101. https://doi.org/10.1016/j.jcat.2022.09.030
19. Alferov K.A., Belov G.P., Meng Y. Chromium catalysts for selective ethylene oligomerization to 1-hexene and 1-octene: Recent results. *Appl. Catal. A*. 2017;542:71–124. https://doi.org/10.1016/j.apcata.2017.05.014

14. Rheingold A.L., Liable-Sands L.M., Trofimenko S. 4,5-Bis(diphenylthiophosphinoyl)-1,2,3-triazole, LT-S2: A new varidentate ligand containing diphenylthiophosphinoyl moieties. *Inorg. Chim. Acta.* 2002;330(1):38–43. https://doi.org/10.1016/S0020-1693(01)00706-X
15. Slutsky Smith E.A., Molev G., Botoshansky M., Gandelman M. Modifiable bidentate systems *via* N–C rearrangement in triazoles. *Chem. Commun*. 2011;47(1):319–321. https://doi.org/10.1039/c0cc02033h
16. Radhakrishna L., Kunchur H.S., Namdeo P.K., Butcher R.J., Balakrishna M.S. New 1,2,3-triazole based bis- and trisphosphine ligands: synthesis, transition metal chemistry and catalytic studies. *Dalton Trans.* 2020;49(11):3434–3449. https://doi.org/10.1039/C9DT04302K
17. Hassin A., Fridman N., Gandelman M. Bidentate Triazolate-Based Ligand System: Synthesis, Coordination Modes, and Cooperative Bond Activation. *Organometallics.* 2020;39(3):425–432. https://doi.org/10.1021/acs.organomet.9b00775
18. Zhao X., Ma X., Kong W., Zhan J. Switchable ethylene tri-/tetramerization with high catalytic performance: Subtle effect presented by P-alkyl substituent of PCCP ligands. *J. Catal.* 2022;415:95–101. https://doi.org/10.1016/j.jcat.2022.09.030
19. Alferov K.A., Belov G.P., Meng Y. Chromium catalysts for selective ethylene oligomerization to 1-hexene and 1-octene: Recent results. *Appl. Catal. A*. 2017;542:71–124. https://doi.org/10.1016/j.apcata.2017.05.014

About the authors

Aleksey A. Senin, Researcher, Laboratory of Polymer Products and Polymer Additives, United Research and Development Center (55/1-2, Leninskii pr., Moscow, 119333, Russia). E-mail: SeninAA@rdc.rosneft.ru. RSCI SPIN-code 1408-6980, https://orcid.org/0000-0002-0015-6588

Kirill B. Polyanskii, Cand. Sci. (Chem.), Leading Researcher, Laboratory of Polymer Products and Polymer Additives, United Research and Development Center (55/1-2, Leninskii pr., Moscow, 119333, Russia). E-mail: PolyanskiyKB@rdc.rosneft.ru. RSCI SPIN-code 3667-1922, https://orcid.org/0000-0002-1302-8868

Aleksey M. Sheloumov, Cand. Sci. (Chem.), Leading Researcher, Laboratory of Polymer Products and Polymer Additives, United Research and Development Center (55/1-2, Leninskii pr., Moscow, 119333, Russia). E-mail: SheloumovAM@rdc.rosneft.ru. https://orcid.org/0000-0002-6930-3451

Vladimir V. Afanasiev, Cand. Sci. (Chem.), Deputy Head, Laboratory of Polymer Products and Polymer Additives, United Research and Development Center" (55/1-2, Leninskii pr., Moscow, 119333, Russia). E-mail: AfanasievVV@rdc.rosneft.ru. https://orcid.org/0000-0001-8388-104X

Tatiana M. Yumasheva, Cand. Sci. (Chem.), Head of the Laboratory of Polymer Products and Polymer Additives, United Research and Development Center (55/1-2, Leninskii pr., Moscow, 119333, Russia). E-mail: YumashevaTM@rdc.rosneft.ru. https://orcid.org/0009-0002-4625-1895

Konstantin B. Rudyak, Dr. Sci. (Eng.), General Director, United Research and Development Center (55/1-2, Leninskii pr., Moscow, 119333, Russia). E-mail: RudyakKB@rdc.rosneft.ru

Stepan V. Vorobyev, Cand. Sci. (Chem.), Associate Professor, Department of Organic Chemistry and Petroleum Chemistry, National University of Oil and Gas "Gubkin University" (65-1, Leninskii pr., Moscow, 119991, Russia). E-mail: vorobyev.o@gubkin.ru. Scopus Author ID 57204359493, ResearcherID O-8748-2016, RSCI SPIN-code 6838-77915, https://orcid.org/0000-0001-6042-6394

Об авторах

Сенин Алексей Александрович, научный сотрудник лаборатории полимерных продуктов и полимерных присадок, ООО «Объединенный центр исследований и разработок» (ООО «РН ЦИР») (119333, Россия, Москва, Ленинский пр-т, д. 55/1, стр. 2). E-mail: SeninAA@rdc.rosneft.ru. SPIN-код РИНЦ 1408-6980, https://orcid.org/0000-0002-0015-6588

Полянский Кирилл Борисович, к.х.н., ведущий научный сотрудник лаборатории полимерных продуктов и полимерных присадок, ООО «Объединенный центр исследований и разработок» (ООО «РН ЦИР») (119333, Россия, Москва, Ленинский пр-т, д. 55/1, стр. 2). E-mail: PolyanskiyKB@rdc.rosneft.ru. SPIN-код РИНЦ 3667-1922, https://orcid.org/0000-0002-1302-8868

Шелоумов Алексей Михайлович, к.х.н., ведущий научный сотрудник лаборатории полимерных продуктов и полимерных присадок, ООО «Объединенный центр исследований и разработок» (ООО «РН ЦИР») (119333, Россия, Москва, Ленинский пр-т, д. 55/1, стр. 2). E-mail: SheloumovAM@rdc.rosneft.ru. https://orcid.org/0000-0002-6930-3451

Афанасьев Владимир Владимирович, к.х.н., заместитель заведующего лабораторией полимерных продуктов и полимерных присадок, ООО «Объединенный центр исследований и разработок» (ООО «РН ЦИР») (119333, Россия, Москва, Ленинский пр-т, д. 55/1, стр. 2). E-mail: AfanasievVV@rdc.rosneft.ru. https://orcid.org/0000-0001-8388-104X

Юмашева Татьяна Модестовна, к.х.н., заведующий лабораторией полимерных продуктов и полимерных присадок, ООО «Объединенный центр исследований и разработок» (ООО «РН ЦИР») (119333, Россия, Москва, Ленинский пр-т, д. 55/1, стр. 2). E-mail: YumashevaTM@rdc.rosneft.ru. https://orcid.org/0009-0002-4625-1895

Рудяк Константин Борисович, д.т.н., генеральный директор ООО «Объединенный центр исследований и разработок» (ООО «РН ЦИР») (119333, Россия, Москва, Ленинский пр-т, д. 55/1, стр. 2). E-mail: RudyakKB@rdc.rosneft.ru.

Воробьев Степан Владимирович, к.х.н., доцент кафедры органической химии и химии нефти, ФГАОУ ВО «Российский государственный университет нефти и газа (национальный исследовательский университет) имени И.М. Губкина» (119991, Россия, Москва, Ленинский пр-т, д. 65, корп. 1). E-mail: vorobyev.o@gubkin.ru. Scopus Author ID 57204359493, ResearcherID O-8748-2016, SPIN-код РИНЦ 6838-77915, https://orcid.org/0000-0001-6042-6394

Translated from Russian into English by V. Glyanchenko
Edited for English language and spelling by Dr. David Mossop

Tonkie Khimicheskie Tekhnologii = Fine Chemical Technologies.
2024;19(1):52–60 ISSN 2686-7575 (Online)

Synthesis and processing of polymers and polymeric composites
Синтез и переработка полимеров и композитов на их основе

UDC 547.245
https://doi.org/10.32362/2410-6593-2024-19-1-52-60

RESEARCH ARTICLE

Synthesis of copolymers based on divinylbenzene and dibenzocyclobutyldimethylsilane and a study of their functional characteristics

Anna V. Lobanova[1,✉], Konstantin S. Levchenko[2], Gregory E. Adamov[2], Pavel S. Smelin[2], Evgeniy P. Grebennikov[1], Alexey D. Kirilin[1]

[1] *MIREA – Russian Technological University (Lomonosov Institute of Fine Chemical Technologies), 119571 Russia*

[2] *Central Research Institute of Technology "Technomash," 121108 Russia*

✉ *Corresponding author, e-mail: anilovand@mail.ru*

Abstract

Objectives. To create new polymer materials based on organosilicon derivatives of benzocyclobutene and to study the possibility of their use as insulating dielectric layers in micro- and microwave electronics devices.

Methods. The synthesis of the dibenzocyclobutyldimethylsilane (diBCB-DMS) monomer was carried out from 4-brombenzocyclobutene through the production stage of the Grignard reagent. Copolymers based on divinylbenzene and dibenzocyclobutyldimethylsilane were obtained by means of thermal polymerization. The properties and structure of the copolymers thus obtained were studied using the following methods: thermogravimetric analysis, infrared spectroscopy, nuclear magnetic resonance (NMR), mass spectroscopy, and by means of high-frequency measurements of volt-ampere characteristics and volumetric resonator.

Results. diBCB-DMS was synthesized with a yield of 81.5%. The composition and structure were confirmed by ^{1}H and ^{13}C NMR spectroscopy. The dielectric constant of the diBCB-DMS homopolymer is ~2.6. The tangent of the dielectric loss angle at 1 GHz of the diBCB-DMS homopolymer is $2.3 \cdot 10^{-4}$. The tangent of the dielectric loss angle at 10 GHz of the diBCB-DMS homopolymer is $2.6 \cdot 10^{-4}$. The study of divinylbenzene and diBCB-DMS copolymers in different molar ratios on a thermogravimetric analyzer showed that the copolymers are able to withstand temperatures up to 470°C. The dielectric permittivity of diBCB-DMS and divinylbenzene copolymers in a molar ratio of 1 : 1 was 2.6. The values of the loss tangent at 1 and 10 GHz of copolymers in a molar ratio of 1 : 1 were $4.0 \cdot 10^{-4}$ and $5.6 \cdot 10^{-4}$, respectively.

Conclusion. Analysis of the obtained results shows that the samples of the diBCB-DMS homopolymer have the same dielectric characteristics as the samples based on diBCB-DMS and divinylbenzene, therefore, the introduction of divinylbenzene into the polymer structure does not worsen the dielectric parameters and such polimer materials can be used at high temperatures.

Keywords

benzocyclobutene, divinylbenzene, dibenzocyclobutyldimethylsilane, dielectric permittivity, loss tangent, TGA, materials for electronics, organosilicon polymers

Submitted: 16.02.2023
Revised: 15.06.2023
Accepted: 24.01.2024

For citation

Lobanova A.V., Levchenko K.S., Adamov G.E., Smelin P.S., Grebennikov E.P., Kirilin A.D. Synthesis of copolymers based on divinylbenzene and dibenzocyclobutyldimethylsilane and a study of their functional characteristics. *Tonk. Khim. Tekhnol. = Fine Chem. Technol*. 2024;19(1):52–60. https://doi.org/10.32362/2410-6593-2024-19-1-52-60

НАУЧНАЯ СТАТЬЯ

Синтез сополимеров на основе дивинилбензола и дибензоциклобутилдиметилсилана и исследование их функциональных характеристик

А.В. Лобанова[1],✉, К.С. Левченко[2], Г.Е. Адамов[2], П.С. Шмелин[2], Е.П. Гребенников[2], А.Д. Кирилин[1]

[1] *МИРЭА – Российский технологический университет (Институт тонких химических технологий им. М. В. Ломоносова), 119571 Россия*

[2] *Центральный научно-исследовательский технологический институт «Техномаш», 121108 Россия*

✉ *Автор для переписки, e-mail: anilovand@mail.ru*

Аннотация

Цели. Создание новых полимерных материалов на основе кремнийорганических производных бензоциклобутена и изучение возможности их использования в качестве изолирующих диэлектрических слоев в устройствах микро- и СВЧ-электроники.

Методы. Синтез мономера дибензоциклобутилдиметилсилана (diBCB-DMS) проводился из 4-бромбензоциклобутена через стадию получения реактива Гриньяра. Сополимеры на основе дивинилбензола и diBCB-DMS получали термополимеризацией. Исследование свойств и строение полученных сополимеров проводилось с помощью термогравиметрического анализа, инфракрасной спектроскопии, ядерного магнитного резонанса (ЯМР), масс-спектроскопии, а также методами высокочастотных измерений вольт-амперных характеристик и объемного резонатора.

Результаты. Синтезирован дибензоциклобутилдиметилсилан с выходом 81.5%, состав и строение которого подтверждены с помощью ^{1}H и ^{13}C ЯМР-спектроскопии. Диэлектрическая проницаемость гомополимера diBCB-DMS составила ~2.6. Тангенс угла диэлектрических потерь при 1 ГГц гомополимера diBCB-DMS равен $2.3\cdot10^{-4}$. Тангенс угла диэлектрических потерь при 10 ГГц гомополимера diBCB-DMS равен $2.6\cdot10^{-4}$. Исследование сополимеров дивинилбензола и diBCB-DMS в разном мольном соотношении на термогравиметрическом анализаторе показало, что сополимеры способны выдерживать температуру до 470°C. Диэлектрическая проницаемость сополимеров diBCB-DMS и дивинилбензола в мольном соотношении 1 : 1 составила 2.6. Значения тангенса угла диэлектрических потерь при 1 ГГц и 10 ГГц сополимеров в мольном соотношении 1 : 1 составили $4.0\cdot10^{-4}$ и $5.6\cdot10^{-4}$ соответственно.

Выводы. Анализ полученных результатов показывает, что образцы гомополимера diBCB-DMS имеют такие же диэлектрические характеристики, как и образцы на основе diBCB-DMS и дивинилбензола, следовательно, введение дивинилбензола в структуру полимера не ухудшает диэлектрические показатели, и такие полимерные материалы можно использовать при высоких температурах.

Ключевые слова

бензоциклобутен, дивинилбензол, дибензоциклобутилдиметилсилан, диэлектрическая проницаемость, тангенс угла потерь, ТГА, материалы для электроники, кремнийорганические полимеры

Поступила: 16.02.2023
Доработана: 15.06.2023
Принята в печать: 24.01.2024

Для цитирования

Лобанова А.В., Левченко К.С., Адамов Г.Е., Шмелин П.С., Гребенников Е.П., Кирилин А.Д. Синтез сополимеров на основе дивинилбензола и дибензоциклобутилдиметилсилана и исследование их функциональных характеристик. *Тонкие химические технологии*. 2024;19(1):52–60. https://doi.org/10.32362/2410-6593-2024-19-1-52-60

INTRODUCTION

The high level of interest in the creation of new polymer materials based on organosilicon derivatives of benzocyclobutene is due to the following reasons: its low dielectric constant (2.65); high breakdown voltage (5.3 MV/cm); high thermal stability (about 470°C); low moisture absorption; and good mechanical properties. These properties enable benzocyclobutene-based materials to be used as insulating dielectric layers, in order to create electronic and electro-optical components, including OLED devices [1], polymer waveguides [2], and others. Furthermore, micro- and microwave electronic devices, volumetric integrated circuits [3], bandpass filters [4], as well as devices using MEMS-on-CMOS technology [5] are manufactured on their basis. These devices are widely used in the military and space industries. The demand for such materials is increasing every year. Therefore, the development of and research into new polymer materials based on benzocyclobutene are still relevant to this day.

The synthesis of monomers of organosilicon derivatives of benzocyclobutene was carried out by several methods: the Heck reaction [6–8]; the Pierce–Rubinstein reaction [9–11]; hydrosilylation with the addition of a Karsted catalyst [12]; and through the stage of obtaining the Grignard reagent [13, 14]. The most convenient of these methods in laboratory conditions is synthesis through the stage of obtaining the Grignard reagent, since this does not require the use of expensive catalysts. For this reason, the dibenzocyclobutyldimethylsilane (diBCB-DMS) monomer was synthesized using the Grignard reagent in this study.

The objective of this study was to create new polymer materials based on organosilicon derivatives of benzocyclobutene and to examine the possibility of their use as insulating dielectric layers in micro- and microwave electronics devices.

EXPERIMENTAL

The diBCB-DMS monomer was synthesized according to the method described in [15]. All reagents were purchased from *Sigma-Aldrich* (USA). Dimethyldichlorosilane was purchased from *abcr GmbH* (Karlsruhe, Germany).

The synthesis of diBCB-DMS was carried out in two stages (Fig. 1).

In order to obtain the Grignard reagent, 4-brom obenzocyclobutene (0.9 mol) was added dropwise with vigorous stirring to a flask containing freshly distilled dry tetrahydrofuran (800 mL) and a mixture of magnesium powder (0.9 mol) and iodine (0.04 mol). The rate was such that the reaction temperature the mixture did not exceed 40°C. The resulting mixture was stirred for another 2 h at this temperature, and then the flask was placed in an ice bath and cooled to 0°C. After cooling the mixture, dimethyldichlorosilane (0.45 mol) was added dropwise at such a rate that the temperature of the reaction mixture did not exceed 10°C. The ice bath was then removed and the mixture was left at room temperature (20°C) overnight. The next day the mixture was diluted with hexane (100 mL). The resulting precipitate was filtered using a column filled with silica gel and washed with several portions of hexane. The filtrate was concentrated on a rotary evaporator. The remaining product was purified by means of vacuum distillation. All the reaction mixtures were analyzed by thin layer chromatography on Merck Silica gel 60 F254 UV-254 plates (*Merck*, Germany). The composition and structure of the resulting compound was confirmed by nuclear magnetic resonance (NMR) spectroscopy and infrared (IR) spectroscopy.

Figure 2 shows the first scheme for obtaining copolymers. According to this scheme, samples were prepared to study thermal stability with different molar ratios. The composition of the mixture was changed by adding diBCB-DMS, starting from 5 to 25 mol %.

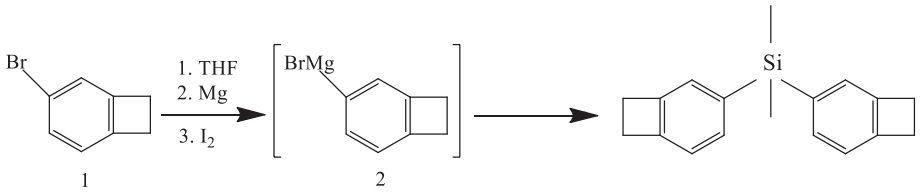

Fig. 1. Dibenzocyclobutyldimethylsilane (diBCB-DMS) synthesis scheme [15]

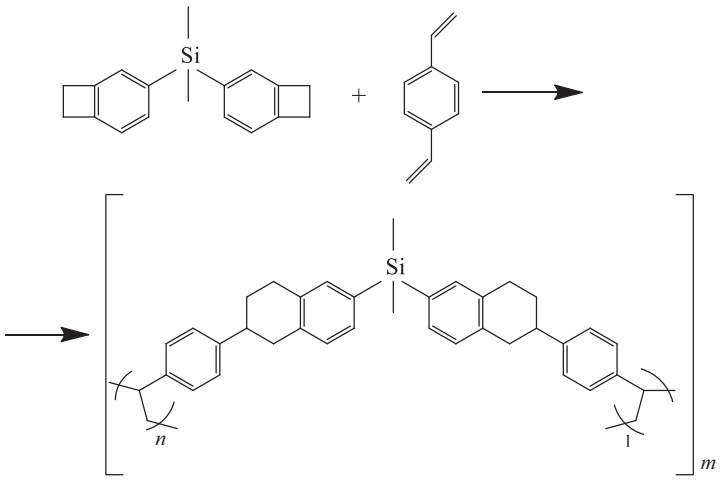

Fig. 2. Scheme for obtaining diBCB-DMS and divinylbenzene copolymers

In order to prepare samples, the mixture was placed in a crucible in an argon atmosphere. The crucibles were placed in an oven at 160–165°C for 30 min. Then the final heat treatment of the samples was carried out at a temperature of 250°C for 4 h.

Figure 3 shows the second production scheme. The addition of an inhibitor into the reaction is due to the fact that the different polymerization temperatures (220°C for diBCB-DMS and 80°C for divinylbenzene) make it difficult to obtain samples. Therefore, an inhibitor was used: 2-methylhydroquinone in an amount of 5% by weight of divinylbenzene.

In order to measure the dielectric constant and loss tangent, samples of 100% diBCB-DMS and a copolymer of diBCB-DMS and divinylbenzene in a 1 : 1 ratio were prepared using thermal polymerization. Samples of 5 × 5 cm in size and a thickness of about 2 mm were obtained. The samples were created using Teflon equipment specially made for this purpose.

Thermal polymerization of 100% diBCB-DMS was carried out in two steps. In the first stage, curing was carried out in a Teflon assembly, filled with ~6 mL of pure diBCB-DMS using a dispenser. The assembly was placed in an OFA-54-8 thermostat (*Esco*, Singapore) at a temperature of 160°C for 5 h, then at 220°C for 1.5 h. At the second stage, the sample was subjected to final heat treatment at a temperature of 250°C for 4 h.

A copolymer of diBCB-DMS and divinylbenzene was prepared in a similar manner. The reaction mixture consisting of diBCB-DMS (4.6 g), divinylbenzene (2.3 g) and 2-methylhydroquinone (0.115 g) was cured in two stages. Primary curing was carried out in a Teflon assembly, filled with ≥7 mL of a reaction mixture containing components in a given ratio using a dispenser. The assembly was placed in a Binder FD240 thermostat (*Binder*, Tuttlingen, Germany), at temperatures of 140°C for 1 h, 160°C for 2 h, 180°C for 1 h, 200°C for 1 h, and 220°C for 1 h. At the second stage, the sample was subjected to the final stage of heat treatment at a temperature of 250°C for 4 h.

Studies of the structure and functional properties of the diBCB-DMS homopolymer and copolymers of diBCB-DMS and divinylbenzene were carried out using the following methods: NMR spectroscopy; Fourier-transform IR spectroscopy; thermogravimetric analysis (TGA); high-frequency current-voltage measurement method (at 1 GHz); and a cavity resonator for measurements at 10 GHz.

DiBCB-DMS NMR spectra were recorded using a Bruker AM-300 spectrometer (*Bruker Corporation*, USA) in $CDCl_3$. Mass spectra were obtained on a Varian MAT CH-6 instrument (*Varian*, USA) using a direct input system. The ionization energy was 70 eV, and the acceleration voltage was 1.75 kV.

In order to obtain IR spectra of materials, an FSM2201 IR Fourier spectrometer (*Infraspec*, Russia) was used. To study polymer samples, they were first ground into powder, then KBr was added and the powder pressed into a tablet. The measurements were carried out in the range of 400–4000 cm^{-1}.

The thermal stability of the copolymer samples was measured by simultaneous TGA using a Shimadzu DTG-60 instrument (*Shimadzu Corporation*, Kyoto, Japan) in dynamic mode in the range of 20–700°C with heating rate of 10°C/min. The measurements were carried out in an argon/air flow at a rate of 50/100 mL/min.

The samples were studied by methods of high-frequency measurements of current-voltage characteristics and a cavity resonator consisting of an Agilent E4991A RF material properties and impedance analyzer. This enabled the dielectric characteristics to be measured at 1 GHz. The Agilent PNA E8361C network analyzer + 85072A 10-GHz cylindrical split resonator (*Agilent Technologies*, Santa Clara, California, USA), enabled dielectric measurements at 10 GHz.

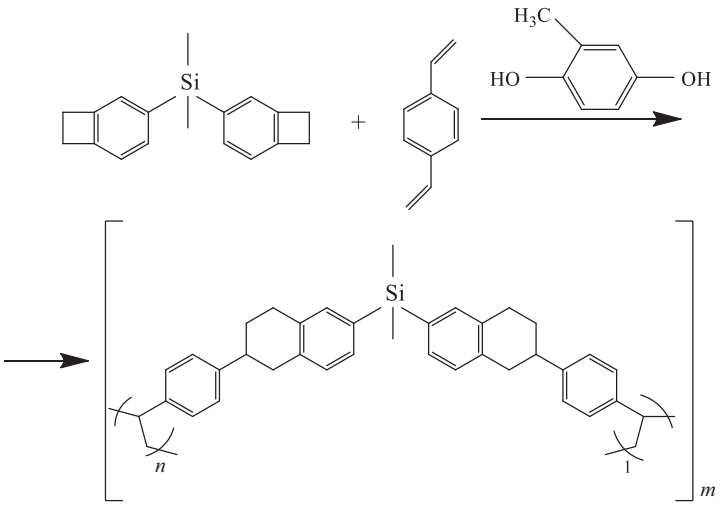

Fig. 3. Scheme for the production of diBCB-DMS and divinylbenzene in the presence of 2-methylhydroquinone

RESULTS AND DISCUSSION

As a result of synthesizing diBCB-DMS through the stage of obtaining the Grignard reagent, the product yield was 95.12 g (81.5%). The compound is a colorless liquid which hardens easily in the refrigerator. ^{1}H NMR spectrum (300 MHz, $CDCl_3$, δ, ppm): 7.62 (d, J = 7.3 Hz, 2H), 7.47 (s, 2H), 7.28 (d, J = 7.3 Hz, 2H), 3.40 (s, J = 3.4 Hz, 8H), 0.76 (s, 6H). ^{13}C NMR spectrum (76 MHz, $CDCl_3$, δ, ppm): 147.30, 145.75, 136.85, 132.73, 128.16, 122.13, 30.14, 30.01, −1.67. Mass spectrum, found: 265.1414; calculated: 265.1407.

Figure 4 shows the IR spectrum of diBCB-DMS. The band at 1463 cm^{-1} is characteristic of the CH_2 group of cyclobutene. The band at 1255 cm^{-1} indicates the presence of a Si–CH_3 bond in the monomer. The band at 1107 cm^{-1} is characteristic of the Si–C_6H_5 bond. Thus, IR spectroscopy data makes it possible to confirm the structure of the synthesized diBCB-DMS monomer.

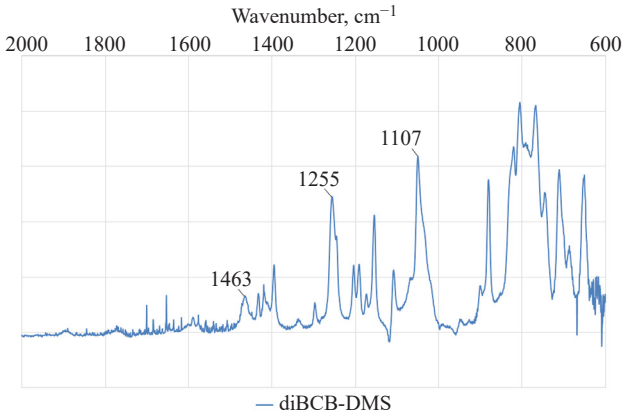

Fig. 4. IR spectrum of diBCB-DMS

Copolymers of diBCB-DMS and divinylbenzene prepared using the first method in different molar ratios were studied by means of TGA. The results of the study are presented in Fig. 5 and in Table 1. Figure 5 shows that polymer samples can withstand temperatures up to 470°C before thermal decomposition.

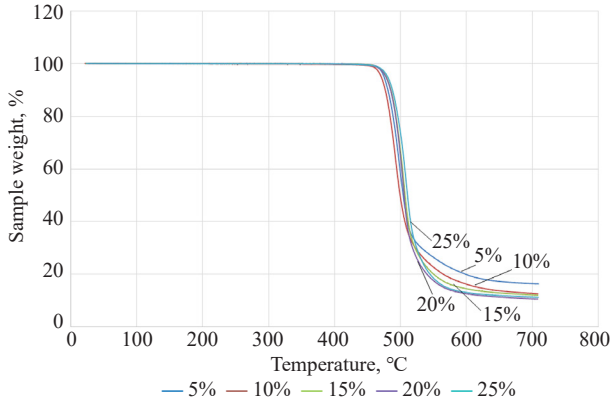

Fig. 5. Curves of polymerized samples with ratios from 5 to 25 mol % diBCB-DMS obtained by the TGA method

Table 1. The initial decomposition temperature of the samples

Ratio of components in the sample	Decomposition temperature, °C
5% diBCB-DMS and 95% divinylbenzene	474.9
10% diBCB-DMS and 90% divinylbenzene	470.7
15% diBCB-DMS and 85% divinylbenzene	478.4
20% diBCB-DMS and 80% divinylbenzene	477.7
25% diBCB-DMS and 75% divinylbenzene	480.4

A sample was obtained as a result of thermal polymerization of the 100% poly-diBCB-DMS monomer. A photograph is shown in Fig. 6. The sample was solid, transparent and had a yellowish tint. After secondary heat treatment, the appearance of the sample did not change.

Fig. 6. 100% diBCB-DMS sample after primary heat treatment: 160°C — 5 h, 220°C — 1.5 h

In the IR spectrum of diBCB-DMS (Fig. 7), a shift of the band 1463 cm^{-1} to 1490 cm^{-1} was observed. This characterizes the process of polymerization of the cyclobutene fragment [4+2]- or [4+4]-cycloaddition (Diels–Alder reaction), with the formation of a six- or eight-membered ring, respectively, containing methylene groups [17].

As a result of copolymerization of diBCB-DMS and divinylbenzene in the presence of an inhibitor in a 1 : 1 molar ratio, a solid, transparent sample with a yellowish tint was obtained (Figs. 8a and 8b). After the second stage of preparation, the sample retained its shape and remained transparent.

The IR spectrum of the resulting copolymer (Fig. 9) showed that during copolymerization, the band at 1630 cm^{-1}, characteristic for C=C vibrations in

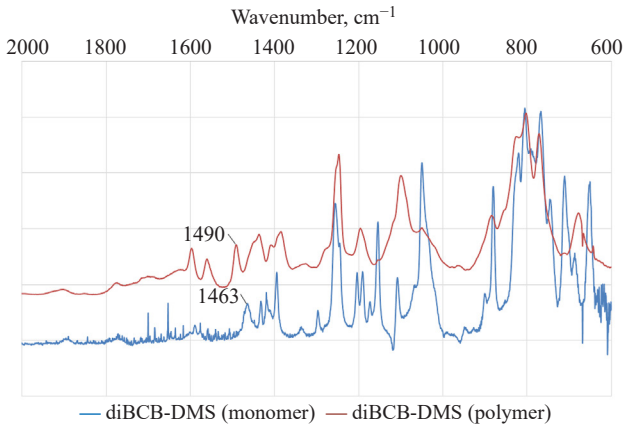

Fig. 7. IR spectrum of diBCB-DMS polymer

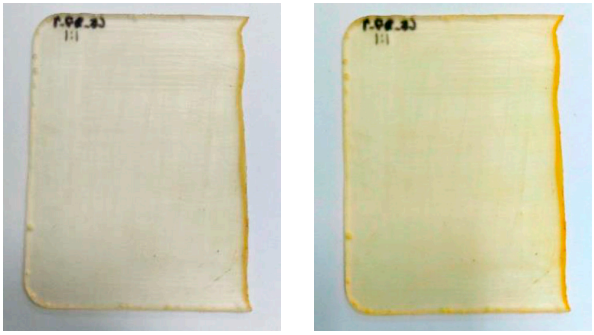

Fig. 8. Photograph of a sample of a diBCB-DMS and divinylbenzene mixture in a molar ratio of 1 : 1. (a) After primary heat treatment at temperature modes: 140°C — 1 h, 160°C — 2 h, 180°C — 1 h, 200°C — 1 h, and 220°C — 1 h; (b) after secondary temperature treatment at 250°C

divinylbenzene, decreases. The band at 985 cm^{-1}, characteristic of the bond of the aromatic ring with the vinyl group in divinylbenzene, also decreases. The band at 1463 cm^{-1}, characteristic of the CH_2 group of cyclobutene, shifts to 1490 cm^{-1}. The presence of changes and the formation of new bands indicates that cyclobutene opens, forming reactive double bonds (Fig. 10). These bonds enter into a [4+2] cycloaddition reaction with vinyl moieties of divinylbenzene. As a result, a copolymer based on diBCB-DMS and divinylbenzene is formed.

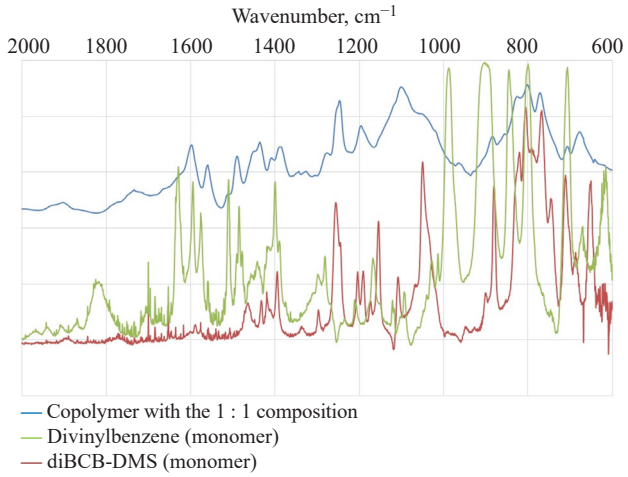

Fig. 9. IR spectrum of diBCB-DMS copolymer and divinylbenzene

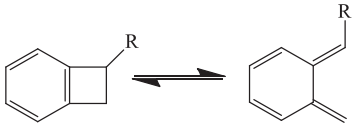

Fig. 10. Process of cyclobutene disclosure in benzocyclobutene

The dielectric characteristics of the samples of 100% diBCB-DMS thus obtained and copolymers of diBCB-DMS and divinylbenzene in a molar ratio of 1 : 1 are presented in Table 2. It can be seen that polymer samples made from a mixture of diBCB-DMS and divinylbenzene monomers in a 1 : 1 molar ratio have a similar dielectric constant and loss tangent when compared to a sample from 100% diBCB-DMS monomer. When divinylbenzene is added to the samples, the dielectric characteristics do not deteriorate. The alues obtained at 1 GHz and 10 GHz remain almost unchanged, allowing the material to be used at higher frequencies.

Table 2. Dielectric characteristics of a 100% diBCB-DMS monomer and a mixture of diBCB-DMS monomers and divinylbenzene

Sample	Dielectric Permittivity at 1 GHz, ε	Loss tangent at 1 GHz, α	Dielectric permittivity at 10 GHz, ε	Loss tangent at 10 GHz, α
Sample of 100% diBCB-DMS before thermal polymerization	2.653	$4.4 \cdot 10^{-4}$	2.730	$4.4 \cdot 10^{-4}$
Sample of 100% diBCB-DMS after thermal polymerization	2.671	$2.3 \cdot 10^{-4}$	2.711	$2.6 \cdot 10^{-4}$
5 cm × 5 cm sample from a monomer mixture before thermal polymerization	2.605	$3.8 \cdot 10^{-4}$	2.674	$7.0 \cdot 10^{-3}$
5 cm × 5 cm sample from a monomer mixture after thermal polymerization	2.619	$4.0 \cdot 10^{-4}$	2.616	$5.6 \cdot 10^{-4}$

CONCLUSIONS

The study shows that, based on organosilicon derivatives of benzocyclobutene, it is possible to obtain polymer materials and use them as insulating dielectric layers in micro- and microwave electronics devices. New thermal polymerizable materials based on diBCB-DMS and divinylbenzene in different molar ratios were obtained for the first time and their functional characteristics were studied. Thus, diBCB-DMS was obtained by a two-stage synthesis method with a yield of 81.5%. Also, the possibility of obtaining copolymers of divinylbenzene and diBCB-DMS was studied. DiBCB-DMS copolymers with divinylbenzene were obtained in the molar ratios: 1 : 1, 1 : 20, 1 : 10, 1 : 6.7, 1 : 5, 1 : 4.

It was established that when producing materials based on copolymers of diBCB-DMS and divinylbenzene, there is no deterioration in dielectric constant and loss tangent relative to the results obtained based on material from 100% diBCB-DMS. The resulting materials have been shown to be capable of withstanding temperatures up to 470°C.

Authors' contribution

All authors equally contributed to the research work.

The authors declare no conflicts of interest.

REFERENCES

1. Zuniga C.A., Abdallah J., Haske W., Zhang Y., Coropceanu I., Barlow S., Kippelen B., Marder S.R. Crosslinking using rapid thermal processing for the fabrication of efficient solution-processed phosphorescent organic light-emitting diodes. *Adv. Mater*. 2013;25(12):1739–1744. https://doi.org/10.1002/adma.201204518
2. Cao L., Grimault-Jacquin A.S., Zerounian N., Aniel F. Design and VNA-measurement of coplanar waveguide (CPW) on benzocyclobutene (BCB) at THz frequencies. *Infrared Phys. Technol.* 2014;63:157–164. https://doi.org/10.1016/j.infrared.2013.12.023
3. Chen Q., Yu W., Huang C., Tan Z., Wang Z. Reliability of through-silicon-vias (TSVs) with benzocyclobutene liners. *Microelectron. Reliab*. 2013;53(5):725–732. https://doi.org/10.1016/j.microrel.2012.12.012
4. Hyeon I.J., Park W.Y., Lim S., Baek C.W. K*u*-band bandpass filters using novel micromachined substrate integrated waveguide structure with embedded silicon vias in benzocyclobutene dielectrics. *Sens. Actuators A: Phys.* 2012;188(12):463–470. https://doi.org/10.1016/j.sna.2012.02.012
5. Makihata M., Tanaka S., Muroyama M., Matsuzaki S., Yamada H., Nakayama T., Esashi M. Integration and packaging technology of MEMS-on-CMOS capacitive tactile sensor for robot application using thick BCB isolation layer and backside-grooved electrical connection. *Sens. Actuators A: Phys.* 2012;188:103–110. https://doi.org/10.1016/j.sna.2012.04.032
6. Yang J., Sun M., Cheng Y., Xiao F. Study of benzocyclobutene-functionalized siloxane thermoset with a cyclic structure. In: *2011 12th International Conference on Electronic Packaging Technology and High Density Packaging*. IEEE. 2011. https://doi.org/10.1109/ICEPT.2011.6066841
7. Yang J., Cheng Y., Xiao F. Synthesis, thermal and mechanical properties of benzocyclobutene-functionalized siloxane thermosets with different geometric structures. *Eur. Polym. J.* 2012;48(4):751–760. https://doi.org/10.1016/j.eurpolymj.2012.01.006
8. Zuo X., Yu R., Shi S., Feng Z., Li Z., Yang S., Fan L. Synthesis and characterization of photosensitive benzocyclobutene-functionalized siloxane thermosets. *J. Polym. Sci. A: Polym. Chem.* 2009;47(22):6246–6258. https://doi.org/10.1002/pola.23668
9. Rabanzo-Castillo K.M., Kumar V.B., Söhnel T., Leitao E.M. Catalytic synthesis of oligosiloxanes mediated by an air stable catalyst, $(C_6F_5)_3B(OH_2)$. *Front. Chem.* 2020;8:477. https://doi.org/10.3389/fchem.2020.00477
10. Li J., Zhang Z., Zhu T., Li Z., Wang J., Cheng Y. Multi-benzocyclobutene functionalized siloxane monomers prepared by Piers-Rubinsztajn reaction for low-k materials. *Eur. Polym. J.* 2020;126:109562. https://doi.org/10.1016/j.eurpolymj.2020.109562
11. Chen X., Wang J., Sun J., Fang Q. High performance low dielectric polysiloxanes with high thermostability and low water uptake. *Mater. Chem. Front.* 2018;2(7):1397–1402. https://doi.org/10.1039/C8QM00104A

12. Shi Q., Pen, Q., Wu S., Long Q., Deng Y., Huan, Yang J. Benzocyclobutene-containing carbosilane monomers as a route to low-κ dielectric and low dielectric loss materials. *ChemistrySelect*. 2022;7(15):e202104413. https://doi.org/10.1002/slct.202104413
13. Yang J., Liu S., Zhu F., Huang Y., Li B., Zhang L. New polymers derived from 4-vinylsilylbenzocyclobutene monomer with good thermal stability, excellent film-forming property, and low-dielectric constant. *J. Polym. Sci. A: Polym. Chem.* 2011;49(2):381–391. https://doi.org/10.1002/POLA.24437
14. Sakellariou G., Ji H., Mays J.W., Baskaran D. Enhanced polymer grafting from multiwalled carbon nanotubes through living anionic surface-initiated polymerization. *Chem. Mater.* 2008;20(19):6217–6230. https://doi.org/10.1021/cm801449t
15. Levchenko K.S., Adamov G.E., Demin D.Y., Chicheva P.A., Chudov K.A., Shmelin P.S., Grebennikov E.P. Di(bicyclo[4.2.0]octa-1(6),2,4-trien-3-yl)dimethylsilane. *Molbank.* 2020;2020(4):M1160. https://doi.org/10.3390/M1160

About the authors

Anna V. Lobanova, Postgraduate Student, K.A. Andrianov Department of Chemistry and Technology of Organoelement Compounds, M.V. Lomonosov Institute of Fine Chemical Technologies, MIREA – Russian Technological University (86, Vernadskogo pr., Moscow, 119571, Russia). E-mail: anilovand@mail.ru. https://orcid.org/0000-0001-6196-3685

Konstantine S. Levchenko, Cand. Sci. (Chem.), Head of the Laboratory for the Development of New Functional Materials for Electronics and Photonics, Technomash (4, Ivana Franko ul., Moscow, 121108, Russia). E-mail: k.s.levchenko@gmail.com. Scopus Author ID 22938411800, RSCI SPIN-code 3126-0823, https://orcid.org/0000-0002-1509-7365

Grigory E. Adamov, Cand. Sci. (Eng.), of the Laboratory for the Development of Technology for Obtaining Functional Structures for Electronics and Photonics, Technomash (4, Ivana Franko ul., Moscow, 121108, Russia). E-mail: adamov@cnititm.ru. Scopus Author ID 24066302800, RSCI SPIN-code 8047-7805, https://orcid.org/0000-0001-8816-1666

Pavel S. Shmelin, Cand. Sci. (Eng.), Head of the Research Department of Functional Materials, Technomash (4, Ivana Franko ul., Moscow, 121108, Russia). E-mail: pshmelin@yandex.ru. Scopus Author ID 37073565000, ResearcherID F-7846-2014, https://orcid.org/0000-0003-4331-7959

Evgeny P. Grebennikov, Dr. Sci. (Eng.), Professor, Deputy Director, Innovation and Engineering Center of Microsensory, MIREA – Russian Technological University (78, Vernadskogo pr., Moscow, 119454, Russia). E-mail: Grebennikov@mirea.ru. Scopus Author ID 36860540400, https://orcid.org/0000-0001-7315-4084

Alexey D. Kirilin, Dr. Sci. (Chem.), Professor, Head of the K.A. Andrianov Department of Chemistry and Technology of Organoelement Compounds, M.V. Lomonosov Institute of Fine Chemical Technologies, MIREA – Russian Technological University (86, Vernadskogo pr., Moscow, 119571, Russia). E-mail: kirilinada@rambler.ru. Scopus Author ID 6603604447, ResearcherID O-9744-215, RSCI SPIN-code 5500-5030, https://orcid.org/0000-0001-9225-9551

Об авторах

Лобанова Анна Васильевна, аспирант кафедры химии и технологии элементоорганических соединений им. К.А. Андрианова, Институт тонких химических технологий им. М.В. Ломоносова, ФГБОУ ВО «МИРЭА – Российский технологический университет» (119571, Россия, Москва, пр-т Вернадского, д. 86). E-mail: anilovand@mail.ru. https://orcid.org/0000-0001-6196-3685

Левченко Константин Сергеевич, к.х.н., начальник лаборатории разработки новых функциональных материалов для электроники и фотоники, АО «ЦНИТИ «Техномаш» (121108, Россия, Москва, ул. Ивана Франко, д. 4). E-mail: k.s.levchenko@gmail.com. Scopus Author ID 22938411800, SPIN-код РИНЦ 3126-0823, https://orcid.org/0000-0002-1509-7365

Адамов Григорий Евгеньевич, к.т.н., начальник лаборатории разработки технологии получения функциональных структур для электроники и фотоники, АО «ЦНИТИ «Техномаш» (121108, Россия, Москва, ул. Ивана Франко, д. 4). E-mail: adamov@cnititm.ru. Scopus Author ID 24066302800, SPIN-код РИНЦ 8047-7805, https://orcid.org/0000-0001-8816-1666

Шмелин Павел Сергеевич, к.т.н., начальник научно-исследовательского отдела функциональных материалов, АО «ЦНИТИ «Техномаш» (121108, Россия, г. Москва, ул. Ивана Франко, д. 4). E-mail: pshmelin@yandex.ru. Scopus Author ID 37073565000, ResearcherID F-7846-2014, https://orcid.org/0000-0003-4331-7959

Гребенников Евгений Петрович, д.т.н. заместитель директора Инновационно-инжинирингового центра микросенсорики, ФГБОУ ВО «МИРЭА – Российский технологический университет» (119454, Россия, г. Москва, пр-т Вернадского, д. 78). E-mail: Grebennikov@mirea.ru. Scopus Author ID 36860540400, https://orcid.org/0000-0001-7315-4084

Кирилин Алексей Дмитриевич, д.х.н., профессор, заведующий кафедрой химии и технологии элементоорганических соединений им. К.А. Андрианова, Институт тонких химических технологий им. М.В. Ломоносова, ФГБОУ ВО «МИРЭА – Российский технологический университет» (119571, Россия, Москва, пр-т Вернадского, д. 86). E-mail: kirilinada@rambler.ru. Scopus Author ID 6603604447, ResearcherID O-9744-215, SPIN-код РИНЦ 5500-5030, https://orcid.org/0000-0001-9225-9551

Translated from Russian into English by H. Moshkov
Edited for English language and spelling by Dr. David Mossop

Tonkie Khimicheskie Tekhnologii = Fine Chemical Technologies.
2024;19(1):61–71 ISSN 2686-7575 (Online)

Chemistry and technology of inorganic materials
Химия и технология неорганических материалов

UDC 546.271
https://doi.org/10.32362/2410-6593-2024-19-1-61-71

RESEARCH ARTICLE

New approaches to the synthesis of substituted derivatives of the $[B_3H_8]^-$ anion

Anna A. Lukoshkova[1,✉], Alexandra T. Shulyak[1], Elizaveta E. Posypayko[1], Nikita A. Selivanov[1], Aleksey V. Golubev[1], Aleksey S. Kubasov[1], Alexander Yu. Bykov[1], Andrey P. Zhdanov[1], Konstantin Yu. Zhizhin[1,2], Nikolay T. Kuznetsov[1]

[1] *Kurnakov Institute of General and Inorganic Chemistry, Russian Academy of Sciences, Moscow, 119991 Russia*

[2] *MIREA – Russian Technological University (M.V. Lomonosov Institute of Fine Chemical Technologies), Moscow, 119571 Russia*

✉ *Corresponding author, e-mail: anya.lukoshkova@yandex.ru*

Abstract

Objectives. To develop methods for the synthesis of substituted derivatives of the octahydrotriborate anion. Such compounds can be considered as hydrogen storage, components of ionic liquids, precursors for the production of boride coatings using the traditional chemical vapor deposition method, and also as a building material for the production of higher boron hydrogen clusters.

Methods. Since substitution reactions are sensitive to moisture and atmospheric oxygen, the syntheses were carried out in a direct flow of argon or in a dry, sealed SPEKS GB02M glove box with a double gas purification unit and two airlocks. The reaction was initiated by cooling to 0°C, in order to avoid the formation of by-products. All the results were characterized using infrared (IR) and nuclear magnetic resonance (NMR) spectroscopies.

Results. The study presents a detailed study of the known methods for preparing substituted derivatives of the octahydrotriborate(1−) anion using dry hydrogen chloride as an electrophilic inductor and makes recommendations for improvement. In this method it is advisable to use cesium octahydrotriborate which facilitates the yield of the target product. New methods were proposed to initiate the substitution reaction in the $[B_3H_8]^-$-anion using *N*-chlorosuccinimide and bromine. Using these inductors, new substituted derivatives of the octahydrotriborate anion with *N*-nucleophiles were obtained and defined by means of IR and NMR spectroscopies: $[B_3H_7NCR]$, (R = Et, *i*-Pr, Ph) and $[B_3H_7NH_2R]$, (R = C_9H_{19} (INA), Bn), $[B_3H_7NHEt_2]$, as well as $Bu_4N[B_3H_7Hal]$, $Bu_4N[B_3H_6Hal_2]$, where Hal = Cl, Br. It was also established that hydrogen bromide is released during the reaction with bromine and amines. This immediately protonates the amine which requires additional heating of the reaction mixture. The study also established that the reaction mechanism with *N*-chlorosuccinimide is not radical.

Conclusions. The main factors influencing the course of the substitution reaction are the possible occurrence of side interactions between the nucleophile and the inducer, steric possibilities, and subsequent isolation of the reactive reaction products.

Keywords

boron, borohydrides, octahydrotriborate(1−) anion, Lewis acids, nucleophilic substitution, succinimide, halogens

Submitted: 01.08.2023
Revised: 17.10.2023
Accepted: 23.01.2024

For citation

Lukoshkova A.A., Shulyak A.T., Posypayko E.E., Selivanov N.A., Golubev A.V., Kubasov A.S., Bykov A.Yu., Zhdanov A.P., Zhizhin K.Yu., Kuznetsov N.T. New approaches to the synthesis of substituted derivatives of the $[B_3H_8]^-$ anion. *Tonk. Khim. Tekhnol.* = *Fine Chem. Technol*. 2024;19(1):61–71. https://doi.org/10.32362/2410-6593-2024-19-1-61-71

НАУЧНАЯ СТАТЬЯ

Новые подходы к синтезу замещенных производных аниона $[B_3H_8]^-$

А.А. Лукошкова[1,✉], А.Т. Шуляк[1], Е.Е. Посыпайко[1], Н.А. Селиванов[1], А.В. Голубев[1], А.С. Кубасов[1], А.Ю. Быков[1], А.П. Жданов[1], К.Ю. Жижин[1,2], Н.Т. Кузнецов[1]

[1] *Институт общей и неорганической химии им. Н.С. Курнакова, Российская академия наук, Москва, 119991 Россия*

[2] *МИРЭА – Российский технологический университет (Институт тонких химических технологий им. М.В. Ломоносова), Москва, 119571 Россия*

✉ *Автор для переписки, e-mail: anya.lukoshkova@yandex.ru*

Аннотация

Цели. Разработка методов синтеза замещенных производных октагидротриборатного аниона, потенциально рассматриваемых в качестве химических аккумуляторов водорода, компонентов ионных жидкостей, прекурсоров для получения боридных покрытий с уникальными свойствами методом Chemical Vapor Deposition (CDV), а также в качестве «строительного материала» для получения высших бороводородных кластеров.

Методы. Ввиду чувствительности реакций замещения к влаге и кислороду воздуха, синтезы проводили в постоянном токе аргона или в сухом герметичном перчаточном боксе СПЕКС ГБ02М с блоком двойной газоочистки и двумя шлюзами. Инициирование реакции проводили при охлаждении до 0°С во избежание образования побочных продуктов. Все результаты были охарактеризованы с помощью инфракравной (ИК) спектроскопии и спектроскопии ядерного магнитного резонанса (ЯРМ).

Результаты. Подробно изучены и усовершенствованы известные методики получения замещенных производных октагидротриборатного (1−) аниона с использованием сухого хлороводорода в качестве электрофильного индуктора. Установлено, что в данном методе целесообразно использовать октагидротриборат цезия, что позволяет облегчить выход целевого продукта. Предложены новые способы инициирования реакции замещения в анионе $[B_3H_8]^-$ с помощью *N*-хлорсукцинимида и брома. С помощью этих индукторов получены и охарактеризованы методами ИК и ЯМР-спектроскопии новые замещенные производные октагидротриборатного аниона с *N*-нуклеофилами: $[B_3H_7NCR]$, (R = Et, *i*-Pr, Ph) и $[B_3H_7NH_2R]$, (R = C_9H_{19} (INA), Bn), $[B_3H_7NHEt_2]$, а также $Bu_4N[B_3H_7Hal]$, $Bu_4N[B_3H_6Hal_2]$, где Hal = Cl, Br. Установлено, что в ходе реакции с бромом и аминами происходит выделение бромоводорода, который сразу протонирует амин, что требует дополнительного нагрева реакционной смеси. Также в ходе работы установлено, что механизм реакции с *N*-хлорсукцинимидом не является радикальным.

Выводы. Усовершенствованы и систематизированы известные методики получения замещенных производных октагидротриборатного аниона. Установлено, что основными факторами, влияющими на ход реакции замещения, являются возможное протекание побочных взаимодействий между нуклеофилом и индуктором, стерические возможности, последующая изоляция реакционноспособных продуктов реакции. В зависимости от нуклеофила выбор метода и условий может быть ограничен.

Ключевые слова

бор, бороводороды, октагидротриборатный (1−) анион, кислоты Льюиса, нуклеофильное замещение, сукцинимид, галогены

Поступила: 01.08.2023
Доработана: 17.10.2023
Принята в печать: 23.01.2024

Для цитирования

Лукошкова А.А., Шуляк А.Т., Посыпайко Е.Е., Селиванов Н.А., Голубев А.В., Кубасов А.С., Быков А.Ю., Жданов А.П., Жижин К.Ю., Кузнецов Н.Т. Новые подходы к синтезу замещенных производных аниона $[B_3H_8]^-$. *Тонкие химические технологии*. 2024;19(1):61–71. https://doi.org/10.32362/2410-6593-2024-19-1-61-71

INTRODUCTION

Substituted derivatives of octahydrotriborate anion act as promising components for chemical hydrogen accumulators [1–3]. They are also precursors for obtaining boride coatings with unique properties [4–6], and play the role of components for obtaining derivatives of higher borohydrates, ionic liquids and liquid crystals [7]. Due to the difficulty of their preparation, the applications of these compounds are still poorly studied.

The preparation of substituted derivatives of the $[B_3H_8]^-$ anion is based on methods using cleavage of the boron backbone of larger clusters, for example, by symmetric cleavage of tetraborane-10 [8]. However, interaction with certain nucleophiles does not lead to substitution, but provokes destruction of the boron backbone [9].

With the development of new and efficient methods for the synthesis of $[B_3H_8]^-$ [10, 11] anion, its substituted derivatives and the methods of their preparation based on

its direct interaction with nucleophiles are of increasing interest. The presence of an aromatic structure allows the octahydrotriborate anion to enter into reactions of electrophile-induced nucleophilic substitution of the hydrogen atom. They are similar to the higher cluster anions [12, 13], where various Lewis acids act as electrophilic inductor [14–16]. The preparation of substituted derivatives by the methods described above is a complex multifactorial process with a number of side reactions. As a result, the yield of the target product can be significantly reduced.

It has been shown that the interaction of $[B_3H_8]^-$ anion with metal halides in the presence of nucleophiles leads to the formation of a large variety of substituted products [14, 17]. By means of nuclear magnetic resonance (NMR) spectroscopy, it has been found that the reaction proceeds through the stage of formation of the transition complex $[B_3H_7–H–MHal_x]^-$. The rate of transformation of this complex is significantly affected by the nature of the Lewis acid. At the same time, the use of metal salts as inductors can significantly complicate the composition of the reaction mixture, complicating the purification of the target products. On the other hand, the use of gaseous hydrogen chloride in the preparation of substituted derivatives is of particular interest due to the almost complete absence of impurities, greatly facilitating the yield of the product. $(CH_3)_4N[B_3H_7Cl]$, $[B_3H_7NCCH_3]$, $[B_3H_7NCCH_3]$, $[B_3H_7DMF]$ (DMF = $(CH_3)_2NCH$) have already been obtained by this method [18], but this method also has a number of disadvantages. It requires a complex multi-component plant with a gas line, as well as cleaning, drying, and carrying out manipulations with gaseous hydrogen chloride gas.

The aim of this study is to improve and systematize the known methods, and develop new ones for the preparation of substituted derivatives of the $[B_3H_8]$ anion. These include: halogen-substituted $Bu_4N[B_3H_7Cl]$, $Bu_4N[B_3H_7Br]$, $Bu_4N[B_3H_6Cl_2]$, $Bu_4N[B_3H_6Br_2]$; nitrilium-substituted $[B_3H_7NCR]$, (R = CH_3, Et, *i*-Pr, Ph); amine-substituted derivatives of $[B_3H_7NH_2R]$, (R = C_9H_{19}, Bn), $[B_3H_7NHEt_2]$, $[B_3H_7NEt_3]$ by interaction of the octahydrotriborate(1−) anion with halogens (Br_2, I_2) and with *N*-chlorosuccinimide (NCS). The compounds $[B_3H_7NCR]$, (R = Et, *i*-Pr, Bn), $[B_3H_7NH_2R]$, (R = C_9H_{19}, Bn) were obtained for the first time using NCS. The use of NCS as an electrophilic inducer was proposed for the synthesis of chloro-substituted, nitrilic and amine-substituted derivatives.

EXPERIMENTAL

Salts of $[B_3H_8]^-$ anion were prepared according to the known method [10] by mild oxidation of sodium borohydride with benzyl chloride. Benzonitrile (99%, *Panreac Sintesis*, Spain), NCS (98%, *Sigma-Aldrich*, USA), bromine (98%, *Sigma-Aldrich*, USA), isononylamine (INA) (98%, *Sigma-Aldrich*, USA), benzylamine (99%, *Panreac Sintesis*, Spain), sulfuric acid (95%, *Chimmed*, Russia), NaCl (99%, *Ruschim*, Russia) were used without further purification.

Dichloromethane, acetonitrile, toluene, and petroleum ether were shaken with $CaCl_2$ and distilled over calcium hydride. The solvents were stored in a dark container over molecular sieves (4 Å) at ≈5°C.

Tetrahydrofuran, diethyl ether was passed through activated aluminum oxide and stored over molecular sieves (4 Å) at ≈5°C.

Triethylamine and diethylamine were purified by shaking with KOH until the darkening of potassium hydroxide stopped, then distilled at atmospheric pressure.

^{11}B and ^1H NMR spectra of solutions of the substances obtained in dichloromethane, deuterodichloromethane, tetrahydrofuran, toluene, and deuteroacetonitrile were recorded on an Avance II-300 NMR spectrometer (*Bruker*, Germany) at 96.32 MHz and 300.21 MHz, respectively, with internal deuterium stabilization. Tetramethylsilane and $BF_3{\cdot}OEt_2$ were used as external standards.

The infrared (IR) spectra of the compounds were recorded on an INFRALUM FT-02 IR Fourier spectrometer (*Lumex*, Russia) in the range 4000–400 cm^{-1} with a resolution of 1 cm^{-1}. Samples were prepared in the form of tablets pressed with KBr (*Sigma-Aldrich*, USA).

Elemental analysis for carbon, hydrogen and nitrogen was carried out on an automatic analyzer CHNS-3 FA 1108 Elemental Analyser (*Carlo Erba Reagents GmbH*, Germany).

Reactions requiring the absence of moisture and air were carried out in a sealed box model SPECS GB02M (*Spectroscopic Systems*, Russia) with a double gas purification unit and two airlocks.

Synthesis of $Bu_4N[B_3H_7Cl]$

$Bu_4N[B_3H_8]$ (100 mg, 0.35 mmol) was placed in a 25-mL flask and dissolved in 5 mL of dichloromethane. The mixture was cooled to −50°C and NCS (47 mg, 0.35 mmol) dissolved in 5 mL of dichloromethane was slowly added. The resulting succinimide was precipitated by addition of diethyl ether. The mixture was filtered off from the precipitate, the filtrate was evaporated at a rotary evaporator. ^{11}B NMR (CD_2Cl_2, 298 K, 96.32 MHz), δ, ppm: −16 (s, 2B), −22 (s, 1B). ^1H NMR (CD_2Cl_2, 298 K, 300 MHz), δ, ppm: 3.05 (m, 8H, Bu_4N), 1.57 (m, 8H, Bu_4N), 1.31 (m, 8H, Bu_4N), 0.93 (t, 12H, Bu_4N), 0.9–0.7 (broad, 7H, HB). IR (KBr), cm^{-1}: ν(BH): 2520, 2448, 2338, ν(BCl): 850.

Synthesis of $Bu_4N[B_3H_6Cl_2]$

$Bu_4N[B_3H_8]$ (100 mg, 0.35 mmol) was placed in a 25-mL flask and dissolved in 5 mL of dichloromethane.

The mixture was cooled to −50°C and NCS (93.1 mg, 0.70 mmol) dissolved in 5 mL of dichloromethane was slowly added. The resulting succinimide was precipitated by addition of diethyl ether. The mixture was filtered from the precipitate; the filtrate was evaporated at a rotary evaporator. ^{11}B NMR (CD_2Cl_2, 298 K, 96.32 MHz), δ, ppm: −5 (s, broad, 1B), −13 (s, 2B); ^{1}H NMR (CD_2Cl_2, 298 K, 300 MHz), δ, ppm: 3.05 (m, 8H, Bu_4N), 1.57 (m, 8H, Bu_4N), 1.31 (m, 8H, Bu_4N), 0.93 (t, 12H, Bu_4N), 0.9–0.7 (broad, 6H, HB). IR (KBr), cm^{-1}: ν(BH): 2517, 2458, 2336, ν(BCl): 811.

Synthesis of $[B_3H_7NCCH_3]$

Method 1. $Cs[B_3H_8]$ (100 mg, 0.57 mmol) was placed in a 10-mL flask and dissolved in 100 μL of acetonitrile. Then 2 mL of toluene was added. The mixture was cooled to −50°C and NCS (75 mg, 0.57 mmol) dissolved in 100 μL of acetonitrile was slowly added. The mixture was stirred for 1 h. Then the precipitate was filtered off and the acetonitrile was distilled off at a rotary evaporator. The filtrate was left in the freezer at T = −5°C for three days until the crystallization of succinimide was complete. The crystals were filtered off. Then the solution was evaporated to a concentrated solution and $[B_3H_7NCCH_3]$ was precipitated with petroleum ether. ^{11}B NMR (CH_3CN, 298 K, 96.32 MHz), δ, ppm: −7.6 (2B), −35.2 (1B); ^{1}H (CD_2Cl_2, 298 K, 300 MHz), δ, ppm: 2.43 (c, 3H, CH_3), 1.68 (broad, 7H, HB). IR (KBr), cm^{-1}: ν(BH): 2516, 2446, 2372, 2340. Calculated/found, %: C (29.83/29.87), H (12.51/12.56), N (17.31/17.29), B (40.27/40.21).

Method 2. Synthesis was conducted using the new method and setup shown in Fig. 1. One gram of sodium chloride was added to the first 250-mL flask, and 1 mL of 95% sulfuric acid was added to a drop funnel with a pressure compensator. A Teflon tube filled with calcium chloride was incorporated for drying and additional purification. The dehydrated gaseous HCl flowed into a three-necked 250-mL flask through a bubbler. The three-necked flask was necessary for gradual sampling. 20 mL of CH_3CN and 0.5 g of dissolved $Cs[B_3H_8]$ were pre-poured into the flask. The interaction was carried out under conditions of slight cooling in an ice bath. The system was equipped with a glycerol bubbler to control the argon flow and two traps, one of which was empty and other contained Et_3N. It should be noted that Teflon hoses were used when working with gaseous HCl. The flasks were equipped with magnetic stirrers.

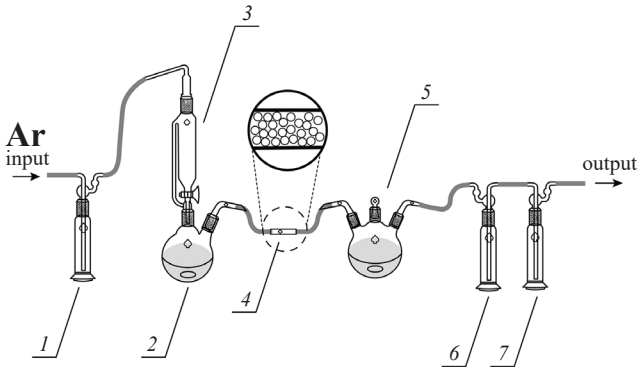

Fig. 1. Scheme of the setup for the synthesis of $[B_3H_7NCCH_3]$:
(*1*) bubbler with glycerin;
(*2*) two-necked flask 250 mL;
(*3*) dropping funnel with pressure compensator;
(*4*) Teflon tube with calcium chloride;
(*5*) three-necked flask 250 mL;
(*6*) empty trap;
(*7*) trap with Et_3N

Synthesis of $[B_3H_7NCPh]$

$Cs[B_3H_8]$ (100 mg, 0.57 mmol) was placed in a 25-mL flask and 5 mL of toluene was added. Benzonitrile (58.8 μL, 0.57 mmol) was added to the suspension and the mixture was cooled to −50°C. Next, NCS (75 mg, 0.57 mmol) dissolved in 1 mL of dichloromethane was added. The mixture was stirred under refrigeration for 1 h. The precipitate was filtered off and left in the refrigerator for three days until the crystallization of succinimide was completed. The crystals were filtered off, the solution was evaporated to a concentrated solution and $[B_3H_7NCBn]$ was precipitated with petroleum ether. ^{11}B NMR ($PhCH_3$, 298 K, 96.32 MHz), δ, ppm: −6.9 (2B), −35.0 (1B).

Synthesis of $[B_3H_7NHEt_2]$

$Cs[B_3H_8]$ (100 mg, 0.57 mmol) was placed in a 25-mL flask and 5 mL of toluene was added. Diethylamine (58.7 μL, 0.57 mmol) was added to the suspension and the mixture was cooled to −50°C. Next, NCS (75 mg, 0.57 mmol) dissolved in 1 mL dichloromethane was added. The mixture was stirred under cooling for 1 h. Then the precipitate was filtered off, kept in the refrigerator for three days, and evaporated under deep vacuum without heating. ^{11}B NMR ($PhCH_3$, 298 K, 96.32 MHz), δ, ppm: −14 (2B), −26 (1B). IR (thin film), cm^{-1}: ν(BH): 2502, 2425, ν(BN): 1455. Calculated/found, %: C, 42.65/42.5; H, 16.11/16.2; N, 12.43/12.4; B, 28.80/28.9.

Synthesis of $[B_3H_7NEt_3]$

Method 1. $Cs[B_3H_8]$ (100 mg, 0.57 mmol) was placed in a 25-mL flask and 5 mL of toluene was added. Triethylamine (79.2 μL, 0.57 mmol) was added to the suspension and the mixture was cooled to −50°C. Next, NCS (75 mg, 0.57 mmol) dissolved in 1 mL of dichloromethane was added. The mixture was stirred under cooling for 1 h. Then the precipitate was filtered off, kept in the refrigerator for three days, and evaporated under deep vacuum without heating. $^{11}B\{^1H\}$ (CD_2Cl_2, 298 K, 96.32 MHz), δ, ppm: −19.9 (2B), −22.4 (1B);

^1H (CD_2Cl_2, 298 K, 300 MHz), δ, ppm: 2.9 (m = 4, 6H, CH_2, J_{HH} = 7.2 Hz), 1.2 (t, 9H, CH_3, J_{HH} = 7.2 Hz), 1.1 (broad, 7H, HB). IR (thin film), cm^{-1}: ν(BH): 2501, 2448, 2424, ν(BN): 1450. Calculated/found, %: C, 51.23/51.4; H, 15.76/15.8; N, 9.96/9.79; B, 23.05/23.0.

Method 2. $Bu_4N[B_3H_8]$ (500 mg, 1.78 mmol) dissolved in 10 mL of dichloromethane was placed in a 50-mL flask, and triethylamine (245 μL, 1.78 mmol) was added. The mixture was cooled and Br_2 (91.7 μL, 1.78 mmol) dissolved in 5 mL of dichloromethane was added. The mixture was slowly warmed to room temperature (20°C), then the precipitate was filtered off and $[B_3H_7NEt_3]$ was separated by column chromatography on silica gel. The elution was carried out by hexane/dichloromethane mixture in the ratio 1 : 1.

Synthesis of $[B_3H_7NH_2Bn]$

$Cs[B_3H_8]$ (100 mg, 0.57 mmol) was placed in a 25-mL flask and 5 mL of toluene was added. Benzylamine (62 μL, 0.57 mmol) was added to the suspension and the mixture was cooled to −50°C. Next, NCS dissolved in 1 mL of dichloromethane was added. The mixture was stirred under cooling for 1 h. The precipitate was then filtered off and evaporated on a vacuum unit without heating. The filtrate was kept in a freezer at −5°C for three days, the succinimide was filtered off and evaporated on a vacuum unit without heating. ^{11}B ($PhCH_3$, 298 K, 96.32 MHz), δ, ppm: −8.1 (2B), −28.3 (1B); IR (thin film), cm^{-1}: ν(BH): 2502, 2429, 2320, ν(BN): 1372. Calculated/found, %: C, 57.33/57.26; H, 10.99/11.01; N, 9.55/9.53; B, 22.11/22.09.

Synthesis of $[B_3H_7INA]$

$Bu_4N[B_3H_8]$ (500 mg, 1.78 mmol) dissolved in 10 mL of tetrahydrofuran was placed in a 50-mL flask, and INA (322 μL, 1.78 mmol) was added. The mixture was cooled and Br_2 (91.7 μL, 1.78 mmol) dissolved in 5 mL of dichloromethane was added. The mixture was slowly warmed to room temperature (20°C) and then heated to the boiling point of tetrahydrofuran for 6 h. $^{11}B\{^1H\}$ (CD_2Cl_2, 298 K, 96.32 MHz), δ, ppm: −13.0 (2B), −30.1 (1B).

RESULTS AND DISCUSSION

Interaction of $Bu_4N[B_3H_8]$ with halogens in dichloromethane

The anion $[B_3H_8]^-$ reacts with Br_2 to form bromo-substituted derivatives $[B_3H_7Br]^-$ and $[B_3H_6Br_2]^-$. The reaction was carried out under conditions of cooling by slowly spiking a solution of Br_2 in dichloromethane; at a ratio of $Bu_4N[B_3H_8]$: Br_2 = 2 : 1. As a result, several signals were observed in the ^{11}B NMR spectrum (Fig. 2a): one signal at −31 ppm with a multiplicity of 9 from the initial octahydrotriborate; and two signals at −13 and −30 ppm with an integral intensity ratio of 2 : 1, related to $[B_3H_7Br]^-$. It can thus be concluded that the reaction is incomplete. At the same time, the formation of a presumably dibromo-substituted derivative was noted in the reaction mixture, as evidenced by the appearance of two signals at −16 and −22 ppm with an integral intensity ratio of 1 : 2. After 24 h, no changes were observed in the ^{11}B NMR spectrum of the reaction mixture (Fig. 2b). After addition of another 0.267 mmol of Br_2, a decrease in signal intensity at −31 ppm from the original octahydrotriborate and an increase in signal intensity at −13 and −30 ppm from the monobromo-substituted derivative were observed (Fig. 2c). Upon subsequent addition of another 0.267 mmol Br_2, the complete disappearance of the signal of the original $[B_3H_8]^-$ and an increase in the intensity of the signals from the mono- and dibromo-substituted products were observed (Fig. 2d).

The addition of acetonitrile to the reaction mixture in the ratio $TBA[B_3H_8]$: CH_3CN = 1 : 1, a stronger nucleophile when compared to bromine, leads to the exchange reaction and the formation of the nitrile mono-substituted product $[B_3H_7NCCH_3]$.

The addition of an equivalent amount of bromine to the mixture of triborate and amine (Et_2NH, Et_3N, $C_9H_{19}NH_2$ (INA)) in dichloromethane leads to a substitution reaction to form the corresponding amine-substituted products $[B_3H_7NHEt_2]$, $[B_3H_7NEt_3]$, $[B_3H_7INA]$. The reaction proceeds incompletely both at −50°C and at room temperature (20°C). HBr is formed during the reaction. Most of this is used for the protonation reaction of the amine which can also act as an inducer of the substitution reaction. However, this reaction requires additional heating. According to the method described in [19], we performed interaction of triborate and isononylamine in tetrahydrofuran at T = 66°C. Bu_4NBr which is insoluble under these conditions precipitated. Carrying out the reaction under the above conditions allowed the yield of the target product $[B_3H_7INA]$ to be significantly increased. However, complete conversion requires the addition of excess bromine. An attempt to carry out a similar interaction with benzylamine led to the formation of only a bromine-substituted derivative, indicating the stronger nucleophilicity of bromine compared to benzylamine.

The interaction of octahydrotriborate with iodine did not lead to the formation of iodine-substituted derivatives. However, when $[B_3H_8]^-$ interacted with triethylamine, diethylamine and isononylamine in the presence of iodine, the ^{11}B NMR spectra of the reaction mixtures in all cases showed two signals characteristic of mono-substituted derivatives with an integral intensity ratio of 2 : 1. From the amine-substituted products they were: −14 and −26 ppm for $[B_3H_7NHEt_2]$; −19.9 and −22.4 ppm for $[B_3H_7NEt_3]$; −13.0 and −30.1 ppm for $[B_3H_7INA]$.

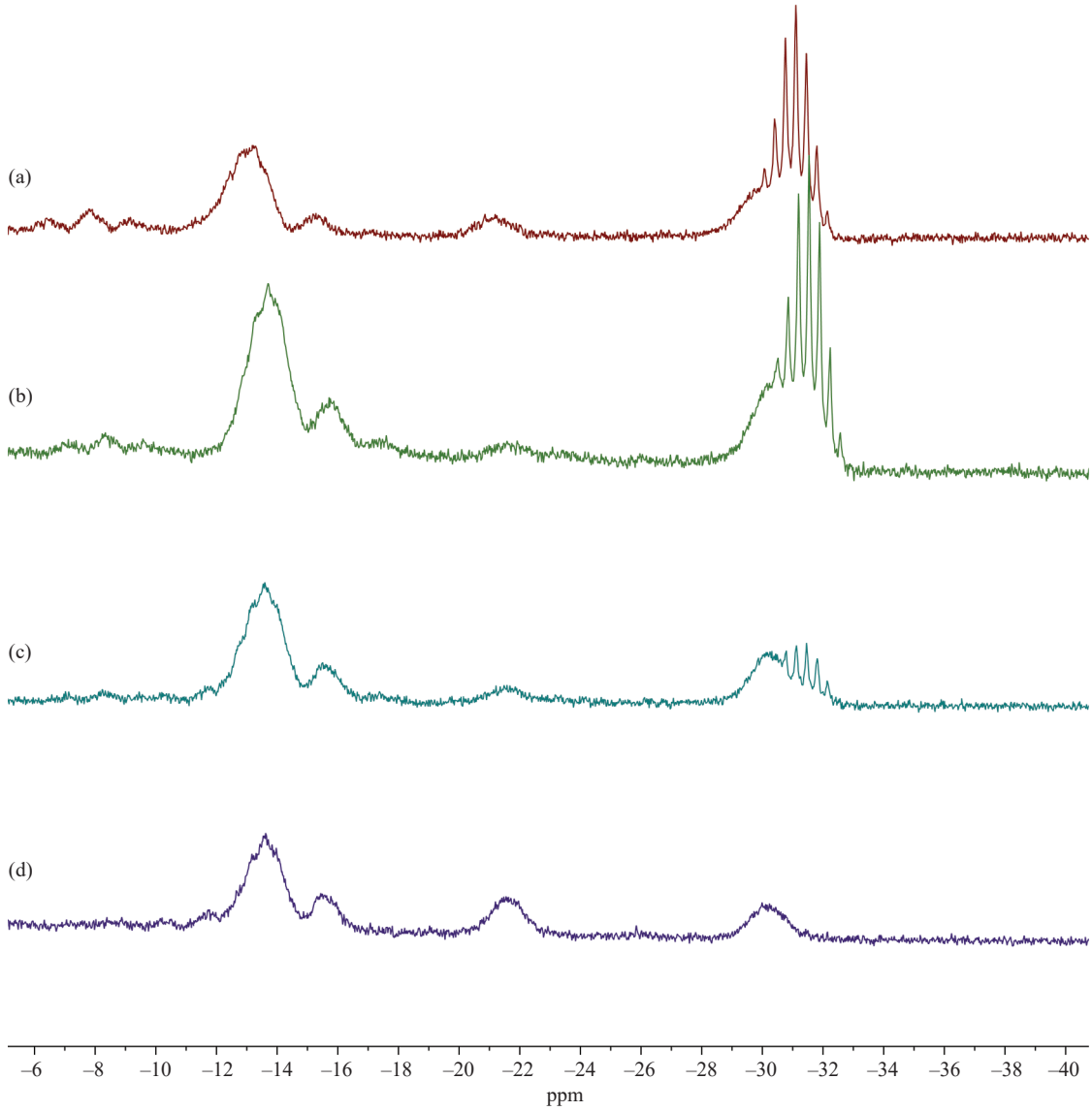

Fig. 2. ^{11}B NMR spectra of a mixture of $Bu_4N[B_3H_8]$ with Br_2:
(a) 1 h after the start of the reaction,
(b) after 24 h,
(c) after adding 0.267 mmol of Br_2,
(d) after adding another 0.267 mmol of Br_2

The highest yield was observed with isonononylamine. In the preparation of substituted derivatives using iodine, excess iodine in the reaction mixture interacts with the substituted derivatives of the $[B_3H_8]^-$ anion to form by-products. Column chromatography helps to get rid of unwanted impurities but reduces the final yield of the target product.

Interaction of $[B_3H_8]^-$ with HCl in acetonitrile

Earlier in [18], a method for the preparation of nitrilium-substituted derivative $[B_3H_7NCCH_3]$ using dry hydrogen chloride was described. The authors used tetramethylammonium salt of octahydrotriborate as a starting substance. The interaction of $(Me_4N)[B_3H_8]$ with HCl in acetonitrile yielded pure acetonitrile-substituted derivative in solution.

This study used the cesium salt of octahydrotriborate, resulting in the relatively fast formation of CsCl precipitate. This simplified the purification and increased the yield of the target product $[B_3H_7NCCH_3]$.

Synthesis using the tetrabutylammonium salt of octahydrotriborate in acetonitrile leads to the formation of a mixture of acetonitrile-substituted derivative and chlorine-substituted derivative. This can be confirmed by the appearance in the ^{11}B NMR spectrum of two pairs of signals with an integral ratio of 2 : 1 at −7.6 and

−35.2 ppm from $[B_3H_7NCCH_3]$ and at –16 and −22 ppm from $[B_3H_7Cl]^-$. Signals from the latter decrease over time. Increasing the amount of added HCl or increasing the synthesis time leads to degradation of the obtained products.

Interaction of $[B_3H_8]^-$ with NCS

Preparation of $Bu_4N[B_3H_7Cl]$ and $Bu_4N[B_3H_6Cl_2]$

NCS is a well-known chlorinating agent in organic chemistry. The interaction of NCS with octahydrotriborate anion leads to the formation of $[B_3H_7Cl]^-$ at the ratio $Bu_4N[B_3H_8]$: NCS = = 1 : 1, and to the formation of $[B_3H_6Cl_2]^-$ at the ratio $Bu_4N[B_3H_8]$: NCS = 1 : 2 (Fig. 3). A subsequent increase in the amount of NCS leads only to the destruction of the boron backbone.

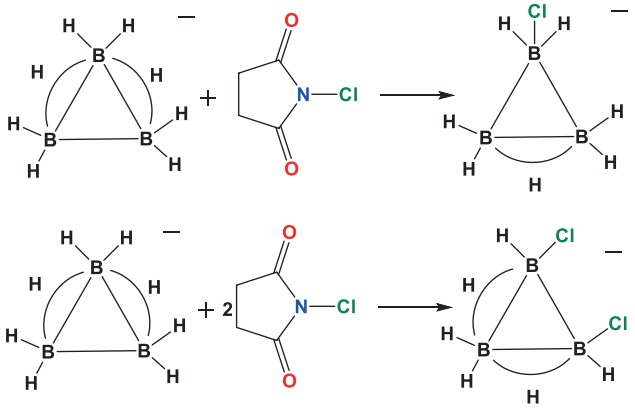

Fig. 3. Scheme of the interaction of NCS with octahydrotriborate anion

The succinimide formed in the reaction interacts with chloro-substituted derivatives to form by-products. This significantly complicates the purification process and reduces the yields of the target compounds. Carrying out the reaction and purification of chloro-substituted derivatives of $[B_3H_8]^-$ anion at cooling to −50°C reduces the solubility of succinimide and, together with its salting with diethyl ether, prevents the occurrence of side processes.

Preparation of nitrile and amine-substituted derivatives

The interaction of the cesium salt of octahydrotriborate with NCS in acetonitrile leads to $[B_3H_7NCCH_3]$. The reaction proceeds through the stage of formation of the monochloro-substituted derivative and is an exchange reaction, in which chlorine is displaced by the nucleophilic stronger acetonitrile. The exchange process of the nucleophilic fragment is equilibrium. The precipitation of cesium chloride shifts the equilibrium towards the formation of the acetonitrile-substituted product (Fig. 4).

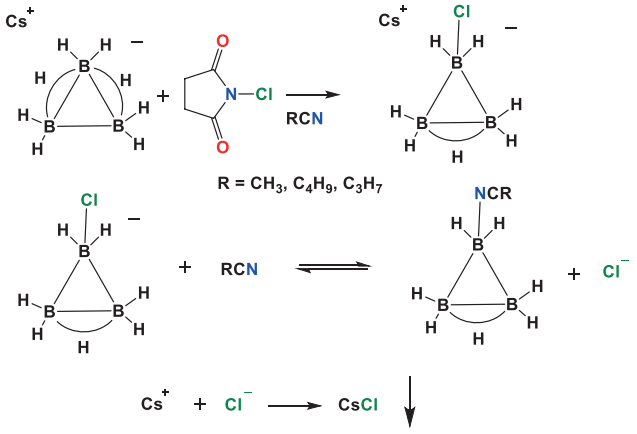

Fig. 4. Scheme of the interaction of the cesium salt of octahydrotriborate with NCS in acetonitrile

Thus, carrying out a similar reaction with the tetrabutylammonium salt of octahydrotriborate in acetonitrile leads to the formation of only chloro-substituted derivatives $[B_3H_7Cl]^-$ and $[B_3H_6Cl_2]^-$. The results of the study are confirmed by ^{11}B NMR spectroscopy data. Two signals were observed in the spectra of the reaction mixture (Fig. 5a) at the first stages: at −7 and −35 ppm with the ratio of integral intensities 2 : 1, belonging to the acetonitrile-substituted derivative. Two signals observed at −16 and −22 ppm correspond to $[B_3H_7Cl]^-$. After 1 h after the beginning of the reaction there was a decrease in the intensity of signals from the chloro-substituted derivative, until their complete disappearance and an increase in the intensity of signals of the acetonitrile-substituted product (Fig. 5b).

The addition of NCS to the mixture of octahydrotriborate with various amines in toluene also leads to the formation of substituted derivatives. However, it significantly increases the reaction time due to the low solubility of the reagents in toluene, while preventing interaction of substituted products with the formed succinimide. In contrast to the neutral substituted derivatives thus formed, succinimide is practically insoluble in toluene, especially at low temperature. For this reason, the synthesis and subsequent isolation of products were carried out at low temperatures, not exceeding 0°C.

In organic chemistry, chlorination reactions using NCS are described as a radical process initiated by a quantum of light. An attempt to carry out two parallel syntheses of monochloro-substituted octahydrotriborate derivative using a red laboratory lamp and under UV irradiation was proposed. According to NMR spectroscopy, absolutely no differences were observed in the reaction masses. Thus, it can be said that the reaction mechanism is still not radical.

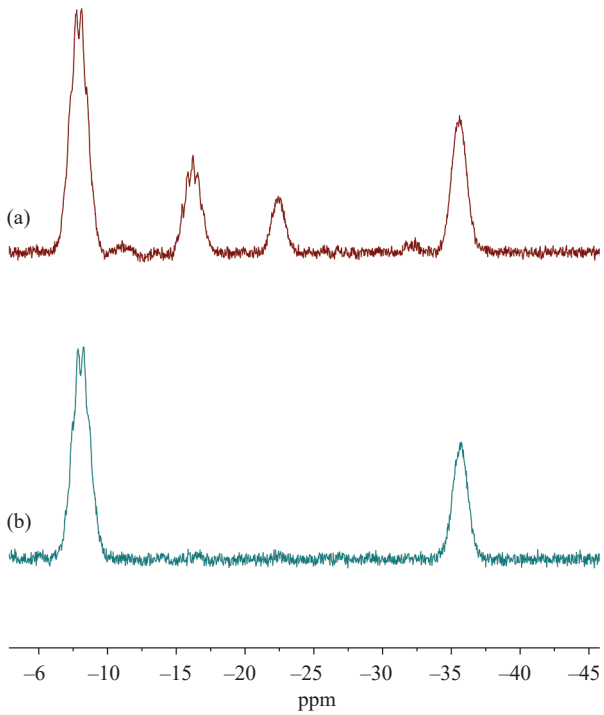

Fig. 5. ^{11}B NMR spectra of a mixture of $Bu_4N[B_3H_8]$ with NCS:
(a) immediately after the start of the reaction,
(b) after 1 h.

Therefore, NCS can act as a chlorinating agent both for the preparation of chloro-substituted derivatives of octahydrotriborate anion by direct interaction with salts of $[B_3H_8]^-$ anion, and for the preparation of other substituted derivatives through the substitution of a nucleophilic fragment.

CONCLUSIONS

All the methods mentioned above are suitable for the preparation of substituted derivatives of the $[B_3H_8]^-$ anion. Depending on the nucleophile, the choice of method and conditions may be limited. The main factors influencing the course of the substitution reaction are the possible occurrence of side interactions between the nucleophile and the inducer, steric possibilities, and the subsequent isolation of reactive reaction products.

This study for this first time proposed the use of NCS as an electrophilic inducer for the synthesis of chloro-substituted, nitrilic and amine-substituted derivatives. Also for the first time, new substituted derivatives of $[B_3H_7NCR]$, (R = Et, *i*-Pr, Bn), $[B_3H_7NH_2R]$, ($R = C_9H_{19}$, Bn) were obtained by this method.

This study also systematizes and improves the known methods for the preparation of substituted octahydrotriborate anion derivatives. For the preparation of nitrilium-substituted derivatives using dry hydrogen chloride, the use of cesium salt enables the product to be isolated.

New methods have been developed for the preparation of halogen-substituted $Bu_4N[B_3H_7Cl]$, $Bu_4N[B_3H_7Br]$, $Bu_4N[B_3H_6Cl_2]$, $Bu4N[B_3H_6Br_2]$; nitrilium-substituted $[B_3H_7NCR]$, (R = CH_3, Et, *i*-Pr, Ph); and amine-substituted derivatives of $[B_3H_7NH_2R]$, ($R = C_9H_{19}$, Bn), $[B_3H_7NHEt_2]$, $[B_3H_7NEt_3]$ by interaction of octahydrotriborate(1−) anion with halogens (Br_2, I_2) and with NCS. The study also found that protonation of the amine occurs during the preparation of amine-substituted derivatives using bromine. In order to avoid this, the synthesis temperature must be increased to 66°C.

When iodine is used as an inducer, its excess can lead to a degradation of the target compound. Thus the isolation of the target product should be carried out immediately after complete conversion of the initial anion $[B_3H_8]^-$.

Acknowledgments

This work was supported by the Ministry of Science and Higher Education of the Russian Federation as part of the State Assignment of the Kurnakov Institute of General and Inorganic Chemistry of the Russian Academy of Sciences (IGIC RAS). This research was performed using the equipment of the Research Sharing Center of Physical Methods for Studying Substances and Materials at IGIC RAS.

Authors' contributions

A.A. Lukoshkova – conducting the experiments, analysis of the results, and writing the text of the manuscript.

A.T. Shulyak – conducting the experiments, analysis of the results, and writing the text of the manuscript.

E.E. Posypayko – conducting the experiments, analysis of the results, and writing the text of the manuscript.

N.A. Selivanov – conducting NMR analysis.

A.V. Golubev – conducting NMR analysis.

A.S. Kubasov – conducting X-ray diffraction analysis.

A.Yu. Bykov – project supervision, development of the research concept, and editing the text of the article.

A.P. Zhdanov – resources.

K.Yu. Zhizhin – project supervision, development of the research concept, and editing the text of the article.

N.T. Kuznetsov – project manager.

The authors declare no conflicts of interest.

REFERENCES

1. Yoon C.W., Carroll P.J., Sneddon L.G. Ammonia triborane: A new synthesis, structural determinations, and hydrolytic hydrogen-release properties. *J. Am. Chem. Soc*. 2009;131(2):855–864. https://doi.org/10.1021/ja808045p
2. Huang Z., Eagles M., Porter S., Sorte E.G., Billet B., Corey R.L., *et al.* Thermolysis and solid state NMR studies of NaB_3H_8, $NH_3B_3H_7$, and $NH_4B_3H_8$. *Dalt. Trans.* 2013;42(3):701–708. https://doi.org/10.1039/c2dt31365k
3. Jensen S.R.H., Paskevicius M., Hansen B.R.S., Jakobsen A.S., Møller K.T., White J.L., *et al*. Hydrogenation properties of lithium and sodium hydride – *closo*-borate, $[B_{10}H_{10}]^{2-}$ and $[B_{12}H_{12}]^{2-}$, composites. *Phys. Chem. Chem. Phys.* 2018;20(23): 16266–16275. https://doi.org/10.1039/c7cp07776a
4. Kher S.S., Romero J.V., Caruso J.D., Spencer J.T. Chemical vapor deposition of metal borides: The formation of neodymium boride thin film materials from polyhedral boron clusters and metal halides by chemical vapor deposition. *Appl. Organomet. Chem.* 2008;22(6):300–307. https://doi.org/10.1002/aoc.1383
5. Chen H., Zou X. Intermetallic borides: structures, synthesis and applications in electrocatalysis. *Inorg. Chem. Front.* 2020;7(11):2248–2264. https://doi.org/10.1039/d0qi00146e
6. Goedde D.M., Girolami G.S. A new class of CVD precursors to metal borides: $Cr(B_3H_8)_2$ and related octahydrotriborate complexes. *J. Am. Chem. Soc.* 2004;126(39):12230–12231. https://doi.org/10.1021/ja046906c
7. Bürchner M., Erle A.M.T., Scherer H., Krossing I. Synthesis and characterization of boranate ionic liquids (BILs). *Chemistry.* 2012;18(8):2254–2262. https://doi.org/10.1002/chem.201102460
8. Dodds A.R., Kodama G. Reactions of tetraborane(10) with mono- and dimethylamine. *Inorg. Chem.* 1977;16(11):2900–2903. https://doi.org/10.1021/ic50177a046
9. Kodama G., Parry R.W. The Preparation and Structure of the Diammoniate of Tetraborane. *J. Am. Chem. Soc.* 1960;82(24):6250–6255. https://doi.org/10.1021/ja01509a012
10. Bykov A.Y., Razgonyaeva G.A., Mal'tseva N.N., Zhizhin K.Y., Kuznetsov N.T. A new method of synthesis of the $B_3H_8^-$ anion. *Russ. J. Inorg. Chem*. 2012;57(4):471–473. https://doi.org/10.1134/s0036023612040055
11. Chen X.M., Ma N., Zhang Q.F., Wang J., Feng X., Wei C., *et al*. Elucidation of the Formation Mechanisms of the Octahydrotriborate Anion ($B_3H_8^-$) through the Nucleophilicity of the B–H Bond. *J. Am. Chem. Soc.* 2018;140(21):6718–6726. https://doi.org/10.1021/jacs.8b03785
12. Zhizhin K.Y., Zhdanov A.P., Kuznetsov N.T. Derivatives of *closo*-decaborate anion $[B_{10}H_{10}]^{2-}$ with *exo*-polyhedral substituents. *Russ. J. Inorg. Chem.* 2010;55(14):2089–2127. https://doi.org/10.1134/s0036023610140019
13. Kuznetsov N.T., Zhizhin K.Yu., Kuznetsov A.N., Avdeeva V.V. *Khimiya poliedricheskikh borovodorodnykh struktur* (*Chemistry of Polyhedral Boron Structures*). Moscow: RAN; 2022. 676 p. (in Russ.). ISBN 978-5-907366-88-6
14. Shulyak A.T., Bortnikov E.O., Selivanov N.A., Grigoriev M.S., Kubasov A.S., Zhdanov A.P., *et al*. Nucleophilic Substitution Reactions in the $[B_3H_8]^-$ Anion in the Presence of Lewis Acids. *Molecules*. 2022;27(3):746. https://doi.org/10.3390/molecules27030746
15. Matveev E.Y., Kubasov A.S., Razgonyaeva G.A., Polyakova I.N., Zhizhin K.Y., Kuznetsov N.T. Reactions of the $[B_{10}H_{10}]^{2-}$ anion with nucleophiles in the presence of halides of group IIIA and IVB elements. *Russ. J. Inorg. Chem.* 2015;60(7):776–785. https://doi.org/10.1134/S0036023615070104
16. Retivov V., Matveev E.Y., Lisovskiy M., Razgonyaeva G., Ochertyanova L., Zhizhin K.Y., *et al*. Nucleophilic substitution in closo-decaborate $[B_{10}H_{10}]^{2-}$ in the presence of carbocations. *Russ. Chem. Bull.* 2010;59(3):550–555. https://doi.org/10.1007/s11172-010-0123-2
17. Drummond A., Morris J.H. Reactions of the octahydrotriborate (−1) ion with mercury salts. *Inorganica Chim. Acta.* 1977;24(C):191–194. https://doi.org/10.1016/s0020-1693(00)93871-4
18. Dolan P.J., Kindsvater J.H., Peters D.G. Electrochemical oxidation and protonation of octahydrotriborate anion. *Inorg. Chem.* 1976;15(9):2170–2173. https://doi.org/10.1021/ic50163a034
19. Das M.K., Bhaumik A. Synthesis and characterization of some amine-triborane(7) adducts. *Indian J. Chem. Sect A.* 1996;35A(9):790–792.

About the authors

Anna A. Lukoshkova, Junior Researcher, Chemistry of Light Elements and Clusters Laboratory, Kurnakov Institute of General and Inorganic Chemistry, Russian Academy of Sciences (IGIC RAS) (31, Leninskii pr., Moscow, 119991, Russia). E-mail: anya.lukoshkova@yandex.ru. Scopus Author ID 58781647200, https://orcid.org/0009-0002-7580-1315

Alexandra T. Shulyak, Postgraduate Student, Junior Researcher, Chemistry of Light Elements and Clusters Laboratory, Kurnakov Institute of General and Inorganic Chemistry, Russian Academy of Sciences (IGIC RAS) (31, Leninskii pr., Moscow, 119991, Russia). E-mail: shulachkaa@gmail.com. Scopus Author ID 57225000199, https://orcid.org/0000-0001-5713-2184

Elizaveta E. Posypayko, Student, Kurnakov Institute of General and Inorganic Chemistry, Russian Academy of Sciences (IGIC RAS) (31, Leninskii pr., Moscow, 119991, Russia). E-mail: lizapos2003@gmail.com. https://orcid.org/0009-0004-4813-4531

Nikita A. Selivanov, Cand. Sci. (Chem.), Researcher, Laboratory of Nanobiomaterials and Bioeffectors for Theranostics of Socially Significant Diseases, Kurnakov Institute of General and Inorganic Chemistry, Russian Academy of Sciences (IGIC RAS) (31, Leninskii pr., Moscow, 119991, Russia). E-mail: Goovee@yandex.ru. Scopus Author ID 57189441382, RSCI SPIN-code 2095-0956, https://orcid.org/0000-0001-7426-5982

Aleksey V. Golubev, Cand. Sci. (Chem.), Researcher, Laboratory of Nanobiomaterials and Bioeffectors for Theranostics of Socially Significant Diseases, Kurnakov Institute of General and Inorganic Chemistry, Russian Academy of Sciences (IGIC RAS) (31, Leninskii pr., Moscow, 119991, Russia). E-mail: golalekseival@mail.ru. Scopus Author ID 57215609169, RSCI SPIN-code 1591-7846, https://orcid.org/0000-0003-2605-4923

Aleksey S. Kubasov, Cand. Sci. (Chem.), Researcher, Chemistry of Light Elements and Clusters Laboratory, Kurnakov Institute of General and Inorganic Chemistry, Russian Academy of Sciences (IGIC RAS) (31, Leninskii pr., Moscow, 119991, Russia). E-mail: fobosax@mail.ru. Scopus Author ID 56118634600, ResearcherID J-5588-2016, RSCI SPIN-code 8266-8605, https://orcid.org/0000-0002-0156-5535

Alexander Yu. Bykov, Cand. Sci. (Chem.), Senior Researcher, Chemistry of Light Elements and Clusters Laboratory, Kurnakov Institute of General and Inorganic Chemistry, Russian Academy of Sciences (IGIC RAS) (31, Leninskii pr., Moscow, 119991, Russia). E-mail: bykov@igic.ras.ru. Scopus Author ID 17433685800, ResearcherID N-7157-2015, RSCI SPIN-code 9498-8148, https://orcid.org/0000-0003-1793-8487

Andrey P. Zhdanov, Cand. Sci. (Chem.), Researcher, Chemistry of Light Elements and Clusters Laboratory, Kurnakov Institute of General and Inorganic Chemistry, Russian Academy of Sciences (IGIC RAS) (31, Leninskii pr., Moscow, 119991, Russia). E-mail: zhdanov@igic.ras.ru. Scopus Author ID 36350472200, RSCI SPIN-code 1544-8482, https://orcid.org/0000-0003-4083-386X

Konstantin Yu. Zhizhin, Dr. Sci. (Chem.), Corresponding Member of the Russian Academy of Sciences, Chief Researcher, Chemistry of Light Elements and Clusters Laboratory, Kurnakov Institute of General and Inorganic Chemistry, Russian Academy of Sciences (IGIC RAS) (31, Leninskii pr., Moscow, 119991, Russia); Professor, Department of Inorganic Chemistry, M.V. Lomonosov Institute of Fine Chemical Technologies, MIREA – Russian Technological University (86, Vernadskogo pr., Moscow, 119571, Russia). E-mail: zhizhin@igic.ras.ru. Scopus Author ID 6701495620, ResearcherID C-5681-2013, RSCI SPIN-code 4605-4065, https://orcid.org/0000-0002-4475-124X

Nikolay T. Kuznetsov, Dr. Sci. (Chem.), Academician of the Russian Academy of Sciences, Head, Chemistry of Light Elements and Clusters Laboratory, Kurnakov Institute of General and Inorganic Chemistry, Russian Academy of Sciences (IGIC RAS) (31, Leninskii pr., Moscow, 119991, Russia). E-mail: ntkuz@igic.ras.ru. Scopus Author ID 56857205300, ResearcherID S-1129-2016, RSCI SPIN-code 3876-6006, https://orcid.org/0000-0002-0131-6387

Об авторах

Лукошкова Анна Анатольевна, младший научный сотрудник лаборатории химии легких элементов и кластеров, ФГБУН Институт общей и неорганической химии им. Н.С. Курнакова, Российская академия наук (ИОНХ РАН) (119991, Россия, Москва, Ленинский пр-т, д. 31). E-mail: anya.lukoshkova@yandex.ru. Scopus Author ID 58781647200, https://orcid.org/0009-0002-7580-1315

Шуляк Александра Тимуровна, аспирант, младший научный сотрудник лаборатории химии легких элементов и кластеров, ФГБУН Институт общей и неорганической химии им. Н.С. Курнакова, Российская академия наук (ИОНХ РАН) (119991, Россия, Москва, Ленинский пр-т, д. 31). E-mail: shulachkaa@gmail.com. Scopus Author ID 57225000199, https://orcid.org/0000-0001-5713-2184

Посыпайко Елизавета Евгеньевна, студент, ФГБУН Институт общей и неорганической химии им. Н.С. Курнакова, Российская академия наук (ИОНХ РАН) (119991, Россия, Москва, Ленинский пр-т, д. 31). E-mail: lizapos2003@gmail.com. https://orcid.org/0009-0004-4813-4531

Селиванов Никита Алексеевич, к.х.н., научный сотрудник лаборатории нанобиоматериалов и биоэффекторов для тераностики социально-значимых заболеваний, ФГБУН Институт общей и неорганической химии им. Н.С. Курнакова, Российская академия наук (ИОНХ РАН) (119991, Россия, Москва, Ленинский пр-т, д. 31). E-mail: Goovee@yandex.ru. Scopus Author ID 57189441382, SPIN-код РИНЦ 2095-0956, https://orcid.org/0000-0001-7426-5982

Голубев Алексей Валерьевич, к.х.н., научный сотрудник лаборатории нанобиоматериалов и биоэффекторов для тераностики социально-значимых заболеваний, ФГБУН Институт общей и неорганической химии им. Н.С. Курнакова, Российская академия наук (ИОНХ РАН) (119991, Россия, Москва, Ленинский пр-т, д. 31). E-mail: golalekseival@mail.ru. Scopus Author ID 57215609169, SPIN-код РИНЦ 1591-7846, https://orcid.org/0000-0003-2605-4923

Кубасов Алексей Сергеевич, к.х.н., научный сотрудник лаборатории химии легких элементов и кластеров, ФГБУН Институт общей и неорганической химии им. Н.С. Курнакова, Российская академия наук (ИОНХ РАН) (119991, Россия, Москва, Ленинский пр-т, д. 31). E-mail: fobosax@mail.ru. Scopus Author ID 56118634600, ResearcherID J-5588-2016, SPIN-код РИНЦ 8266-8605, https://orcid.org/0000-0002-0156-5535

Быков Александр Юрьевич, к.х.н., старший научный сотрудник лаборатории химии легких элементов и кластеров, ФГБУН Институт общей и неорганической химии им. Н.С. Курнакова, Российская академия наук (ИОНХ РАН) (119991, Россия, Москва, Ленинский пр-т, д. 31). E-mail: bykov@igic.ras.ru. Scopus Author ID 17433685800, ResearcherID N-7157-2015, SPIN-код РИНЦ 9498-8148, https://orcid.org/0000-0003-1793-8487

Жданов Андрей Петрович, к.х.н., научный сотрудник лаборатории химии легких элементов и кластеров, ФГБУН Институт общей и неорганической химии им. Н.С. Курнакова, Российская академия наук (ИОНХ РАН) (119991, Россия, Москва, Ленинский пр-т, д. 31). E-mail: zhdanov@igic.ras.ru. Scopus Author ID 36350472200, SPIN-код РИНЦ 1544-8482, https://orcid.org/0000-0003-4083-386X

Жижин Константин Юрьевич, д.х.н., профессор, чл.-корр. РАН, главный научный сотрудник лаборатории химии легких элементов и кластеров, ФГБУН Институт общей и неорганической химии им. Н.С. Курнакова, Российская академия наук (ИОНХ РАН) (119991, Россия, Москва, Ленинский пр-т, д. 31); профессор кафедры неорганической химии, Институт тонких химических технологий им. М.В. Ломоносова, ФГБОУ ВО «МИРЭА – Российский технологический университет» (119571, Россия, Москва, пр-т Вернадского, д. 86). E-mail: zhizhin@igic.ras.ru. Scopus Author ID 6701495620, ResearcherID C-5681-2013, SPIN-код РИНЦ 4605-4065, https://orcid.org/0000-0002-4475-124X

Кузнецов Николай Тимофеевич, д.х.н., профессор, академик РАН, заведующий лабораторией химии легких элементов и кластеров, ФГБУН Институт общей и неорганической химии им. Н.С. Курнакова, Российская академия наук (ИОНХ РАН) (119991, Россия, Москва, Ленинский пр-т, д. 31). E-mail: ntkuz@igic.ras.ru. Scopus Author ID 56857205300, ResearcherID S-1129-2016, SPIN-код РИНЦ 3876-6006, https://orcid.org/0000-0002-0131-6387

Translated from Russian into English by H. Moshkov
Edited for English language and spelling by Dr. David Mossop

Tonkie Khimicheskie Tekhnologii = Fine Chemical Technologies.
2024;19(1):72–87 ISSN 2686-7575 (Online)

UDC 621.315.5
https://doi.org/10.32362/2410-6593-2024-19-1-72-87

REVIEW ARTICLE

Methods for the synthesis of barium titanate as a component of functional dielectric ceramics

Anastasia A. Kholodkova[1,2], Alexander V. Reznichenko[1], Alexander A. Vasin[1], Andrey V. Smirnov[1,✉]

[1] *MIREA – Russian Technological University, Moscow, 119454 Russia*

[2] *Faculty of Chemistry, Lomonosov Moscow State University, Moscow, 119991 Russia*

✉ *Corresponding author, e-mail: smirnov_av@mirea.ru*

Abstract

Objectives. To examine the general principles and recent advances in the synthesis of high-purity and high-homogeneity barium titanate powders in the manufacture of electronic components.

Results. The main publications regarding the synthesis of barium titanate powder, including the works of recent years, were analyzed. The technological advantages and disadvantages of various synthesis methods were identified. Groups of methods based on solid-state interaction of reagents and methods of "wet chemistry" were also considered. The possibilities of producing barium titanate particles of non-isometric shapes for creating textured ceramics were discussed separately.

Conclusions. Barium titanate is a well-known ferroelectric with a high dielectric constant and low dielectric loss. It is used as a component in ceramic electronic products, for example, capacitors, memory devices, optoelectronic devices, and piezoelectric transducers. The possibilities of producing functional ceramics based on barium titanate powder largely depend on its state and morphological characteristics, determined during the synthesis stage. The most important factors affecting the functional characteristics of ceramics are the purity and morphology of the powder raw materials used.

Keywords

barium titanate, ferroelectrics, piezoceramics, perovskite-like oxide ferroelectrics, solid-state synthesis, sol–gel method, hydrothermal synthesis, supercritical water

Submitted: 31.12.2022
Revised: 03.10.2023
Accepted: 26.01.2024

For citation

Kholodkova A.A., Reznichenko A.V., Vasin A.A., Smirnov A.V. Methods for the synthesis of barium titanate as a component of functional dielectric ceramics. *Tonk. Khim. Tekhnol. = Fine Chem. Technol.* 2024;19(1):72–87. https://doi.org/10.32362/2410-6593-2024-19-1-72-87

ОБЗОРНАЯ СТАТЬЯ

Методы синтеза титаната бария как компонента функциональной диэлектрической керамики

А.А. Холодкова[1,2], А.В. Резниченко[1], А.А. Васин[1], А.В. Смирнов[1,✉]

[1] *МИРЭА – Российский технологический университет, Москва, 119454 Россия*

[2] *Химический факультет, Московский государственный университет им. М.В. Ломоносова, Москва, 119234 Россия*

✉ *Автор для переписки, e-mail: smirnov_av@mirea.ru*

Аннотация

Цели. Проанализировать общие принципы и последние достижения в области синтеза порошков титаната бария высокой чистоты и гомогенности для изготовления электронных компонентов.

Результаты. Рассмотрены основные публикации о синтезе порошка титаната бария, включая работы последних лет, отмечены достоинства и недостатки различных методов синтеза с технологической точки зрения. Проанализированы группы методов, основанные на твердофазном взаимодействии реагентов, и методы «мокрой химии». Отдельно обсуждены возможности получения частиц титаната бария неизометричной формы, предназначенные для создания текстурированной керамики.

Выводы. Титанат бария является широко известным сегнетоэлектриком с высокой диэлектрической проницаемостью и низким значением диэлектрических потерь и применяется в качестве компонента керамических изделий электроники, например, для конденсаторов, запоминающих устройств, оптоэлектронных устройств, пьезоэлектрических преобразователей. Возможности производства функциональной керамики на основе порошка титаната бария во многом зависят от его фазовых и морфологических характеристик, которые определяются на этапе синтеза. Одними из важнейших факторов, влияющих на функциональные характеристики керамики, выступают чистота и морфология используемого порошкового сырья.

Ключевые слова

титанат бария, сегнетоэлектрики, пьезокерамика,
перовскитоподобные оксидные сегнетоэлектрики, твердофазный синтез,
золь-гель метод, гидротермальный синтез, сверхкритический водный флюид

Поступила: 31.12.2022
Доработана: 03.10.2023
Принята в печать: 26.01.2024

Для цитирования

Холодкова А.А., Резниченко А.В., Васин А.А., Смирнов А.В. Методы синтеза титаната бария как компонента функциональной диэлектрической керамики. *Тонкие химические технологии*. 2024;19(1):72–87. https://doi.org/10.32362/2410-6593-2024-19-1-72-87

INTRODUCTION

The synthesis of complex oxides can often be a challenging task in both laboratory and industrial practice. Along with oxygen, such compounds contain two or more other chemical elements. Depending on their quantitative ratio and the conditions of the synthesis process, stable compounds of various compositions can be obtained from the same components. Thus, the targeted synthesis of a single-state product with a strictly defined stoichiometry requires the use of certain technological approaches. Currently, several groups of methods for producing complex oxides have been developed in solid-state chemistry. They include high-temperature treatment of reagents, flow synthesis, melt synthesis, hydrothermal synthesis, and other methods using solutions, as well as their combinations. The article discusses the principles of the most important and popular methods.

METHODS FOR THE SYNTHESIS OF BARIUM TITANATE

At temperatures below 120°C, barium titanate has ferroelectric properties. The most important requirements for fine-crystalline $BaTiO_3$ powder are a high level of purity, uniformity of state composition, narrow size distribution of crystals, identical (usually round) shape, and a low degree of agglomeration [1]. To date, a large number of methods for the synthesis of $BaTiO_3$ powder have been developed. They can be attributed to one or another of the main groups of methods for the synthesis of complex oxides. There are also many hybrid methods (sol–gel hydrothermal process, sol–gel process in a supercritical medium, etc.).

High-temperature solid-state synthesis

In the solid-state synthesis of pure $BaTiO_3$, the reactants are typically $BaCO_3$ and TiO_2. They are mixed by grinding

in a mill for 2 to 24 h in air or in an alcohol medium. The prepared mixture is then dried in air at a temperature of about 80°C. The synthesis is carried out at temperatures from 800 to 1400°C for up to 8 h [2–6]. The process of transforming the reactants into the final product, barium metatitanate, can be divided into three stages [2]. During heating of the reaction mixture, barium carbonate decomposes to form oxide, and barium ions diffuse into the structure of titanium dioxide. Pure $BaCO_3$ releases CO_2 at a temperature of 825°C [4], while in the presence of TiO_2, decomposition begins at a lower temperature. The removal of BaO from the decomposition reaction due to its interaction with TiO_2 accelerates the process at the initial stage. The formation of $BaTiO_3$ can be observed already at 650°C [7]. As a new $BaTiO_3$ state is formed on the TiO_2 surface, the reaction becomes diffusion-controlled and is hampered by the low solubility of BaO in metatitanate (less than 100 ppm). This leads to the formation of the orthotitanate Ba_2TiO_4 state [8]. The processes occurring in the solid-state reaction front can be expressed by the following equations:

$$BaO + TiO_2 = BaTiO_3 \quad (1)$$

$$BaTiO_3 + BaO = Ba_2TiO_4 \quad (2)$$

$$Ba_2TiO_4 + TiO_2 = 2BaTiO_3 \quad (3)$$

In practice, the reaction (3) does not always proceed completely, and the final product of the synthesis contains undesirable impurities of Ba_2TiO_4. The particle size of the initial $BaCO_3$ is usually of the order of 1 μm, and their interaction with TiO_2 requires fairly high temperatures (up to 1100°C). As a result, the product obtained consists of large agglomerates which require grinding.

The grinding procedure was carried out in one of three ways: once over a long period of time (12 h, 270 rpm) [2]; with the use of dispersants (ammonium polyacrylate) [7]; or repeatedly, alternating with heating the oxide mixture [6]. In some works, grinding was performed in liquid media such as water, alcohols, etc. [9, 10]. It was noted that, in this case, the surface of the reactants was found to be enriched with hydroxyl and/or alkoxy groups. This slowed down their solid-state interaction at the stage of heat treatment [10, 11]. At the same time, the reactivity of the components of the mixture increased, facilitating the diffusion of Ba^{2+} ions into the TiO_2 matrix. Grinding the reagents to a nanocrystalline state enabled the synthesis temperature to be reduced to 800°C. This also reduced the formation of Ba_2TiO_4, and eliminated the need to grind the final product. It was shown [12] that a similar effect persisted at grinding durations of up to 20 h, after which the particles reagglomerated. Due to the diffusion control of the process, the shape and size of the product particles in the absence of intensive agglomeration at low temperatures were close to the shape and size of the particles of the initial TiO_2 [7]. The morphology inheritance allowed for the characteristics of the final product to be controlled at the synthesis planning stage.

It was noted that by lowering the pressure of air or CO_2 over the oxides during the process, their reactivity increased due to easier release of CO_2 [7]. However, in this case, Ba_2TiO_4 is formed to a greater extent. Increasing the CO_2 pressure over the reaction mixture (up to 100 kPa), in turn, allows for the formation of orthotitanate to be completely suppressed. Pre-grinding of the reactants and control of CO_2 pressure create conditions for the synthesis of pure nanocrystalline $BaTiO_3$ by high-temperature solid-state transformation (Fig. 1).

Ultrasonic treatment is used as an alternative to grinding for preparing the reaction mixture for solid-state transformation [13–16]. Depending on the nature of the medium in which the reactants are placed, ultrasonic treatment has a dispersing effect (e.g., in ethanol [16]) and can also lead to chemical activation of the surface. $BaCO_3$ can partially dissolve in non-alkaline aqueous solutions. It was determined that ultrasonic radiation causes a rearrangement of barium ions on the surface of TiO_2 particles, which has a negative ζ potential [14]. As a result of these processes, the temperature required to transform the treated mixture of reactants into barium titanate is lower than in the case of grinding. The average particulate size of the product is also smaller.

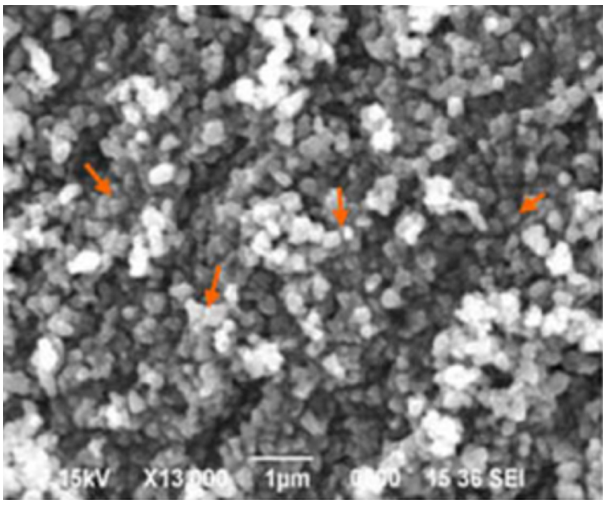

Fig. 1. Scanning electron microscope (SEM) image of a $BaTiO_3$ sample synthesized by high-temperature solid-state method at 800°C [6]

Mechanochemical synthesis

Mechanical treatment of the reactants in the solid-state production of $BaTiO_3$ is often a preparatory step before high-temperature heating. However, a number of studies have showed that the preparation of barium titanate can feasibly be achieved by entirely mechanochemical methods [17–21].

As in high-temperature synthesis, the source of titanium ions in such a process is TiO_2, and a more efficient source of barium ions is BaO or $Ba(OH)_2$[17]. It should be noted that these barium compounds tend to interact with carbon dioxide and water from the surrounding air. In order to estimate the amount of the reactant correctly, operations with BaO and $Ba(OH)_2$ must be carried out in an inert atmosphere. The path from the reactants to the final product passes through the formation of the intermediate compound Ba_2TiO_4 [22]. The near-room temperature at which mechanochemical synthesis is carried out is insufficient to decompose $BaCO_3$. As a result, the reaction is slow or inhibited. For the same reason, the reaction between barium and titanium oxides was performed without CO_2 access in a nitrogen atmosphere or in vacuum [22]. The medium in which the mechanical treatment of the reaction mixture is carried out significantly affects not only the completeness of the reaction, but also the size of the $BaTiO_3$ particles [23]. Replacing a gaseous medium with a liquid medium (e.g., toluene) allows a product to be obtained which consists of smaller crystals. The important role of mill design was also noted. For example, a ball mill enables a nearly 100% conversion of a mixture of BaO and TiO_2 into $BaTiO_3$ to be achieved in 4 h. When using an attritor, 12 min are sufficient for the complete reaction between TiO_2 and $BaCO_3$ [17, 19]. In order to increase the mechanical action intensity in the synthesis in a ball mill, a sufficiently high weight ratio of the balls and the reaction mixture was chosen: from 20 : 1 to 25 : 1 [17, 22, 23]. The range of energies imparted by the ball upon impact to ensure the transformation of a mixture of barium and titanium oxides into $BaTiO_3$ was established as 50–160 mJ [20]. Based on these values, efficient conditions for mechanochemical synthesis can be chosen.

Soft mechanochemical synthesis without thermal treatment of reactants can produce crystalline $BaTiO_3$ particles close in size to nanoparticles (Fig. 2). It is easy to perform, and has low energy consumption.

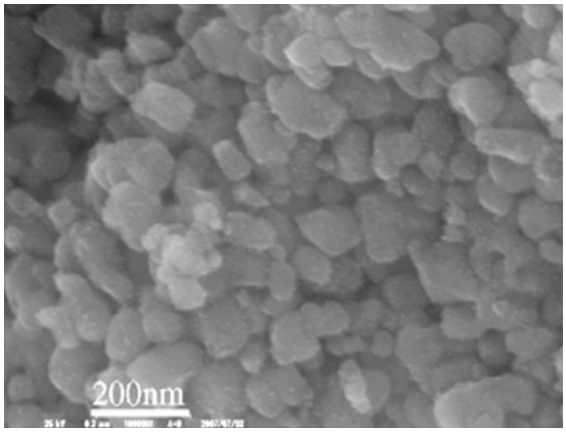

Fig. 2. SEM image of a $BaTiO_3$ sample obtained by mechanochemical synthesis [19]

Complexation methods

In complexation methods for the synthesis of crystalline $BaTiO_3$, the reactants are, as a rule, barium salts ($Ba(NO_3)_2$, $BaCO_3$, $BaCl_2$, $Ba(CH_3COO)_2$) and various titanium compounds (butoxide, isopropoxide, tetrachloride, dioxide). The chelating agent is citric or ethylenediaminetetraacetic (EDTA) acid. The auxiliary reagents can also be ethylene glycol, ammonium hydroxide, and nitric acid.

At the beginning of the citrate process, the titanium-containing reactant is hydrolyzed in the acidic medium of a complexing agent. A barium salt solution is also prepared (if the reactant is $BaCO_3$, it is also dissolved in the acidic medium). By mixing the prepared solutions, a solution of barium titanium citrate is obtained [24]. At this stage, it is important to control the acidity of the medium, since the composition of the mixed citrate depends on the pH. At a low pH value, a complex of the composition $BaTi(C_6H_6O_7)_3 \cdot 6H_2O$ with a molar ratio of cations of 1 : 1 is formed. By increasing pH, $Ba_2Ti(C_6H_5O_7)_2(C_6H_6O_7) \cdot 7H_2O$ with a Ba : Ti ratio of 2 : 1 is produced [25]. In order to maintain the stoichiometry of the final product ($BaTiO_3$) in the precursor, pH 5–6 is maintained in the reaction medium by adding the required amount of NH_4OH or HNO_3 [26, 27]. In some studies, citric acid was replaced with EDTA, which is a stronger complexing agent [27, 28]. The operations described herein are similar to those in the Pechini method, with the exception of the addition of ethylene glycol to the reaction system at one of the stages [29]. A simpler scheme was also proposed for preparing a precursor by dissolving $BaCl_2$ and TiO_2 in a solution of citric acid with heating and stirring until a viscous gel is formed [30].

Then, water is evaporated from the solutions (90°C, 1–2 h) and the precursor obtained is dried. In the Pechini method, the temperature is raised to 180°C for several hours, in order to esterify ethylene glycol and citric acid and form a polymer.

The final stage of synthesis in each of the methods is high-temperature heating of the precursor. At this stage, organic components are removed and $BaTiO_3$ crystallizes. Heating for up to 8 h is carried out in air at temperatures from 600 to 1000°C. The aim of the synthesis stages preceding heating is to achieve a high degree of reagent mixing. The heating conditions, in turn, determine the state purity and morphological features of $BaTiO_3$ crystals.

The literature presents two points of view on the mechanism of the process which occurs when the precursor is heated. According to one point of view, in the temperature range from 380 to 525°C, the precursor transforms into an intermediate compound of the composition $BaTi_2O_5CO_3$. This decomposes at a temperature of about 690°C to form the final barium titanate [31]. Other observations

of the decomposition of the precursor establish that heating leads to only partial formation of an intermediate compound [32]. Most of the precursor decomposes into $BaCO_3$ and TiO_2 (X-ray amorphous) in the temperature range from 435 to 500°C which interact at a temperature of about 600°C [25, 26, 32]. The decomposition mechanism depends on the heating conditions [32]. A systematic study [33] showed that the formation of $BaCO_3$ can be avoided by removing organic components for a longer time up to 24 h at lower temperatures (about 300°C), at which no carbonate has yet been formed. Before further increasing the temperature, the precursor is ground. It is recommended to heat to the upper temperature at the maximum possible rate [27] and to apply a long holding time (about 8 h) [33]. Subject to such conditions, the purity of the product increases. It does not contain $BaCO_3$ impurities.

A significant conclusion which can be drawn from studies of the mechanism of precursor decomposition is the fact of the formation of $BaCO_3$ and TiO_2 in the form of separate states at temperatures lower than the temperature of the beginning of $BaTiO_3$ crystallization. This means that the mixing of cations at the atomic level, achieved by preparing complex compounds, is violated by heat treatment of the precursor. $BaTiO_3$ is formed by the solid-state reaction of $BaCO_3$ and TiO_2 [25]. An advantage of complexation over conventional solid-state synthesis is the smaller size of interacting particles (nanometers). This cannot be achieved by mechanical processing of coarser reactants. As a result, the crystals of the product are also micro- and nanosized (up to 130 nm). Under certain conditions, one can obtain samples consisting of crystals smaller than 50 nm in size with a narrow size distribution [29, 32, 34] (Fig. 3).

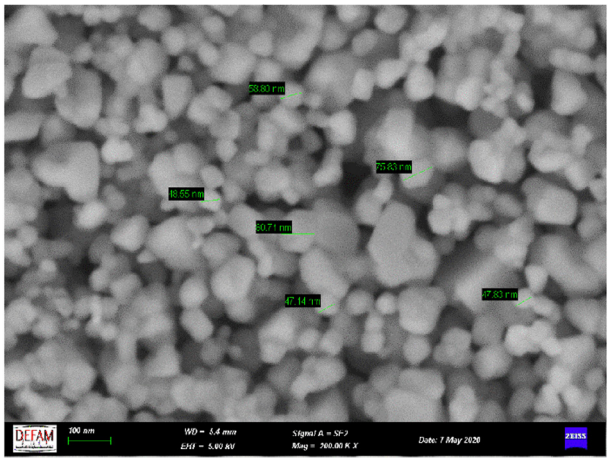

Fig. 3. SEM image of $BaTiO_3$ nanocrystals obtained by the Pechini method [29]

Another advantage of the technology under consideration is its high level of control over the stoichiometry of the product. This is due to the possibility of the formation of mixed complexes with a given Ba : Ti ratio in the solution [35]. However, nanocrystals are highly prone to agglomeration due to low ζ potential values at the pH of the solution above 1.5 [36]. Heat treatment at the final stage of the process reduces their size [34]. A high degree of powder agglomeration creates difficulties during the sintering of ceramics. This is because the behavior of the structure of workpieces containing agglomerates during firing has been insufficiently studied [35]. According to various data, $BaTiO_3$ nanocrystals obtained by complexation methods form agglomerates ranging in size from 0.2 to 2.0 μm [32, 37].

Sol–gel method

The sol–gel method is used to obtain crystalline $BaTiO_3$ powders, as well as thin films, coatings, and aerogels [38–43]. This method allows the stoichiometry of the final product to be easily adjusted, and facilitates the production of powders of various barium titanates ($BaTiO_3$, Ba_2TiO_4, $BaTi_2O_5$, $BaTi_4O_9$) by varying the molar ratio of the reactants [44, 45].

In the sol–gel synthesis of $BaTiO_3$, as in most other complex oxides, one of the reactants is a transition metal alkoxide (titanium isopropylate or titanium butoxide). This is due to its high activity in the hydrolysis and condensation reactions [46, 47]. Barium ions are introduced into the reaction mixture as an alcohol solution of hydroxide, acetate, acetylacetonate, or also alkoxides [44, 46, 48, 49]. The reactants are mixed in a dry inert atmosphere, in order to prevent them from interacting with water vapor or carbon dioxide [46, 48]. In this regard, the more suitable choice is acetylacetonate or barium acetate, since they are more moisture-resistant [46]. The mixing of the reactants leads to the rapid and complete alcoholysis of alkoxides and polycondensation, in order to form Ti–O–Ti and Ti–O–Ba^{2+} bonds [48]. In an acidic medium (pH 2.5–3.5), the acidity of which is provided by adding acetic acid, the mixture is converted into a sol by hydrolysis [46, 50]. In this case, water molecules contribute to the redistribution of fragments of the condensed system by the formation of hydrogen bonds [48]. With an increase in the pH, the hydrolysis of alkoxides leads to crystallization of metal hydroxides and oxides from the solution, rather than to the formation of a gel [51]. The hydrolysis rate decreases with the length of the carbon chain of alkoxides [46] and also depends on the presence of auxiliary reagents. The addition of chelating agents (e.g., acetylacetone) or surfactants to the reaction mixture enables the progress of condensation and polymer growth to be controlled by reducing the reaction rate [46, 52]. Gelation is often carried out at room temperature, in order to achieve a more uniform structure, since heating naturally accelerates the process [50]. The gel thus prepared is

dried at temperatures from 50 to 110°C from several hours to several days. According to various observations, the structure of the gel and the precursor, as well as the temperature required for calcination, depends on the nature of the Ba-containing reactant. Heating the precursor to 200°C is accompanied by the evaporation of solvent residues, and then, with further heating to 400°C, organic fragments are pyrolyzed. When heated to 500°C, the powder has an amorphous structure. $BaTiO_3$ begins to crystallize at about 550°C in the case of synthesis from barium acetate or isopropylate [44, 49], at 600°C when synthesized from hydroxide [48], and at 620°C when using barium acetylacetonate [46]. The mechanism of crystallization of $BaTiO_3$ from gel has no unambiguous interpretation. Some studies reported the absence of any intermediate compounds and the direct formation of $BaTiO_3$ from the precursor [44, 48]. There is a point of view that, during the decomposition of the gel, barium titanate is preceded by oxycarbonate $Ba_2Ti_2O_5CO_3$ [49]. It is more likely that the gel will decompose to form $BaCO_3$ and TiO_2, which then enter into solid-state interaction [46, 49, 52], as in the complexation methods.

In most studies, calcination of the gel for up to 2 h is carried out at temperatures up to 900°C [44, 46, 49, 52]. It was noted the product is weakly crystallized [46] and contains small amounts of $BaCO_3$ [52–54]. The crystals in single-state $BaTiO_3$ powders obtained by the sol–gel method had a narrow size distribution in the range from 37 to 70 nm (Fig. 4) [49, 52, 55].

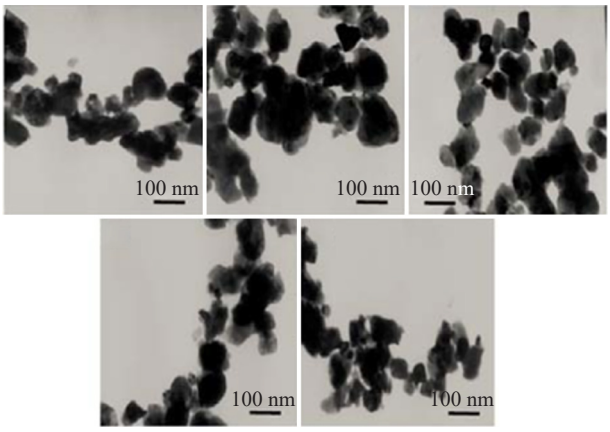

Fig. 4. Transmission electron microscope (TEM) images of $BaTiO_3$ crystals obtained by the sol–gel method [52]

Hydrothermal method

The hydrothermal method is one of the main methods used to obtain $BaTiO_3$. The reactants are typically barium salts ($BaCl_2$, $Ba(NO_3)_2$), or $Ba(OH)_2$ and titanium dioxide in the amorphous or crystalline state [56–58]. The reactivity of amorphous TiO_2 under hydrothermal conditions is higher than that of crystalline TiO_2 [59]. Therefore, it is often synthesized *in situ* using titanium alkoxides or chlorides as reactants which at the beginning of the process are hydrolyzed, in order to form $TiO_2 \cdot H_2O$ [57, 60, 61]. A mixture of reactants in an aqueous solution is placed in a closed reactor and maintained at a temperature from 130 to 250°C and at an equilibrium pressure [56–58, 61] for a time ranging from several hours [34, 56, 61] to several days [58, 62]. The product is cooled, washed with an acid solution and distilled water, in order to remove $BaCO_3$, and dried in air or vacuum [34, 56, 61, 62].

The literature shows two points of view on the mechanism of formation of $BaTiO_3$ under hydrothermal conditions. According to one of them, the transformation occurs by means of a solid-state mechanism without dissolving TiO_2 [63, 64]. In this case, the solution facilitates the transport of Ba^{2+} ions to the TiO_2 surface in comparison with high-temperature solid-state synthesis. The model of product formation remains the same: the formation of a $BaTiO_3$ layer on the TiO_2 surface and the gradual propagation of the reaction front into the initial particles. According to the other point of view, a dissolution–precipitation mechanism takes place in which the nucleation occurs homogeneously in the solution as a result of the reaction of Ba^{2+} and $Ti(OH)_n^{4-n}$ [58, 63–65]. This point of view garnered more experimental confirmations and is thus shared by most researchers.

An important advantage of hydrothermal synthesis is that $BaTiO_3$ is the only form of the complex oxide stable under these conditions. For the reaction system, thermodynamic parameters of ions in an equilibrium state were calculated. Taking solubility into account, diagrams were constructed to determine the conditions for obtaining a $BaTiO_3$ precipitate at different temperatures [68]. As an example, Fig. 5 shows such a diagram for 160°C. It can be seen that the $BaTiO_3$ precipitate forms at high pH values. However, the pH of the initial $Ba(OH)_2$ solution may be insufficiently high for the precipitate to form [69] (Fig. 6). Therefore, in order to maintain the required basicity of the medium, an excess of strong alkalis (KOH, NaOH) is initially added to the reaction mixture [56, 57, 60]. A study of the attenuation of X-ray radiation in samples of reaction mixtures and products of hydrothermal synthesis of barium titanate for 15–120 min at a temperature of 100–200°C revealed the presence of various polytitanates in the reaction medium [68]. The first product to form is the titanium dioxide-enriched state $BaTi_2O_5$. Metatitanate $BaTiO_3$ is formed in tandem with it. After further progress of the process, the third state, Ba_2TiO_4, is produced. At the final stage, the only remaining product is $BaTiO_3$. The formation of different states in a hydrothermal process may indicate that its mechanism is more complex than suggested by the dissolution–precipitation model and is complemented by the *in situ* model.

The problem in obtaining stoichiometric $BaTiO_3$ is the partial leaching of Ba^{2+} ions from the crystal surface, observed in both acidic and basic media [24, 66, 71, 72]. This process occurs least intensely at pH 7–11 [71].

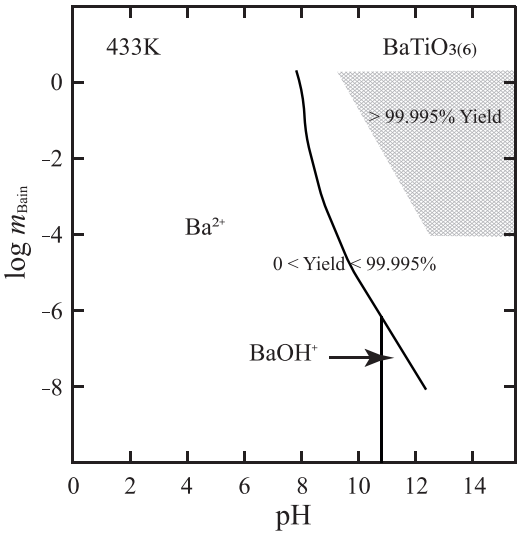

Fig. 5. Stable forms of barium ions in the Ba^{2+}–TiO_2 reaction system at 160°C and the yield of the product ($BaTiO_3$), depending on the pH and the input total molality of barium ions [68]

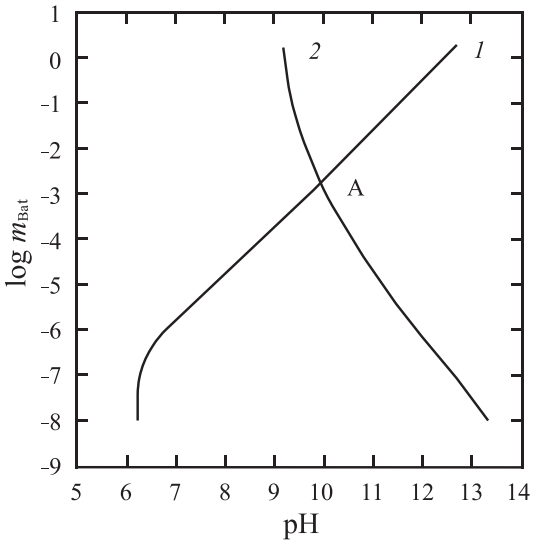

Fig. 6. Comparison of (*1*) the pH of an aqueous $Ba(OH)_2$ solution and (*2*) the pH required for crystallization of $BaTiO_3$ at various total molalities [69]

Hydrothermally produced $BaTiO_3$ crystals are usually round in shape and tend to form agglomerates. They can be characterized by narrow size distribution and an average size from 20 to 500 nm [32, 56, 58, 61, 62]. In some cases, it was possible to synthesize cubic-cut nanocrystals ranging in size from 5 to 15 nm [57] (Fig. 7).

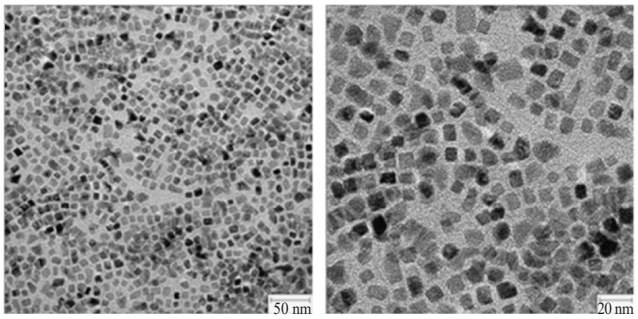

Fig. 7. TEM images of $BaTiO_3$ nanocrystals synthesized hydrothermally at 130°C in 16 h [57]

The different solubility of different forms of the initial TiO_2 makes it possible for small $BaTiO_3$ crystals (up to 110 nm) to be obtained from amorphous oxide and larger ones (from 200 to 700 nm) from sparingly soluble rutile [59]. Increasing the basicity of the medium accelerates the dissolution of TiO_2, resulting in the formation of smaller $BaTiO_3$ crystals [58]. The growth of larger crystals is promoted by an excess of Ba^{2+} in the reaction medium [62] and an increase in the temperature and duration of the process [58, 61].

Synthesis in a supercritical water medium

Under supercritical conditions, the synthesis of $BaTiO_3$ powder can be performed both in a flow reactor and in a batch reactor. The reactants are barium salts or hydroxide (oxide), and titanium dioxide or chloride. It is recommended to perform manipulations with BaO and $Ba(OH)_2$ for the preparation of the reaction mixture in an inert atmosphere. Under stationary conditions, the synthesis is carried out at 400°C and 26 MPa for 20 h [73]. The product of the reaction is pure crystalline $BaTiO_3$ powder consisting of round crystals with an average size of about 80 nm. Individual crystals reach 370 nm (Fig. 8) without the use of auxiliary reagents.

The results of the use of the flow conditions were presented for the synthesis at temperatures from 380 to 420°C and pressures from 25 to 40 MPa [74, 75]. The flow reactor was equipped with two mixers. One was supplied with solutions of reactants and auxiliary substances (e.g., alkali). In the other mixer, the reactant solution was combined with water preheated above the critical point. The mixture prepared in this way entered the reactor at a controlled flow rate and was then cooled in the downstream part of the reactor. The process took from a few milliseconds to 4 s. For the crystallization of $BaTiO_3$, the pH was maintained at 11–12 by adding a KOH solution to the reaction system or taking an excess amount of $Ba(OH)_2$. The suspension removed

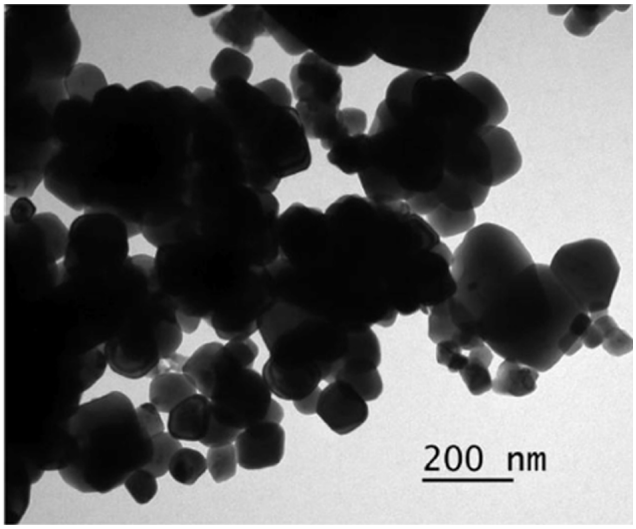

Fig. 8. TEM image of $BaTiO_3$ crystals synthesized in supercritical water at 400°C and 26 MPa in a batch reactor [73]

from the reactor was filtered. It was then successively washed with a solution of acetic acid and distilled water, and dried in air. Pure crystalline $BaTiO_3$ was obtained. The size of the crystals indicates its dependence on the duration of the process. Within 4 to 8 ms, nanocrystals (from 5 to 13 nm) were obtained [74], while at a duration of several seconds, the crystal size increased to 100 nm [75] (Fig. 9). Crystal growth was also observed with increasing process temperature and basicity of the medium. Due to the reduced surface tension of water in the supercritical state in comparison with the liquid state, the degree of particle aggregation in $BaTiO_3$ powders was found to be lower.

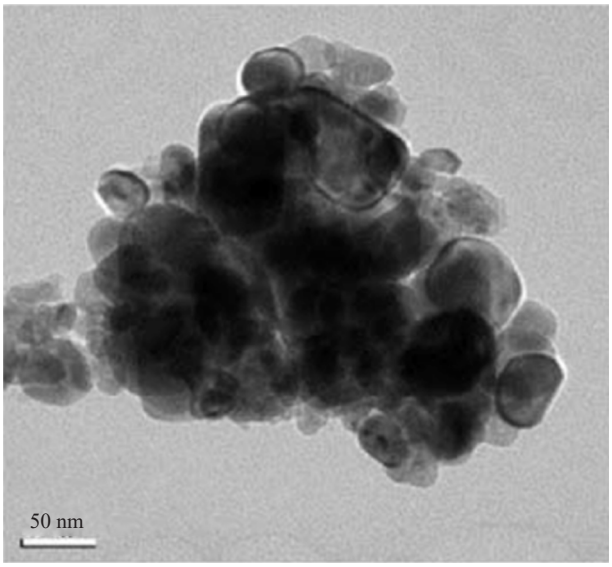

Fig. 9. TEM image of $BaTiO_3$ crystals synthesized in supercritical water at 400°C in a flow reactor [75]

SYNTHESIS OF CRYSTALINE BARIUM TITANATE OF DIFFERENT MORPHOLOGY

Effect of morphology on the properties of $BaTiO_3$ crystals

As noted earlier, the most important factor in the production of functional ceramics is to synthesize isometric submicron and nanosized $BaTiO_3$ crystals. At the same time, the ferroelectric properties of $BaTiO_3$ depend not only on temperature, but also on the size of its particles [76]. At temperatures below the Curie point, the thermodynamically stable tetragonal state is replaced by a metastable pseudocubic state in crystals the size of which is smaller than the critical size. The pseudocubic state is paraelectric, i.e., it does not possess ferroelectric properties. One explanation for this phenomenon is the lack of an external electric field capable of neutralizing the own field of polarized particles with a high specific surface area. A certain role is played by the excess surface energy of nanosized particles. Small particles are characterized by a noticeable increase in the effect of structural defects which have a charge disrupting spontaneous polarization. Moreover, spontaneous polarization is a bulk process based on long-range interactions which is difficult to achieve if the crystal volume is very small [77, 78]. Data on the critical size of $BaTiO_3$ crystals varies between different sources, indicating on average a value of several tens of nanometers [77, 79, 80].

The manifestation of ferroelectric properties depends on the size of the particles, as well as on their geometry [81]. In comparison with round submicron and nanoparticles, which can be considered 0-dimensional, 1- and 2-dimensional $BaTiO_3$ particles possess special properties. Interest in 1-dimensional particles (needles, bars, fibers, etc.) is caused by their ability to maintain spontaneous polarization when the thickness is reduced to several nanometers [82]. This is justified by the minimal effect of the depolarizing field on cylindrical particles [83]. Furthermore, for such particles, the emergence of a new type of dipole ordering was theoretically predicted [84]. Powders consisting of 2-dimensional crystals (plates) show advantages over isometric ones in the manufacture of ceramic materials. They facilitate control of the thickness of a sample of the material, increase surface hardness, and make it possible for the piezoelectric modulus to be increased due to a high degree of grain orientation [84, 85].

Anisotropic $BaTiO_3$ particles are difficult to obtain due to the isotropy of the perovskite structure [86]. Synthesis is carried out mainly by the hydrothermal method or in molten salt [81, 86]. Crystals of a given shape are often obtained using templates which can act as reactants or porous membranes subsequently removed by etching or calcination [81].

Control of the morphology of $BaTiO_3$ under hydrothermal conditions

One of the possibilities for controlling the shape of crystals during hydrothermal synthesis is to maintain a certain basicity of the medium. The layer-by-layer formation of the $BaTiO_3$ structure in an aqueous medium is accompanied by competition between the formation of Ti–O–Ba and Ti–OH bonds [84]. At a high pH, the formation of a Ti bond with the hydroxyl group is more likely and leads to inhibition of crystal growth. The faces corresponding to different crystallographic planes contain different specific numbers of Ti atoms. Therefore, the slowdown in their growth is not uniform. The (111) face is most susceptible to the effect of OH groups. Taking advantage of this, plate-like $BaTiO_3$ crystals (average thickness 5.8 nm, average diameter 27.1 nm) were obtained from $Ba(OH)_2$ and titanium isopropoxide at 225°C for 5 h with maintaining the pH of the solution around 13 [84].

The growth of certain $BaTiO_3$ faces can be inhibited by introducing additives into the reaction medium. For example, a synthesis was reported using polyacrylic acid, which is selectively adsorbed on the high-energy (111) face and impedes crystal growth in this direction [83]. As a result, plate-like crystals were also obtained.

Additives can promote the formation of extended structures. The introduction of ammonia into the reaction medium leads to the growth of fibrous $BaTiO_3$ crystals [81]. However, the mechanism of this effect has not yet been established.

A more complex, but also more efficient way of controlling the morphology of the product is to use a titanium-containing template reactant. Such templates are typically alkali metal polytitanates with a layered structure which are active in ion-exchange reactions ($Na_2Ti_3O_7$, $K_2Ti_4O_9$, etc.). The synthesis using such reactants requires preparation. Polytitanates can be obtained hydrothermally by treating TiO_2 in a medium of NaOH or KOH (K_2CO_3) [82]. $BaTiO_3$ is formed by the exchange of Na^+ or K^+ ions for Ba^{2+} ions and subsequent restructuring with a shift of the layers of TiO_6 octahedra relative to each other.

Under conditions of the dissolution–precipitation mechanism with the formation of nuclei of a new state in a liquid medium, the reaction produces isometric $BaTiO_3$ crystals, regardless of the morphology of the reactants. However, if the goal is to obtain a product with the preserved morphology of the reactant, reaction must take place by means of an alternative mechanism which excludes dissolution [87–90]. The shape of particles of the initial layered polytitanates can be best preserved at a relatively short reaction time, low temperature, low $Ba(OH)_2$ concentration, and the use of an alcohol additive [88, 90]. Lowering the temperature to 100°C reduces the solubility of polytitanates. Polytitanates are highly soluble in a highly alkaline medium. Therefore, decreasing the $Ba(OH)_2$ concentration also leads to the desired result. The introduction of ethyl alcohol reduces the solubility of $Ba(OH)_2$ and ensures saturation of the solution with Ba^{2+} ions with a smaller amount of this reagent. Using this information, the synthesis at temperatures from 100 to 150°C for 24 h yielded plate-like crystals and fibers of $BaTiO_3$ (Figs. 10, 11).

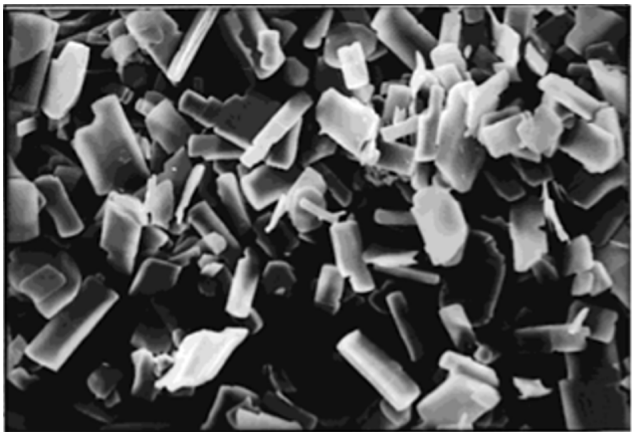

Fig. 10. SEM image of $BaTiO_3$ crystals obtained hydrothermally using plate-like $K_{0.8}Ti_{1.73}Li_{0.27}O_4$ particles as a template [87]

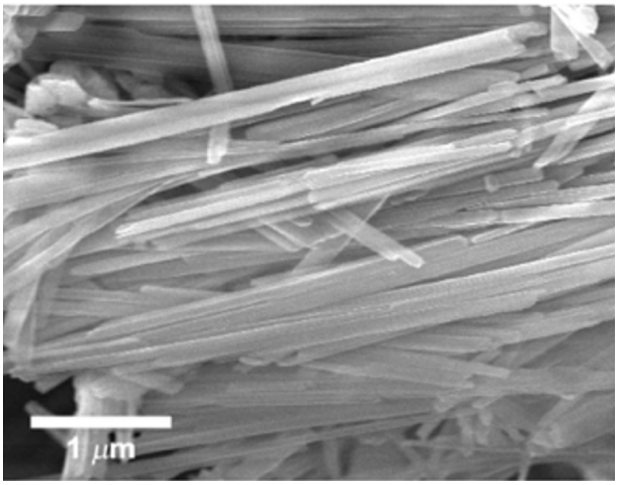

Fig. 11. SEM image of $BaTiO_3$ crystals obtained hydrothermally using bar $K_2Ti_4O_9$ particles as a template [88]

By varying the $Ba(OH)_2$ concentration, it is possible to direct the process along a path which combines both mechanisms of hydrothermal reaction. Depending on the contribution of one or the other mechanism, the shape of the product particles changes. Using extended $Na_2Ti_3O_7$ particles, $BaTiO_3$ crystals of various shapes were synthesized under hydrothermal conditions (Fig. 12) [91].

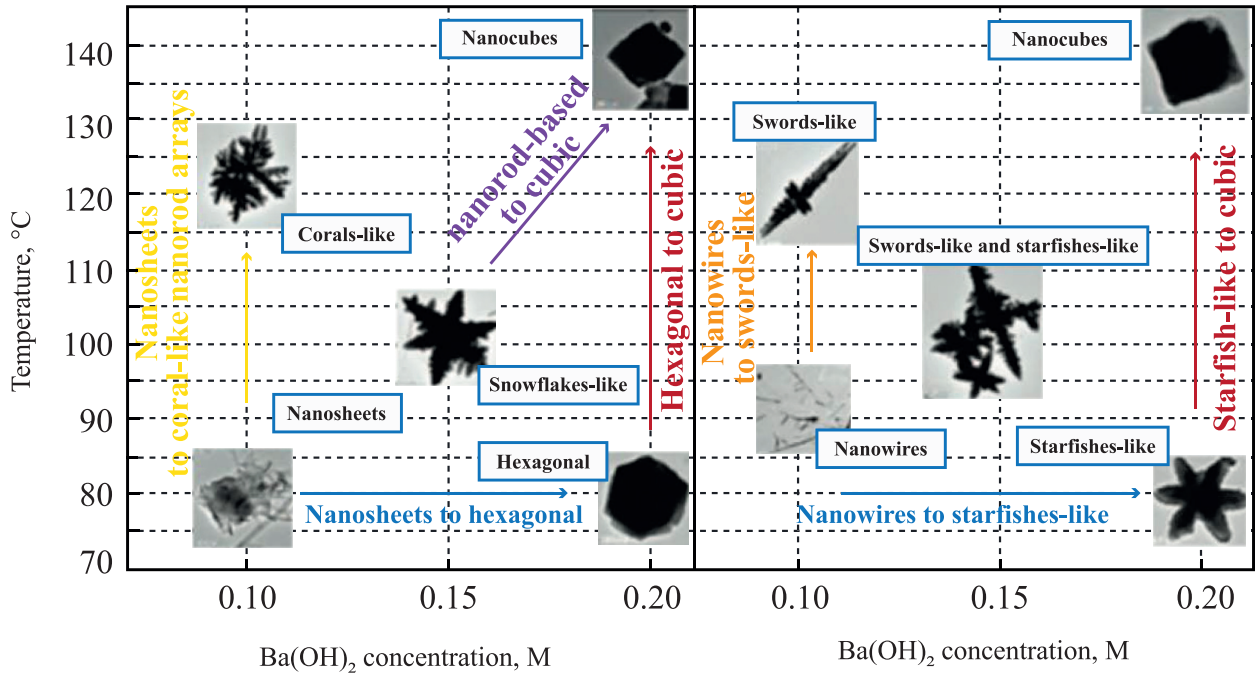

Fig. 12. Effect of the $Ba(OH)_2$ concentration and the hydrothermal process temperature on the morphology of $BaTiO_3$ synthesized using $Na_2Ti_3O_7$ particles as a template in the form of (a) nanotubes and (b) nanobars [91]

Control of the morphology of $BaTiO_3$ during molten salt synthesis

Due to features of the reaction medium, melt synthesis lacks many of the disadvantages of the previously discussed methods, but it also has its own. The melt is most often a eutectic mixture of alkali and alkaline earth metal halides, but salts with other anions, as well as hydroxides, are also used [92, 93]. The synthesis temperature ranges from 300 to 1000°C, depending on the nature of the melt and reactants. In the future, a decrease in temperature through the use of ionic liquids as a medium can be considered.

The process consists of grinding together calculated amounts of reactants and salts which will serve as a medium, then maintaining this mixture at a temperature above the melting point of the salts. $BaTiO_3$ is synthesized from TiO_2 and various barium compounds (BaO, $Ba(OH)_2$, $BaCO_3$, $Ba(NO_3)_2$) [86, 93–96]. The liquid medium facilitates the transport of ions, when compared with the conventional solid-state reaction and also slows down the growth and aggregation of $BaTiO_3$ crystals [95]. Upon completion of the high-temperature holding, the system is cooled and salts are removed by washing with water. In the synthesis of $BaTiO_3$, it is very important to control the molar ratio of the reactants, since polytitanates can be formed [94]. It was also noted that the use of amorphous TiO_2 as a reactant enables the purity of the product to be increased. The complete removal of salt ions from the final product is impossible, and $BaTiO_3$ inevitably contains impurities of other cations [94].

The principles of producing crystals with a given morphology are aimed at restraining the growth of certain crystal faces by choosing the composition of the salt mixture. A high molar ratio of salts and reactants inhibits the growth of high-energy faces. It was found that in a KCl–NaCl medium, the growth in the direction of the (101) and (001) planes is inhibited, resulting in cubic crystals. In a K_2SO_4–Na_2SO_4 medium, the growth of the (111) face slows down, and the product consists of plate-like crystals [93]. In molten salt, template reactants are also used. These can be layered polytitanates and TiO_2 with a required morphology [86, 96]. It is recommended that the source of Ba^{2+} ions be easily soluble compounds such as oxide or hydroxide, rather than salts [86]. It is important that the dissolution rate of the Ba-containing reactant should be higher than the dissolution rate of the Ti-containing reactant, and the reaction should occur by a solid-state mechanism by saturating TiO_2 with Ba^{2+} ions. Otherwise, the template morphology may be lost. Figure 13 presents an example of $BaTiO_3$ crystals synthesized from BaO and TiO_2 in a NaCl–KCl medium.

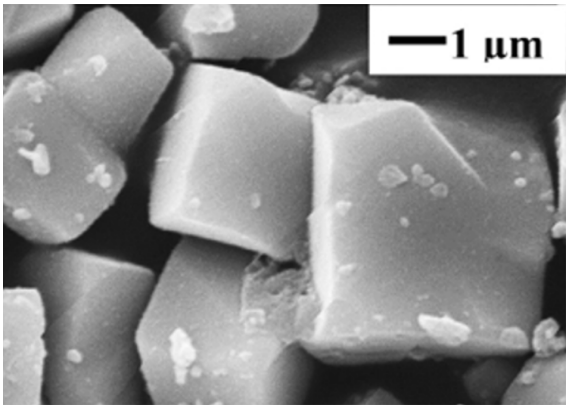

Fig. 13. SEM image of $BaTiO_3$ particles synthesized in a NaCl–KCl melt at 1080°C for 1 h [93]

CONCLUSIONS

The objective of this review was to analyze the literature data regarding for obtaining micro- and nanocrystals of $BaTiO_3$ of high purity and homogeneity, in order to find a method suitable for the synthesis of powder materials. The formation of various polytitanates in many cases complicates the production of pure $BaTiO_3$.

Experimental data on complexation methods and the sol–gel method, which were developed in order to achieve a high degree of mixing of reactants and to obtain a product of a given composition, does not always support the implementation of this idea. The data does not eliminate the formation of by-products such as carbonates and nonstoichiometric compounds. This was clearly confirmed by studies of synthesized powders by IR spectrometry and X-ray fluorescence analysis. The product typically contained traces of carbonates. Auxiliary reagents are often incompletely removed from the surface and from the bulk of the synthesized oxide. Despite the labor-intensive and expensive preparation of precursors, the temperature of their calcination can be comparable to the temperature of conventional solid-state synthesis.

The conventional solid-state synthesis method has some well-known disadvantages. It is inferior to wet chemistry methods in the homogeneity of the initial mixture of reactants and requires high temperatures to carry out the reaction. Thanks to the long-term development and improvement of this method, techniques have been found which make it possible to produce pure fine-crystalline oxides using this method (grinding the reactants and the product, repeated firing). Although the process of synthesizing complex oxides usually takes a long time, it is technically quite simple and does not require high costs for reagents and equipment.

The hydrothermal method uses mild conditions and also inexpensive reactants. Process planning requires careful monitoring of the solubility of the reactants. This method is suitable for the production of $BaTiO_3$ without impurities of polytitanates, even if the molar ratio of reactants is not 1 : 1. One general disadvantage of this method is the presence of adsorbed water on the surface of oxide crystals and OH groups as structural defects. Under hydrothermal conditions, the barium titanate particles are characterized by leaching of barium ions from the surface. The resulting local nonstoichiometry can manifest itself during further sintering of the ceramic as the undesirable growth of anomalous grains and a decrease in dielectric characteristics. The product of hydrothermal synthesis is often calcined before further use as a ceramic raw material. The hydrothermal method provides ample opportunities for controlling the shape of crystals of complex oxides.

The method for producing $BaTiO_3$ in supercritical water is promising. At the present time, the number of works on synthesis under these conditions is very limited. As such, they do not allow us to form an objective picture of the advantages and disadvantages of the method.

Acknowledgments

The study was conducted as part of the implementation of indicators for projects funded from the state budget or other external sources: The National Project “Science and Universities” to achieve the result “Creation of new laboratories, including under the guidance of young promising researchers (growing result),” FSFZ-2022-0003.

Authors’ contributions

A.A. Kholodkova, A.V. Reznichenko, A.A. Vasin – writing the text of the article, analysis and formulation of the results.

A.A. Kholodkova, A.V. Reznichenko, A.A. Vasin, A.V. Smirnov – conceptualization.

A.V. Smirnov – scientific editing, general management.

The authors declare no obvious and potential conflicts of interest related to the publication of this article.

REFERENCES

1. Pithan C., Hennings D., Waser R. Progress in the Synthesis of Nanocrystalline $BaTiO_3$ Powders for MLCC: Progress in Synthesis of Nanocrystalline $BaTiO_3$ Powders. *Int. J. Appl. Ceram. Technol.* 2006;2(1):1–14. https://doi.org/10.1111/j.1744-7402.2005.02008.x
2. Brzozowski E., Castro M.S. Synthesis of barium titanate improved by modifications in the kinetics of the solid state reaction. *J. Eur. Ceram. Soc*. 2000;20(14–15):2347–2351. https://doi.org/10.1016/S0955-2219(00)00148-5
3. Chaisan W., Yimnirun R., Ananta S., Cann D.P. Dielectric properties of solid solutions in the lead zirconate titanate-barium titanate system prepared by a modified mixed-oxide method. *Mater. Lett.* 2005;59(28):3732–3737. https://doi.org/10.1016/j.matlet.2005.06.045
4. Kambale K.R.R., Kulkarni A.R.R., Venkataramani N. Grain growth kinetics of barium titanate synthesized using conventional solid state reaction route. *Ceram. Int*. 2014;40(1A):667–673. https://doi.org/10.1016/j.ceramint.2013.06.053
5. Mikhailov M.M., Neshchimenko V.V., Utebekov T.A., Yuriev S.A. Features high-temperature synthesis of barium zirconium titanate powder by using zirconium dioxide nanopowders. *J. Alloys Compd*. 2015;652:364–370. https://doi.org/10.1016/j.jallcom.2015.08.124
6. Roy A.C., Mohanta D. Structural and ferroelectric properties of solid-state derived carbonate-free barium titanate ($BaTiO_3$) nanoscale particles. *Scr. Mater*. 2009;61(9):891–894. https://doi.org/10.1016/j.scriptamat.2009.07.022
7. Buscaglia M.T., Bassoli M., Buscaglia V., Alessio R. Solid-State Synthesis of Ultrafine $BaTiO_3$ Powders from Nanocrystalline $BaCO_3$ and TiO_2. *J. Am. Ceram. Soc*. 2005;88(9):2374–2379. https://doi.org/10.1111/j.1551-2916.2005.00451.x
8. Kainth S., Choudhary R., Upadhyay S., Bajaj P., Sharma P., Brar L.K., *et al*. Non-isothermal solid-state synthesis kinetics of the tetragonal barium titanate. *J. Solid State Chem*. 2022;312:123275. https://doi.org/10.1016/j.jssc.2022.123275
9. Qian H., Zhu G., Xu H., Zhang X., Zhao Y., Yan D., *et al*. Preparation of tetragonal barium titanate nanopowders by microwave solid-state synthesis. *Appl. Phys. A*. 2020;126(4):294. https://doi.org/10.1007/s00339-020-03472-y
10. Sundararajan T., Prabu S.B., Vidyavathy S.M. Combined effects of milling and calcination methods on the characteristics of nanocrystalline barium titanate. *Mater. Res. Bull*. 2012;47(6):1448–5144. https://doi.org/10.1016/j.materresbull.2012.02.044
11. Clabel H J.L., Awan I.T., Pinto A.H., Nogueira I.C., Bezzon V.D.N., Leite E.R., *et al.* Insights on the mechanism of solid state reaction between TiO_2 and $BaCO_3$ to produce $BaTiO_3$ powders: The role of calcination, milling, and mixing solvent. *Ceram. Int*. 2020;46(3):2987–3001. https://doi.org/10.1016/j.ceramint.2019.09.296
12. Nath A.K., Jiten C., Singh K.C., Laishram R., Thakur O.P., Bhattacharya D.K. Effect of Ball Milling Time on the Electrical and Piezoelectric Properties of Barium Titanate Ceramics. *Integr. Ferroelectr*. 2010;116(1):51–58. https://doi.org/10.1080/10584587.2010.488572
13. Rotaru R., Peptu C., Samoila P., Harabagiu V. Preparation of ferroelectric barium titanate through an energy effective solid state ultrasound assisted method. *J. Am. Ceram. Soc*. 2017;100(10):4511–4518. https://doi.org/10.1111/jace.15003
14. Lee H.W., Kim N.W., Nam W.H., Lim Y.S. Sonochemical activation in aqueous medium for solid-state synthesis of $BaTiO_3$ powders. *Ultrason. Sonochem*. 2022;82:105874. https://doi.org/10.1016/j.ultsonch.2021.105874
15. Akbas H.Z., Aydin Z., Yilmaz O., Turgut S. Effects of ultrasonication and conventional mechanical homogenization processes on the structures and dielectric properties of $BaTiO_3$ ceramics. *Ultrason. Sonochem*. 2017;34:873–880. https://doi.org/10.1016/j.ultsonch.2016.07.027
16. Jin S.H., Lee H.W., Kim N.W., Lee B.W., Lee G.G., Hong Y.W., *et al*. Sonochemically activated solid-state synthesis of $BaTiO_3$ powders. *J. Eur. Ceram. Soc*. 2021;41(9):4826–4834. https://doi.org/10.1016/j.jeurceramsoc.2021.03.043
17. Stojanovic B.D., Simoes A.Z., Paiva-Santos C.O., Jovalekic C., Mitic V.V., Varela J.A. Mechanochemical synthesis of barium titanate. *J. Eur. Ceram. Soc*. 2005;25(12):1985–1989. https://doi.org/10.1016/j.jeurceramsoc.2005.03.003
18. Stojanovic B.D. Mechanochemical synthesis of ceramic powders with perovskite structure. *J. Mater. Process. Techno*l. 2003;143–144(1):78–81. https://doi.org/10.1016/S0924-0136(03)00323-6
19. Ohara S., Kondo A., Shimoda H., Sato K., Abe H., Naito M. Rapid mechanochemical synthesis of fine barium titanate nanoparticles. *Mater. Lett*. 2008;62(17–18):2957–2959. https://doi.org/10.1016/j.matlet.2008.01.083
20. Kozma G., Lipták K., Deák C., Rónavári A., Kukovecz Á., Kónya Z. Conversion Study on the Formation of Mechanochemically Synthesized $BaTiO_3$. *Chemistr*y. 202215;4(2):592–602. https://doi.org/10.3390/chemistry4020042
21. Kudłacik-Kramarczyk S., Drabczyk A., Głąb M., Dulian P., Bogucki R., Miernik K., *et al*. Mechanochemical Synthesis of $BaTiO_3$ Powders and Evaluation of Their Acrylic Dispersions. *Materials*. 2020;13(15):3275. https://doi.org/10.3390/ma13153275
22. Kong L.B., Zhang T.S., Ma J., Boey F. Progress in synthesis of ferroelectric ceramic materials *via* high-energy mechanochemical technique. *Prog. Mater. Sci*. 2008;53(2):207–322. https://doi.org/10.1016/j.pmatsci.2007.05.001
23. Apaydin F., Parlak T.T., Yildiz K. Low temperature formation of barium titanate in solid state reaction by mechanical activation of $BaCO_3$ and TiO_2. *Materials Research Express*. 2020;6(12):126330. https://doi.org/10.1088/2053-1591/ab6c0d
24. More S.P., Khedkar M.V., Jadhav S.A., Somvanshi S.B., Humbe A.V., Jadhav K.M. Wet chemical synthesis and investigations of structural and dielectric properties of $BaTiO_3$ nanoparticles. *J. Phys.: Conf. Se*r. 2020;1644(1):012007. https://doi.org/10.1088/1742-6596/1644/1/012007
25. Hennings D., Mayr W. Thermal Decomposition of (BaTi) Citrates into Barium Titanate. *J. Solid State Chem*. 1978;26(4):329–338. https://doi.org/10.1016/0022-4596(78)90167-6
26. Kao C.F., Yang W.D. Preparation of barium strontium titanate powder from citrate precursor. *Appl. Organomet. Chem*. 1999;13(5):383–397. http://doi.org/10.1002/(SICI)1099-0739(199905)13:5<383::AID-AOC836>3.0.CO;2-P
27. Wang H. Inhibition of the formation of barium carbonate by fast heating in the synthesis of $BaTiO_3$ powders *via* an EDTA gel method. *Mater. Chem. Phys*. 2002;74:1–4. https://doi.org/10.1016/S0254-0584(01)00410-2
28. Sen S., Choudhary R.N.P., Pramanik P. Synthesis and characterization of nanostructured ferroelectric compounds. *Mater. Lett.* 2004;58(27–28):3486–3490. https://doi.org/10.1016/j.matlet.2004.06.063
29. Aktaş P. Synthesis and Characterization of Barium Titanate Nanopowders by Pechini Process. *Celal Bayar University Journal of Science* (*CBUJOS*). 2020;16(3):293–300. https://doi.org/10.18466/cbayarfbe.734061
30. Turky A.O., Rashad M.M., Bechelany M. Tailoring optical and dielectric properties of $Ba_{0.5}Sr_{0.5}TiO_3$ powders synthesized using citrate precursor route. *Mater. Des*. 2016;90:54–59. https://doi.org/10.1016/j.matdes.2015.10.113

31. Hsieh T.-H., Yen S.-C., Ray D.-T. A study on the synthesis of (Ba,Ca)(Ti,Zr)O_3 nano powders using Pechini polymeric precursor method. *Ceram. Int*. 2012;38(1):755–759. https://doi.org/10.1016/j.ceramint.2011.08.001
32. Durán P., CapelF., Tartaj J., Moure C. $BaTiO_3$ formation by thermal decomposition of a (BaTi)-citrate polyester resin in air. *J. Mater. Res.* 2001;16(1):197–209. https://doi.org/10.1557/JMR.2001.0032
33. Ries A., Simões A.Z., Cilense M, Zaghete M.A, Varela J.A. Barium strontium titanate powder obtained by polymeric precursor method. *Mater. Charact*. 2003;50(2–3):217–221. https://doi.org/10.1016/S1044-5803(03)00095-0
34. Prado L.R., de Resende N.S., Silva R.S., Egues S.M.S., Salazar-Banda G.R. Influence of the synthesis method on the preparation of barium titanate nanoparticles. *Chem. Eng. Process.: Process Intensif.* 2015;103:12–20. https://doi.org/10.1016/j.cep.2015.09.011
35. Duran P., Gutierrez D., Tartaj J., Moure C. Densification behaviour, microstructure development and dielectric properties of pure $BaTiO_3$ prepared by thermal decomposition of (Ba, Ti)-citrate polyester resins. *Ceram. Int*. 2002;28(3):283–292. https://doi.org/10.1016/S0272-8842(01)00092-X
36. Luan W., Gao L. Influence of pH value on properties of nanocrystalline $BaTiO_3$ powder. *Ceram. Int*. 2001;27(6):645–648. https://doi.org/10.1016/S0272-8842(01)00012-8
37. Lazarević Z.Ž., Vijatović M., Dohčević-Mitrović Z., Romčević N.Ž., Romčević M.J., Paunović N., *et al.* The characterization of the barium titanate ceramic powders prepared by the Pechini type reaction route and mechanically assisted synthesis. *J. Eur. Ceram. Soc*. 2010;30(2):623–628. https://doi.org/10.1016/j.jeurceramsoc.2009.08.011
38. Ashiri R., Nemati A., Sasani Ghamsari M. Crack-free nanostructured $BaTiO_3$ thin films prepared by sol–gel dip-coating technique. *Ceram. Int.* 2014;40(6):8613–8619. https://doi.org/10.1016/j.ceramint.2014.01.078
39. Hayashi T., Ohji N., Hiraoka K., Fukunaga T., Maiwa H. Preparation and Properties of Ferroelectric $BaTiO_3$ Thin Films by Sol–Gel Process. *Jpn. J. Appl. Phys.* 1993;32(9S):4092–4094. https://doi.org/10.1143/JJAP.32.4092
40. Demydov D., Klabunde K.J. Characterization of mixed metal oxides ($SrTiO_3$ and $BaTiO_3$) synthesized by a modified aerogel procedure. *J. Non-Cryst. Solids*. 2004;350:165–172. https://doi.org/10.1016/j.jnoncrysol.2004.06.022
41. Suslov A., Kobylianska S., Durilin D., Ovchar O., Trachevskii V., Jancar B., *et al*. Modified Pechini Processing of Barium and Lanthanum–Lithium Titanate Nanoparticles and Thin Films. *Nanoscale Res. Lett*. 2017;12(1):350. https://doi.org/10.1186/s11671-017-2123-8
42. Teh Y.C., Saif A.A., Poopalan P. Sol–Gel Synthesis and Characterization of $Ba_{1-x}Gd_xTiO_{3+\delta}$ Thin Films on SiO_2/Si Substrates Using Spin-Coating Technique. *Mater. Sci*. 20179;23(1):51–56. https://doi.org/10.5755/j01.ms.23.1.13954
43. Devi L.R., Sharma H.B. Structural and optical parameters of sol–gel derived Barium Strontium Titanate (BST) thin film. *Mater. Today Proc*. 2022;65(5):2801–2806. https://doi.org/10.1016/j.matpr.2022.06.219
44. Pfaff G. Sol–gel synthesis of barium titanate powders of various compositions. *J. Mater. Chem.* 1992;2(6):591–594. https://doi.org/10.1039/JM9920200591
45. Phule P.P., Risbud S.H. Sol–gel synthesis and characterization of $BaTi_4O_9$ and $BaTiO_3$ powders. In: *Materials Research Society Symposium Proceedings* (*MRS Online Proceedings Library*). 1988:121:275–280. https://doi.org/10.1557/PROC-121-275
46. Cernea M. Sol–gel synthesis and characterization of $BaTiO_3$ powder. *J. Optoelectron. Adv. Mater*. 2005;7(6):3015–3022.
47. Omar A.F.C., Hatta F.F., Kudin T.I.T., Mohamed M.A., Hassan O.H. Calcination Effect on Structural Trasformation of Barium Titanite Ferroelectric Ceramic by Sol Gel Method. *Int. J. Eng. Adv. Technol.* 2019;9(1):5893–5896. https://doi.org/10.35940/ijeat.A3023.109119
48. Lemoine C., Gilbert B., Michaux B., Pirard J.P., Lecloux A. Synthesis of barium titanate by the sol–gel process. *J. Non-Cryst. Solids*. 1994;175(1):1–13. https://doi.org/10.1016/0022-3093(94)90309-3
49. Ianculescu A.C., Vasilescu C.A., Crisan M., Raileanu M., Vasile B.S., Calugaru M., *et al.* Formation mechanism and characteristics of lanthanum-doped $BaTiO_3$ powders and ceramics prepared by the sol–gel process. *Mater. Charact*. 2015;106:195–207. https://doi.org/10.1016/j.matchar.2015.05.022
50. Phule P.P., Risbud S.H. Low-temperature synthesis and processing of electronic materials in the BaO–TiO_2 system. *J. Mater. Sci*. 1990;25:1169–1183. https://doi.org/10.1007/BF00585422
51. Nanni P., Viviani M., Buscaglia V. Synthesis of Dielectric Ceramic Materials. In: Nalwa H.S. (Ed.). *Handbook of Low and High Dielectric Constant Materials and Their Applications*. Academic Press; 1999. p. 429–55. https://doi.org/10.1016/B978-012513905-2/50011-X
52. Zheng C., Cui B., You Q., Chang Z. Characterization of $BaTiO_3$ Powders and Ceramics Prepared Using the Sol–gel Process, with Triton X-100 Used as a Surfactant. In: *The 7th National Conference on Functional Materials and Applications*. 2010. P. 341–346.
53. Bakken K., Pedersen V.H., Blichfeld A.B., Nylund I.-E., Tominaka S., Ohara K., Grande T., Einarsrud M.-A. Structures and Role of the Intermediate Phases on the Crystallization of $BaTiO_3$ from an Aqueous Synthesis Route. *ACS Omega*. 2021;6(14):9567–9576. https://doi.org/10.1021/acsomega.1c00089
54. Singh M., Yadav B.C., Ranjan A., Kaur M., Gupta S.K. Synthesis and characterization of perovskite barium titanate thin film and its application as LPG sensor. *Sensors and Actuators B: Chemical*. 2017;241:1170–1178. https://doi.org/10.1016/j.snb.2016.10.018
55. Nagdeote S.B. Sol–gel Synthesis, Structural and Dielectric Characteristics of Nanocrystalline Barium Titanate Solid. *Macromol. Symp*. 2021;400(1):2100060. https://doi.org/10.1002/masy.202100060
56. Boulos M., Guillemet-Fritsch S., Mathieu F., Durand B., Lebey T., Bley V. Hydrothermal synthesis of nanosized $BaTiO_3$ powders and dielectric properties of corresponding ceramics. *Solid State Ion.* 2005;176(13–14):1301–1309. https://doi.org/10.1016/j.ssi.2005.02.024
57. Cai W., Rao T., Wang A., Hu J., Wang J., Zhong J., *et al.* A simple and controllable hydrothermal route for the synthesis of monodispersed cube-like barium titanate nanocrystals. *Ceram. Int*. 2015;41(3):4514–4522. https://doi.org/10.1016/j.ceramint.2014.11.146
58. Lee W.W., Chung W.H., Huang W.S., Lin W.C., Lin W.Y., Jiang Y.R., *et al*. Photocatalytic activity and mechanism of nano-cubic barium titanate prepared by a hydrothermal method. *J. Taiwan Inst. Chem. Eng*. 2013;44(4):660–669. https://doi.org/10.1016/j.jtice.2013.01.005
59. Kumazawa H., Kagimoto T., Kawabata A. Preparation of barium titanate ultrafine particles from amorphous titania by a hydrothermal method and specific dielectric constants of sintered discs of the prepared particles. *J. Mater. Sci*. 1996;31(10):2599–2602. https://doi.org/10.1007/BF00687288
60. Ávila H.A., Ramajo L.A., Reboredo M.M., Castro M.S., Parra R. Hydrothermal synthesis of $BaTiO_3$ from different Ti-precursors and microstructural and electrical properties of sintered samples with submicrometric grain size. *Ceram. Int.* 2011;37(7):2383–2390. https://doi.org/10.1016/j.ceramint.2011.03.032

61. Zhu X., Zhang Z., Zhu J., Zhou S., Liu Z. Morphology and atomic-scale surface structure of barium titanate nanocrystals formed at hydrothermal conditions. *J. Cryst. Growth*. 2009;311(8): 2437–2442. https://doi.org/10.1016/j.jcrysgro.2009.02.016
62. Zhu K., Qiu J., Kajiyoshi K., Takai M., Yanagisawa K. Effect of washing of barium titanate powders synthesized by hydrothermal method on their sinterability and piezoelectric properties. *Ceram. Int.* 2009;35(5):1947–1951. https://doi.org/10.1016/j.ceramint.2008.10.018
63. Hertl W. Kinetics of Barium Titanate Synthesis. *J. Am. Ceram. Soc*. 1988;71(10):879–883. https://doi.org/10.1111/j.1151-2916.1988.tb07540.x
64. MacLaren I., Ponton C.B. A TEM and HREM study of particle formation during barium titanate synthesis in aqueous solution. *J. Eur. Ceram. Soc*. 2000;20(9):1267–1275. https://doi.org/10.1016/S0955-2219(99)00287-3
65. Eckert J.O., Hung-Houston C.C., Gersten B.L., Lencka M.M., Riman R.E. Kinetics and Mechanisms of Hydrothermal Synthesis of Barium Titanate. *J. Am. Ceram. Soc*. 1996;79(11):2929–2939. https://doi.org/10.1111/j.1151-2916.1996.tb08728.x
66. Pinceloup P., Courtois C., Vincens J., Leriche A., Thierry B. Evidence of a dissolution-precipitation mechanism in hydrothermal synthesis of barium titanate powders. *J. Eur. Ceram. Soc*. 1999;19(6–7):973–977. https://doi.org/10.1016/S0955-2219(98)00356-2
67. Walton R.I., Millange F., Smith R.I., Hansen T.C., O'Hare D. Real Time Observation of the Hydrothermal Crystallization of Barium Titanate Using *in Situ* Neutron Powder Diffraction. *J. Am. Chem. Soc.* 2001;123(50):12547–12555. https://doi.org/10.1021/ja011805p
68. Lencka M.M., Riman R.E. Hydrothermal synthesis of perovskite materials: Thermodynamic modeling and experimental verification. *Ferroelectrics*. 1994;151(1): 159–164. https://doi.org/10.1080/00150199408244737
69. Lencka M.M., Riman R.E. Thermodynamic Modeling of Hydrothermal Synthesis of Ceramic Powders. *Chem. Mater*. 1993;5(1):61–70. https://doi.org/10.1021/cm00025a014
70. Akbulut Özen S., Özen M., Şahin M., Mertens M. Study of the hydrothermal crystallization process of barium titanate by means of X-ray mass attenuation coefficient measurements at an energy of 59.54 keV. *Mater. Charact*. 2017;129:329–335. https://doi.org/10.1016/j.matchar.2017.05.006
71. Neubrand A., Lindner R., Hoffmann P. Room-Temperature Solubility Behavior of Barium Titanate in Aqueous Media. *J. Am. Ceram. Soc*. 2004;83(4):860–864. https://doi.org/10.1111/j.1151-2916.2000.tb01286.x
72. Kholodkova A.A., Danchevskaya M.N., Ivakin Y.D., Muravieva G.P. Synthesis of fine-crystalline tetragonal barium titanate in low-density water fluid. *J. Supercrit. Fluids*. 2015;105:201–208. https://doi.org/10.1016/j.supflu.2015.05.004
73. Kholodkova A.A., Danchevskaya M.N., Ivakin Y.D., Muravieva G.P., Tyablikov A.S. Crystalline barium titanate synthesized in sub- and supercritical water. *J. Supercrit. Fluids.* 2016;117:194–202. https://doi.org/10.1016/j.supflu.2016.06.018
74. Hayashi H., Noguchi T., Islam N.M., Hakuta Y., Imai Y., Ueno N. Hydrothermal synthesis of $BaTiO_3$ nanoparticles using a supercritical continuous flow reaction system. *J. Cryst. Growth*. 2010;312(12–13):1968–1972. https://doi.org/10.1016/j.jcrysgro.2010.03.034
75. Hakuta Y., Ura H., Hayashi H., Arai K. Effect of water density on polymorph of $BaTiO_3$ nanoparticles synthesized under sub and supercritical water conditions. *Mater. Lett*. 2005;59(11): 1387–1390. https://doi.org/10.1016/j.matlet.2004.11.063
76. Aoyagi S., Kuroiwa Y., Sawada A., Kawaji H., Atake T. Size effect on crystal structure and chemical bonding nature in $BaTiO_3$ nanopowder. *J. Therm. Anal. Calorim*. 2005;81(3):627–630. https://doi.org/10.1007/s10973-005-0834-z
77. Frey M.H., Payne D.A. Grain-size effect on structure and phase transformations for barium titanate. *Phys. Rev. B. Condens. Matter*. 1996;54(5):3158–3168. https://doi.org/10.1103/physrevb.54.3158
78. Hennings D., Schnell A., Simon G. Diffuse Ferroelectric Phase Transitions in $Ba(Ti_{1-y}Zr_y)O_3$ Ceramics. *J. Am. Ceram. Soc.* 1982;65(11):539–544. https://doi.org/10.1111/j.1151-2916.1982.tb10778.x
79. Lee T., Aksay I.A. Hierarchical Structure−Ferroelectricity Relationships of Barium Titanate Particles. *Cryst. Growth Des*. 2001;1(5):401–419. https://doi.org/10.1021/cg010012b
80. Kozawa T., Onda A., Yanagisawa K. Accelerated formation of barium titanate by solid-state reaction in water vapour atmosphere. *J. Eur. Ceram. Soc.* 2009;29(15):3259–3264. https://doi.org/10.1016/j.jeurceramsoc.2009.05.031
81. Buscaglia V., Buscaglia M.T. Synthesis and Properties of Ferroelectric Nanotubes and Nanowires: A Review. In: Alguero M., Gregg J.M., Mitoseriu L. (Eds.). *Nanoscale Ferroelectrics and Multiferroics: Key Processing and Characterization Issues, and Nanoscale Effects*. First Edit. John Wiley & Sons; 2016. P. 200–231. https://doi.org/10.1002/9781118935743.ch8
82. Bao N., Shen L., Gupta A., Tatarenko A., Srinivasan G., Yanagisawa K. Size-controlled one-dimensional monocrystalline $BaTiO_3$ nanostructures. *Appl. Phys. Lett*. 2009;94(25):253109. https://doi.org/10.1063/1.3159817
83. Maxim F., Ferreira P., Vilarinho P. Strategies for the Structure and Morphology Control of $BaTiO_3$ Nanoparticles. In: *New Applications for Nanomaterials*. *Series: Micro and Nanoengineering*. 2014. V. 22. P. 83–97.
84. Yosenick T.J., Miller D.V., Kumar R., Nelson J.A., Randall C.A., Adair J.H. Synthesis of nanotabular barium titanate *via* a hydrothermal route. *J. Mater. Res.* 2005;20(4):837–843. https://doi.org/10.1557/JMR.2005.0117
85. Kong X., Hu D., Ishikawa Y., Tanaka Y., Feng Q. Solvothermal Soft Chemical Synthesis and Characterization of Nanostructured $Ba_{1-x}(Bi_{0.5}K_{0.5})_xTiO_3$ Platelike Particles with Crystal-Axis Orientation. *Chem. Mater*. 2011;23(17): 3978–3986. https://doi.org/10.1021/cm2015252
86. Huang K.C., Huang T.C., Hsieh W.F. Morphology-controlled synthesis of barium titanate nanostructures. *Inorg. Chem*. 2009;48(19):9180–9184. https://doi.org/10.1021/ic900854x
87. Feng Q., Hirasawa M., Yanagisawa K. Synthesis of crystal-axis-oriented $BaTiO_3$ and anatase platelike particles by a hydrothermal soft chemical process. *Chem. Mater*. 2001;13(2):290–296. https://doi.org/10.1021/cm000411e
88. Kang S.O., Park B.H., Kim Y.Il. Growth mechanism of shape-controlled barium titanate nanostructures through soft chemical reaction. *Cryst. Growth Des*. 2008;8(9):3180–3186. https://doi.org/10.1021/cg700795q
89. Li Y., Gao X.P., Pan G.L., Yan T.Y., Zhu H.Y. Titanate nanofiber reactivity: Fabrication of $MTiO_3$ (M = Ca, Sr, and Ba) perovskite oxides. *J. Phys. Chem. C*. 2009;113(11): 4386–4394. https://doi.org/10.1021/jp810805f
90. Xue L., Yan Y. Controlling the morphology of nanostructured barium titanate by hydrothermal method. *J. Nanosci. Nanotechnol*. 2010;10(2):973–979. https://doi.org/10.1166/jnn.2010.1884
91. Bao N., Shen L., Srinivasan G., Yanagisawa K., Gupta A. Shape-controlled monocrystalline ferroelectric barium titanate nanostructures: From nanotubes and nanowires to ordered nanostructures. *J. Phys. Chem. C*. 2008;112(23):8634–8642. https://doi.org/10.1021/jp802055a
92. Kanatzidis M.G., Poeppelmeier K.R., Bobev S., Guloy A.M., Hwu S.J., Lachgar A., *et al.* Report from the third workshop on future directions of solid-state chemistry: The status of solid-state chemistry and its impact in the physical sciences. *Prog. Solid State Ch*em. 2008;36(1–2):1–133. https://doi.org/10.1016/j.progsolidstchem.2007.02.002

93. Özen M., Mertens M., Snijkers F., Hondt H.D., Cool P. Molten-salt synthesis of tetragonal micron-sized barium titanate from a peroxo-hydroxide precursor. *Adv. Powder Technol*. 2017;28(1):146–154. https://doi.org/10.1016/j.apt.2016.09.007
94. Gorokhovsky A.V., Escalante-Garcia J.I., Sánches-Monjarás T., Vargas-Gutierrez G. Synthesis of barium titanate powders and coatings by treatment of TiO_2 with molten mixtures of $Ba(NO_3)_2$, KNO_3 and KOH. *Mater. Lett*. 2004;58(17–18): 2227–3220. https://doi.org/10.1016/j.matlet.2004.01.025
95. Zhang Y., Wang L., Xue D. Molten salt route of well dispersive barium titanate nanoparticles. *Powder Technol*. 2012;217: 629–633. https://doi.org/10.1016/j.powtec.2011.11.043
96. Zhao W., E L., Ya J., Liu Z., Zhou H. Synthesis of High-Aspect-Ratio $BaTiO_3$ Platelets by Topochemical Conversion and Fabrication of Textured $Pb(Mg_{1/3}Nb_{2/3})O_3$-32.5$PbTiO_3$ Ceramics. *Bull. Korean Chem. Soc*. 2012;33(7):2305–2308. https://doi.org/10.5012/bkcs.2012.33.7.2305

About the authors

Anastasia A. Kholodkova, Cand. Sci. (Chem.), Senior Researcher, Laboratory of Ceramic Materials and Technologies, MIREA – Russian Technological University (78, Vernadskogo pr., Moscow, 119454, Russia); Junior Researcher, Department of Physical Chemistry, Faculty of Chemistry, Lomonosov Moscow State University (1–3, Kolmogorova ul., Moscow, 119234, Russia). E-mail: anakholo@gmail.com. Scopus Author ID 56530861400, ResearcherID M-2169-2016, RSCI SPIN-code 7256-7784, https://orcid.org/0000-0002-9627-2355

Alexander V. Reznichenko, Research Engineer, Laboratory of Ceramic Materials and Technologies, MIREA – Russian Technological University (78, Vernadskogo pr., Moscow, 119454, Russia). E-mail: 250871rav@gmail.com. Scopus Author ID 56600221500, RSCI SPIN-code 2167-7678

Alexander A. Vasin, Cand. Sci. (Eng.), Senior Researcher, Laboratory of Ceramic Materials and Technologies, MIREA – Russian Technological University (78, Vernadskogo pr., Moscow, 119454, Russia). E-mail: alexandrvasin123@gmail.com. Scopus Author ID 57211840246, ResearcherID K-3214-2015, RSCI SPIN-code 3864-9132, https://orcid.org/0000-0002-9501-2316

Andrey V. Smirnov, Cand. Sci. (Eng.), Head of the Laboratory of Ceramic Materials and Technologies, MIREA – Russian Technological University (78, Vernadskogo pr., Moscow, 119454, Russia). E-mail: smirnov_av@mirea.ru. Scopus Author ID 56970389000, ResearcherID J-2763-2017, RSCI SPIN-code 2919-9250, https://orcid.org/0000-0002-4415-5747

Об авторах

Холодкова Анастасия Андреевна, к.х.н., старший научный сотрудник, Лаборатория керамических материалов и технологий, ФГБОУ ВО «МИРЭА – Российский технологический университет» (119454, Россия, Москва, пр-т Вернадского, д. 78); младший научный сотрудник, кафедра физической химии, Химический факультет, ФГБОУ ВО «Московский государственный университет им. М.В. Ломоносова» (119234, Россия, Москва, ул. Колмогорова, 1, стр. 3). E-mail: anakholo@gmail.com. Scopus Author ID 56530861400, ResearcherID M-2169-2016, SPIN-код РИНЦ 7256-7784, https://orcid.org/0000-0002-9627-2355

Резниченко Александр Владимирович, инженер-исследователь, Лаборатория керамических материалов и технологий, ФГБОУ ВО «МИРЭА – Российский технологический университет» (119454, Россия, Москва, пр-т Вернадского, д. 78). E-mail: 250871rav@gmail.com. Scopus Author ID 56600221500, SPIN-код РИНЦ 2167-7678

Васин Александр Александрович, к.т.н., старший научный сотрудник, Лаборатория керамических материалов и технологий, ФГБОУ ВО «МИРЭА – Российский технологический университет» (119454, Россия, Москва, пр-т Вернадского, д. 78). E-mail: alexandrvasin123@gmail.com. Scopus Author ID 57211840246, ResearcherID K-3214-2015, SPIN-код РИНЦ 3864-9132, https://orcid.org/0000-0002-9501-2316

Смирнов Андрей Владимирович, к.т.н., заведующий Лабораторией керамических материалов и технологий, ФГБОУ ВО «МИРЭА – Российский технологический университет» (119454, Россия, Москва, пр-т Вернадского, д. 78). E-mail: smirnov_av@mirea.ru. Scopus Author ID 56970389000, ResearcherID J-2763-2017, SPIN-код РИНЦ 2919-9250, https://orcid.org/0000-0002-4415-5747

Translated from Russian into English by V. Glyanchenko
Edited for English language and spelling by Dr. David Mossop

MIREA – Russian Technological University
78, Vernadskogo pr., Moscow, 119454, Russian Federation.
Publication date *February 29, 2024.*
Not for sale

МИРЭА – Российский технологический университет
119454, РФ, Москва, пр-т Вернадского, д. 78.
Дата опубликования *29.02.2024.*
Не для продажи

www.finechem-mirea.ru